Strengthening of an Orthotropic Steel Deck with Blind Bolted Steel Plates

Enhancing the fatigue performance with a light-weight and quick-to-install strengthening solution

L.K. Juric

TUDelft

ARUP

Strengthening of an Orthotropic Steel Deck with Blind Bolted Steel Plates

Enhancing the fatigue performance with a light-weight and quick-to-install strengthening solution

by

L.K. Juric

to obtain the degree of Master of Science

at the Delft University of Technology,

to be defended publicly on Monday April 14th, 2025 at 11:00.

An electronic version of this thesis is available at `http://repository.tudelft.nl/`.

TUDelft

Acknowledgements

The important thing is not to stop questioning.
Curiosity has its own reason for existing.
- Albert Einstein

This thesis marks the end of my time at TU Delft and brings together everything I've learned during these past years. It's been a time of growth, both academically and personally. I've always been drawn to bridges—their complexity, function, and presence in the landscape. Being able to work on a topic that explores how we can extend the life of these structures felt like a natural fit with my interests and values. I've remained driven by curiosity throughout my studies, and this project gave me the chance to explore that curiosity in a way that was both challenging and rewarding.

Along the way, I've had the privilege of working with people who have supported me at every step. Marko, thank you for encouraging critical thinking and for our inspirational monthly meetings. Abishek, your support, both technical and personal, meant so much, especially during the moments when stress was high. Roel, I'm grateful for how generously you shared your time and knowledge. You helped me find focus when I wanted to explore everything, and I learned a lot from you, both in modelling and structural understanding. Daan, thank you for introducing this topic and helping shape it into something that truly fit my interests. I really appreciated our early brainstorming sessions. And to Frans, thank you for your valuable feedback and for being part of the committee.

To my family: mom and dad, even though we were more than a 1,000 kilometres apart, it never felt like it. You were always just one call away. Tata, in many ways, I feel like I'm living your dream by studying this—thank you for that inspiration. Kad god želim pričati o zakovicama ili o drugim (techničkim) temama, tu si. Mama, you've always been the best listener, always present. Vjeruješ u mene ponekad više nego ja sama. Hvala vam puno.

To Emma, I'm so thankful for how close we are. To Jurr, thank you for being my favourite support system. Van koffie voor me maken of koken tot luisteren naar mijn verhaal in positieve en lastige momenten. And to Deborah, we've been through it all together, bachelor weekends, late-night study sessions, and now graduating just a month apart. Bedankt voor je vriendschap.

To all my friends throughout these years, from the bachelor and master, from U-BASE, the book club, Pluto, committees, and beyond, thank you. You've made my time in Delft unforgettable. I'm grateful for everything we've shared and the friendships I'll take with me into the next phase.

Laura Katharina Jurić
Delft, April 2025

Summary

Orthotropic steel decks are widely used in bridge construction due to their high strength-to-weight ratio. However, they are particularly prone to fatigue cracking at welded joints, an issue intensified by increased traffic and heavier vehicles over time. This poses significant challenges for the maintenance and safety of ageing steel bridges, both in the Netherlands and internationally.

This thesis investigates a novel strengthening method using blind bolted steel plates to enhance the fatigue performance of orthotropic steel decks. The central research question is:

To what extent can a strengthening solution with blind bolted steel plates contribute to the extension of the fatigue life of orthotropic steel decks?

A case study of the Second Van Brienenoord Bridge forms the focus of the research. Two fatigue-critical details within the heavy traffic lane are identified and targeted for strengthening. The strengthening solution involves attaching a thin steel plate to the existing deck using blind bolts, offering a lightweight and practical alternative to conventional methods such as Ultra High Performance Concrete (UHPC) overlays.

A detailed finite element model of the bridge deck is developed in GSA Oasys to analyse hot spot stresses under fatigue loading before and after strengthening. A parametric model is also developed using Grasshopper to efficiently generate and assess different strengthening schemes by varying design parameters: plate thickness, bolt size, bolt spacing, number of bolt rows, and transverse bolt configuration.

A comprehensive parametric study identifies plate thickness as the most influential factor in reducing hot spot stresses. Interactions between parameters, such as bolt arrangement and plate thickness, are identified. Based on these findings, a selection of promising strengthening schemes is made for further evaluation.

These schemes are assessed using three criteria: fatigue life extension, added weight, and estimated installation time. Additionally, static verifications under thermal loading and heavy vehicle loading (Eurocode Load Model 2) are performed to ensure that the bolts do not fail prematurely in shear. Some schemes require denser bolt patterns at plate edges to pass these checks. The most effective schemes achieve over 60% reduction in hot spot stresses and extend fatigue life by up to 30 years, with moderate weight and relatively quick installation times.

In conclusion, this research demonstrates that blind bolted steel plate strengthening can effectively enhance the fatigue performance of orthotropic steel decks, providing a cost-efficient and quick to implement solution. The use of blind bolts enhances applicability by enabling one-sided installation, even above closed stiffeners. The methodology and insights developed here can guide future applications in bridge maintenance.

Recommendations for further research include experimental testing to validate bolt preload and slip resistance, more detailed fatigue damage assessments based on full stress histories, and investigation of the strengthening method's applicability to varying deck geometries and damage levels. Practical aspects such as the interaction between deck and strengthening plate, emergency repair potential, and long-term durability should also be explored.

Contents

List of Figures

List of Tables

<div align="right">

1

</div>

Introduction

1.1. Research context

Many steel bridges currently in service in the Netherlands were built shortly after the Second World War, with most constructed between 1960 and 1980 [1]. These bridges often utilise a stiffened steel plate as the bridge deck, called an orthotropic steel deck, whose benefits are its relatively low weight and short construction time [2]. Examples from the Dutch highway network include the Suurhoff and Van Brienenoord bridges, while internationally renowned examples are the Millau Viaduct in France and the Akashi Kaikyo suspension bridge in Japan.

Although orthotropic steel decks have demonstrated a high load-carrying capacity, a significant disadvantage has emerged over the years: their susceptibility to fatigue cracking. Fatigue cracks develop due to high localised stresses caused by heavy cyclic loads, with certain details of the deck being especially vulnerable to peak stresses, such as the welds between connecting elements. Since an orthotropic steel deck contains numerous welds, connecting the deck plate, troughs, and cross beams, many locations are vulnerable to fatigue cracking, as illustrated in Figure 1.1. This issue has been confirmed in practice, as a considerable number of existing orthotropic steel deck bridges, both fixed and movable, have exhibited fatigue problems.
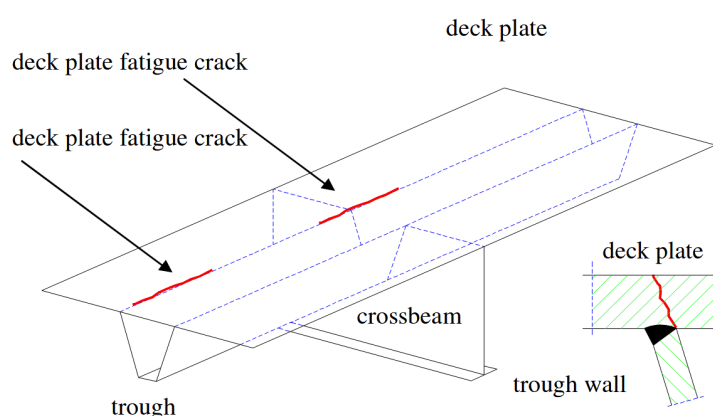
Figure 1.1: Orthotropic Steel Deck: overview of components & fatigue crack locations [1]

The extent of this problem was underestimated during construction of the bridges, partly due to lack of in-depth knowledge of fatigue behaviour at the time. As a result, fatigue was given less

consideration in both design and execution. Additionally, these structures are now subjected to substantially higher traffic loads than initially designed for, as a result of the ever-increasing number and weight of vehicles on the motorways. For example, the design code used at the time of construction, VOSB1963, considered 50% lower axle loads and 125% lower uniformly distributed loads (for the heaviest loaded lane) compared to the currently used EN 1991-2 [3]. An extreme case of unexpected fatigue cracking is the Van Brienenoord bascule bridge, where cracks were detected in the heavy vehicle lane after only seven years of service [4].

With the growing prevalence of fatigue cracking in ageing bridges and its potential to compromise structural integrity, addressing these issues has become increasingly urgent. This is particularly critical as vehicle traffic is expected to increase further in the coming years. Full replacement of bridge decks affected by fatigue damage is not a desirable solution due to its high cost and environmental impact. Instead, Rijkswaterstaat, in collaboration with engineering firms, is conducting a large-scale assessment of bridges in the Netherlands and developing strengthening strategies to extend the fatigue life of orthotropic steel deck bridges.

1.1.1. Current fatigue strengthening techniques

When critical fatigue cracks suddenly appear in orthotropic steel deck bridges, an emergency repair method known as the "gutsen-lassen" solution is often applied. This technique involves placing a steel plate over the cracked area and welding it along its perimeter to the deck plate. While this emergency repair method is quick to implement, the additional welds are prone to development of new cracks, often adding to the fatigue problem [5].

For long-term improvements in fatigue resistance, strengthening methods are typically employed. One commonly applied technique is applying an Ultra High Performance Concrete (UHPC) overlay to the deck. This increases the deck's stiffness and, consequently, enhances fatigue resistance. However, this solution has disadvantages: the large additional weight imposed on the bridge's super- and substructure, as well as the relatively long installation time due to the curing of the concrete, which can take over six months for a highway bridge [5]. This results in significant disruption time of traffic, which can be problematic for bridges that form important links on the highway network.

Given the limitations of current fatigue enhancement techniques, alternative strengthening solutions are being investigated by research institutes and engineering firms. An example is strengthening using a bolted steel plate, which was successfully implemented by engineering firm Arup for the Suurhoff bridge. The strengthening solution consisted of a 30 mm steel plate with preloaded injection bolts as connectors. Between the strengthening plate and the deck plate, an epoxy layer was applied to aid force transfer and account for surface imperfections. The installation was completed in four weeks [6], demonstrating the potential of this technique.

1.2. Research problem

The Suurhoff bridge demonstrates the feasibility of strengthening orthotropic decks with bolted steel plates, but the applied design was conservative, using thick plates and covering the entire bridge deck area. Additionally, the need for epoxy layers and access beneath the deck for tightening of bolts complicated the installation process. Although this method reduced installation time and weight compared to the UHPC overlay, there is potential to explore strengthening solutions that could further improve these factors.

Furthermore, there is limited research on whether a more targeted strengthening approach, such as focusing on strengthening only the heavy traffic lanes, can effectively extend fatigue life while minimising installation time and additional weight. The effectiveness of such partial

strengthening, which can be adaptable to varying degrees of fatigue damage, has not been sufficiently explored. This is particularly relevant for secondary roads (*N-wegen*), which experience fatigue damage but do not justify full-scale strengthening interventions. Further investigation could be particularly useful, as it would help optimise the strengthening approach for many bridges in the Netherlands.

1.3. **Aim and research objectives**

This thesis aims to develop a strengthening design for improving the fatigue resistance of orthotropic steel decks. The design objectives are to create a lightweight solution, minimise installation time, and allow for flexible strengthening, meaning the strengthening can be tailored to the extent of fatigue damage, the desired additional service life, and the accepted level of future repairs.

The research builds upon the Suurhoff bridge concept of using a bolted steel plate for strengthening but proposes modifications to the design to enhance performance. Specifically, the design incorporates a thin steel plate and blind bolts as connectors. Using a thin plate reduces the weight and eliminates the need for an epoxy mid-layer, since the plates can deform together, which in turn simplifies the installation procedure. Blind bolts, which require access on only one side of the connection, further reduce the installation time by removing the need for access beneath the bridge deck during installation.

To evaluate the effectiveness of this strengthening concept, a case study bridge deck will be numerically modelled to conduct fatigue assessment and determine the improvement in fatigue life after strengthening. If proven effective, this method could provide a practical strengthening solution for many ageing steel bridges.

To achieve these goals, the following research objectives are identified:

- Investigate the applicability of blind bolt technologies for strengthening orthotropic steel bridge decks.
- Conduct fatigue calculation of a bridge deck and obtain hot spot stresses of critical details.
- Design different strengthening schemes using blind bolted steel plates and assess their fatigue performance.
- Compare the proposed strengthening schemes in terms of weight, installation time and fatigue life improvements.

1.4. **Research scope**

Developing and evaluating a new design concept for strengthening orthotropic steel decks is a complex process that involves multiple steps. Due to the time constraints of this thesis, certain limitations have been set to define the scope of the research.

The strengthening design is developed for a single case study bridge deck with known geometry and documented fatigue damages. Several fatigue-critical locations with the most significant damage are selected, located in the heavy vehicle lane, and a tailored strengthening design is developed to improve their fatigue resistance. While the findings provide valuable insights, further research is required to validate the applicability of this approach to other critical details and different bridge deck geometries.

Although this research aims to identify different blind bolt technologies, a detailed investigation into their performance, such as fatigue behaviour or slip resistance, is beyond the scope of this thesis. Instead, reasonable estimations are made regarding the preload and slip resistance of

the selected blind bolts. Additionally, the study simplifies real-world conditions by assuming perfect contact between the strengthening plate and the deck plate, ignoring potential surface unevenness that could affect bolt preloading.

The fatigue assessment in this research is also conducted in a simplified manner. Rather than performing a full fatigue life evaluation with a stress range history analysis, this study identifies the most critical load position for each selected fatigue detail and determines the corresponding hot spot stress. The effectiveness of the strengthening is then assessed by comparing hot spot stresses before and after strengthening. An approximate estimation of fatigue life extension is made using the ratio of these stresses and a reference damage value obtained from the fatigue assessment of the case study bridge deck without strengthening.

While fatigue performance is the primary focus, the strengthening design must also meet ultimate limit state (ULS) requirements to ensure it does not introduce failures in other load scenarios. Since a slip-resistant connection is desired, the bolts are checked in ULS for slip capacity under temperature effects and Load Model 2 loading. However, other ULS and serviceability limit state (SLS) checks are beyond the scope of this research. It is assumed that the added strengthening does not negatively impact the overall bridge deck and structural integrity.

1.5. Research questions

The following research question will be answered in the report:

To what extent can a strengthening solution with blind bolted steel plates contribute to the extension of fatigue life of orthotropic steel decks?

The sub-questions that will help to derive an answer are as follows:

- Which blind bolt technologies, considering their preload characteristics and other performance criteria, are the most suitable for application in strengthening orthotropic steel decks?

- To what degree can the hot spot stresses of the case study bridge deck be reduced with a strengthening with blind-bolted steel plates?

- To what extent do the preload level, bolt configuration and thickness of the strengthening plate influence the hot spot stress reductions?

- How sensitive is the strengthening method for ultimate limit state verifications?

- Which strengthening schemes using blind-bolted steel plates provide the best balance of fatigue life extension, weight, and installation time?

1.6. Methodology

This research follows a structured approach to develop and assess a strengthening design using blind-bolted steel plates for orthotropic steel decks. The methodology consists of the following steps.

1.6.1. Literature review

Firstly, a literature review is conducted to understand the background of the fatigue issues in orthotropic steel decks and investigate existing strengthening techniques. Additionally, a study of available blind bolt types is performed to determine the most suitable option for this application.

1.6.2. Strengthening design
The bridge deck of the Second Van Brienenoord bridge is adopted as the case study of this research. The geometric and material properties of the deck are inventoried. The fatigue critical locations are identified based on existing fatigue assessments. A strengthening design using blind-bolted steel plates is developed for the heavy vehicle lane of the bridge deck, tailored to improve the fatigue behaviour of several most critical details. The design parameters include thickness of strengthening plate, bolt size and bolt configuration. The latter is further subdivided into the spacing between two bolt rows, number of bolt rows, number of bolts per trough and number of bolts between troughs, leading to six strengthening design parameters in total.

1.6.3. Numerical modelling
A finite element model of the bridge deck is created and the hot spot stresses of the critical details prior to strengthening are determined. The FE model of the bridge deck is extended by adding the strengthening. A parametric model is created where the design parameters of the strengthening can be varied and a finite element model is automatically generated, with which the hot spot stresses of the strengthened bridge deck are obtained.

1.6.4. Parametric study and Evaluation of strengthening schemes
Firstly, a parametric study of the strengthening schemes is performed to asses the impact of the various design parameters on hot spot stress reduction. Among the considered parameters, some might have a more significant effect on stress reduction, while others have a more limited influence. The outcomes of the parametric study will help in selecting strengthening schemes for further analysis. This final selection of strengthening schemes is verified in ultimate limit state, by performing shear checks of the bolts. Finally, several strengthening schemes are assessed using the following criteria: fatigue life extension, additional weight and installation time.

1.7. Thesis outline
The report is organised into several chapters, following the steps presented in the Methodology. First, the literature review is given in Chapter 2, where the fatigue phenomenon and characteristics of orthotropic steel decks are explained. Additionally, the various blind bolt types are summarised. In Chapter 3, the case study is introduced and the strengthening design is defined, explaining which components it consist of and which design parameters are considered in the analysis. The development of the finite element model for fatigue assessment is presented in Chapter 4, together with the explanation of the parametric model for generation of different strengthening schemes. The effect of the design parameters on hot spot stress reduction is studied with a parametric study, for which the results are summarised in Chapter 5. Chapter 6 gives the results of the ultimate limit state verifications and assesses a final selection of strengthening schemes on fatigue life extension, weight and installation time. Finally, the conclusions of the thesis are compiled in Chapter 7, and recommendations for further research provided in Chapter 8.

<div align="right">

2

</div>

Literature Review

This chapter serves as the theoretical framework of the research, first presenting the basic principles of fatigue and orthotropic steel decks, in Sections 2.1 and 2.2 respectively. Next, a study of available blind bolted technologies is performed, with the findings summarised in Section 2.3.

2.1. Fatigue

Fatigue is a structural damage mechanism that occurs when structures are exposed to cyclic loading. The stress ranges under which failure occurs are usually lower than the static strength of the material [7]. Fatigue failure is considered one of the most catastrophic failure mechanisms, as there is often little warning beforehand [4].

A clear understanding of the fatigue phenomenon is crucial for mitigating fatigue failure in structures. This section elaborates on the initiation and growth of fatigue cracking, as well as the susceptibility of welded joints to fatigue. Furthermore, it explains how to calculate the fatigue resistance of a structural element and presents the method for estimating its fatigue life.

2.1.1. Fatigue process

The fatigue process can be divided into three phases: initiation, crack growth and final failure, as visualised in Figure 2.1 [8] [7]. Each of these stages is explained below.
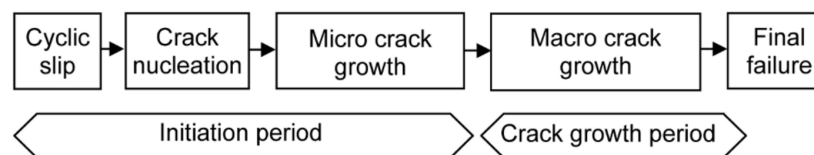
Figure 2.1: Phases of fatigue process [8]

Initiation period

The fatigue process initiates with cyclic slip in certain grains of the specimen, caused by cyclic shear stresses from fatigue loading. This cyclic slip occurs on microscopic level. If the specimen contains surface defects, such as scratches, small cracks, or notches, these defects act as stress raisers, leading to stress concentrations and eventually crack initiation [8].

However, even in a polished specimen without surface defects, cyclic slip can still occur. Fatigue cracking may develop before the material reaches its yield strength. This happens

because some grains, which are favourably oriented with respect to the loading axis, experience micro-yielding before the entire specimen yields. This localised microplastic deformation often occurs in the surface grains, where slip planes continuously change direction due to cyclic loading, leading to formation of surface intrusions and extrusions on the material's surface. This phenomenon is called a "slip band" [8]. At these intrusions, microcracks can nucleate. Figure 2.2 visualises the formation of a slip band. Internal defects, such as porosity, can also serve as initiation points for crack formation.
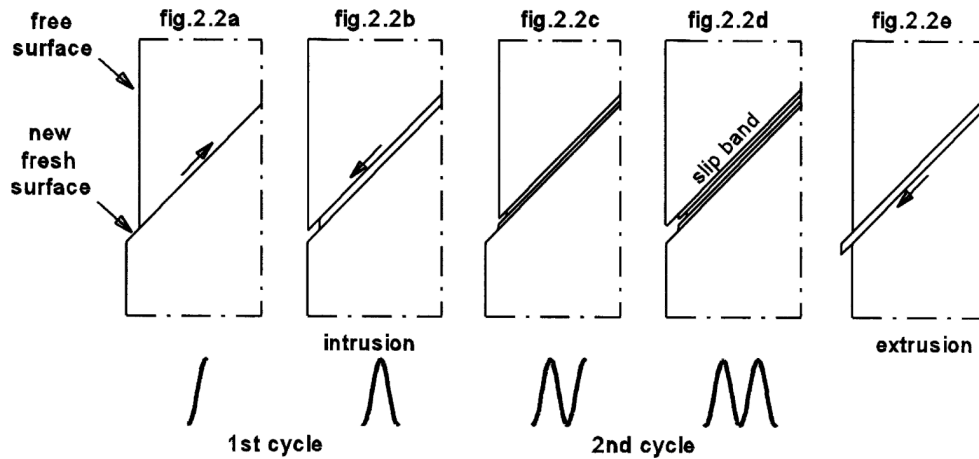
Figure 2.2: Initiation of fatigue crack [8]

Crack growth period

At the beginning of crack propagation, the microcrack is in the order of one single grain, and its path is crystallographic, meaning that it changes direction based on the grain orientation. As the crack growths, this single-slip system is replaced with multiple-slip planes, and the crack path reorients to become perpendicular to the loading direction [8]. This behaviour is shown in Figure 2.3a.
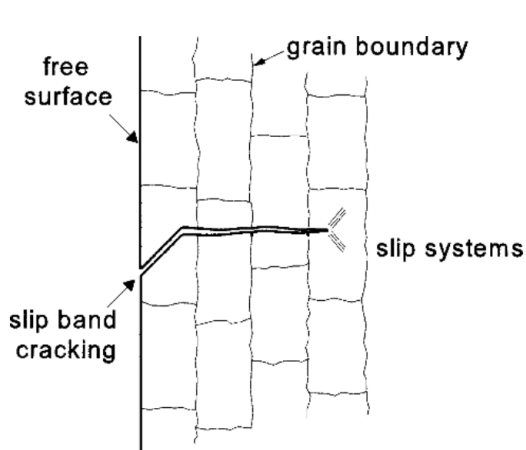
(a) Growth direction of microcrack [8]
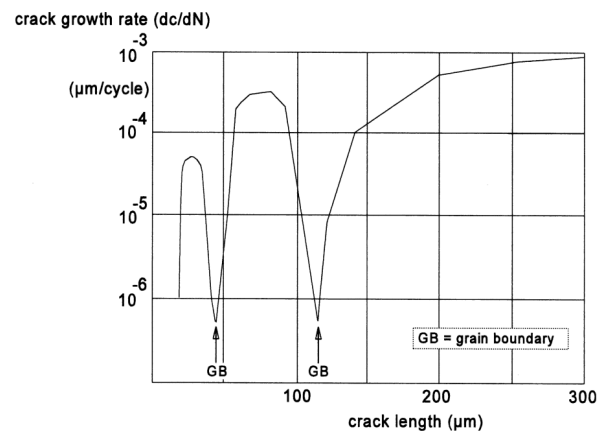
(b) Fatigue crack growth rate changes along crack length [8]

Figure 2.3: Crack growth behaviour

The crack growth rate varies along the crack length. Initially, while the crack width is limited, the growth rate fluctuates: it accelerates while the crack moves through a grain but slows down at grain boundaries. As the crack front increases and spans multiple grains along its width, its

growth rate becomes influenced by all these grains collectively. Now, the crack growth is not affected any more by the surface conditions and, instead, depends on the overall resistance of the material. This transition marks the shift from the initiation phase to the crack growth stage [8]. Figure 2.3b illustrates the described crack growth behaviour.

Final failure

Final failure occurs when the fatigue crack reaches a critical length, and the remaining cross-section of the specimen can no longer withstand the applied load. Some plastic deformation may be observed in ductile materials [8], but in some cases, no noticeable deformation occurs, leading to sudden brittle failure [4]. Figure 2.4 illustrates a typical fatigue crack fracture surface, which appears smooth and features concentric rings known as "beach marks". These marks indicate the progression of crack growth over time.
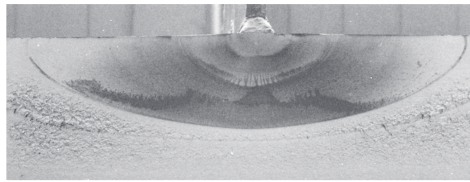
Figure 2.4: Fracture surface of a fatigue crack [4]

Welded joints

If a specimen contains no significant defects, such as welds or surface imperfections, the majority of its fatigue life is spent in the crack initiation phase. However, when defects are present, they act as stress raisers, reducing the time required for crack initiation. In such cases, microcracks form more rapidly and are larger from the start. For materials with severe defects, such as welded joints, the initiation phase may be almost entirely skipped, leading to a significantly shorter fatigue life [8].

Welded joints are particularly susceptible to fatigue cracking due to intrusions at the weld toe, stiffness differences between the weld and the connected members, and geometric discontinuities (in case of a rough weld profile). These factors cause stress concentrations, for example near the weld toe, as shown in Figure 2.5. If the applied cyclic loading is high enough, crack formation occurs within a short time period. In welded joints, fatigue cracks usually initiate at the weld toe or weld root [4].

Another critical aspect in welded joints is the presence of residual stresses from the welding processes. While these stresses may not significantly affect static loading conditions, they have a major impact under cyclic loading. For example, when cyclic loading is in the compressive range, residual tensile stresses can shift the effective stress range into tension, resulting in crack growth even when external tensile loads are minimal [4].

2.1.2. Fatigue resistance

The fatigue resistance of a structural element is defined as its ability to withstand fatigue loading without failure. It can be determined through experimental testing, where a specimen is subjected to cyclic loading with either constant or variable amplitude. The number of cycles until failure is recorded, and a graph can be plotted that relates the load ranges to the number of load cycles [9].

Fatigue strength curves

The relation between the applied stress ranges (S) and number of load cycles until failure (N) can be approximated linearly on a logarithmic scale, resulting in an S-N curve [9]. With these
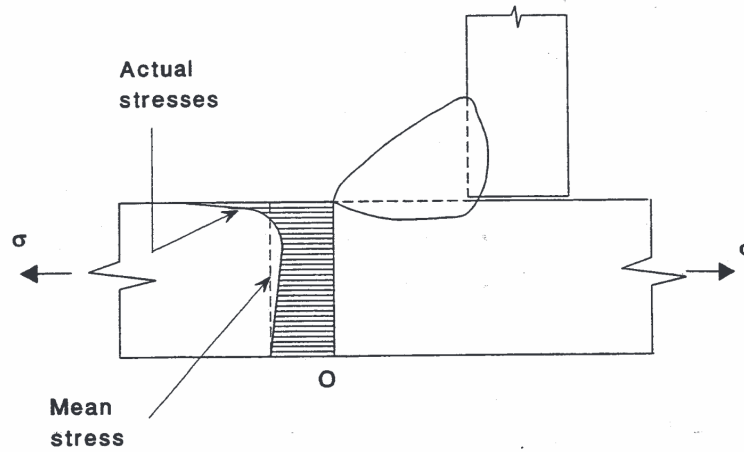
Figure 2.5: Visualisation of stress concentration at weld toe [4]

curves, it can be estimated how long a structural detail can last under cyclic loading, once the stress history has been determined. In fatigue life calculations, the stress ranges acting on a structure are first determined, and then compared to the corresponding S-N curve to estimate the number of cycles the material can endure before failure (see Section 2.1.3).

Figure 2.6 displays examples of S-N curves for welded steel details. Three regions can be distinguished in the plot, with parameter $m = 3$ representing the slope of the S-N curve:

1. Region with $m = 3$ in the cycle range of $1 \times 10^6 \geq N \geq 5 \times 10^5$

2. Region with $m = 5$ in the cycle range of $5 \times 10^5 \geq N \geq 1 \times 10^7$

3. Region with $m = \infty$ in the cycle range of $N \geq 1 \times 10^7$
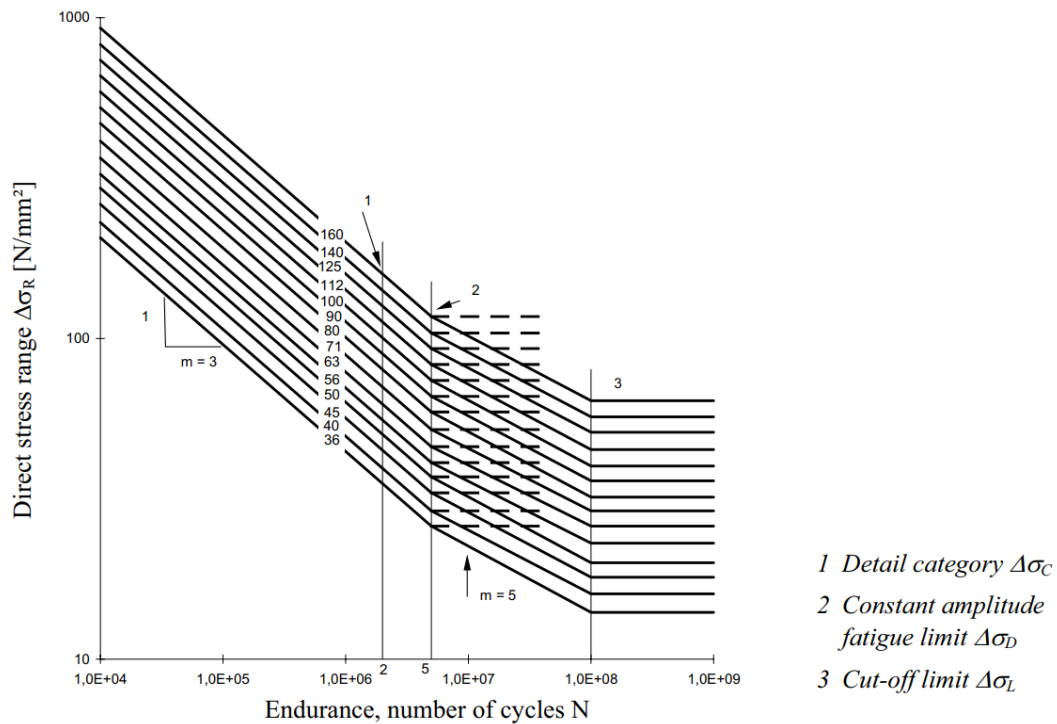
Figure 2.6: Fatigue strength curves for direct stress ranges [10]

The first region shows a steeper relation between stress range and number of cycles compared to the second region, which has a shallower slope, meaning that changes in stress ranges have less impact on the fatigue life. Infinite fatigue life refers to a loading condition where crack propagation does not occur [4], and in the fatigue strength plot, it is represented by a horizontal line (third region). If stress ranges fall below a certain limit, called the cut-off limit or endurance limit, the Eurocode permits neglecting fatigue damage, as it is assumed that the material can endure an infinite number of loading cycles without fatigue failure [4].

Multiple curves are shown, representing different detail categories. The number assigned to each curve corresponds to the reference value of the fatigue strength at 2 million cycles, $\Delta\sigma_c$. The fatigue strength is calculated using different formulas [4], depending on the part of the curve that is applicable. Equation 2.1 describes the first segment, and Equation 2.2 the second segment, while the calculation of $\Delta\sigma_D$ is presented in Equation 2.3. The fatigue strength at the cut-off limit is calculated with Equation 2.4.

$$\Delta\sigma_R^m N_R = \Delta\sigma_C^m 2.10^6 \tag{2.1}$$

$$\Delta\sigma_R^m N_R = \Delta\sigma_D^m 5.10^6 \tag{2.2}$$

$$\Delta\sigma_D = (2/5)^{\frac{1}{3}}\Delta\sigma_C = 0.737\Delta\sigma_C \tag{2.3}$$

$$\Delta\sigma_L = (5/100)^{\frac{1}{5}}\Delta\sigma_D = 0.549\Delta\sigma_D \tag{2.4}$$

2.1.3. Fatigue life

This section aims to explain how the fatigue life of a structure is determined, focusing on welded joints, as they are highly susceptible to fatigue, and are the primary focus of this thesis. The procedure for calculating the fatigue life of a structural element is usually performed with the following steps [9]:

1. *Classification of detail category*: determines which S-N curve applies

2. *Calculation of stresses*: computes the stress ranges acting on the component

3. *Analysis of stress history*: organises stress cycles from variable loading with cycle counting

4. *Determination of fatigue damage*: uses S-N curve to estimate fatigue life and apply damage accumulation models

Note that the approach explained here is the S-N curve method, but there are also other approaches available, e.g. the fracture mechanics method, which analyses the stresses at the crack tip in order to study the initiation and propagation of fatigue cracks [11].

Detail classes

As mentioned in Section 2.1.2, the fatigue strength curve of a structural element or detail depends on its assigned detail category. Reference fatigue strength values ($\Delta\sigma_c$) are determined by conducting tests on various (welded) joints to determine their fatigue resistance at 2 million load cycles. The joints are then categorised into different detail classes [10]. The specifics to the fatigue behaviour of welded joints, as explained in Section 2.1.1, such as the influence of residual stresses and geometric discontinuities, are incorporated into this detail classification. The use of detail classes eliminates the need for extensive testing since the fatigue resistance

can be estimated directly from design standards [9]. Eurocode 1993-1-9 [10] provides detail categories for various structural components, such as plain members, load-carrying welded joints, hollow sections, and orthotropic decks [4]. The assigned detail category determines which S-N curve should be used in fatigue life calculations.

Calculation of stresses
Different methods can be used to determine stresses in fatigue-critical details. Abdelbaset and Zhu [11] have presented the most commonly applied methods, which are explained below.

Nominal stress approach
The nominal stress approach is one of the most widely used methods for fatigue assessment. It calculates the fatigue strength based on the average, nominal stress of a cross-sectional area of the component. This method accounts for geometric modifications, such as holes or notches, but does not consider high stress concentrations that occur at locations like welded connections. Nominal stresses can be determined using structural mechanics principles for simple structures or with the finite element method (FEM) for more complex components. The approach is incorporated into design standards such as the Eurocode, by providing S-N curves for various detail categories. The S-N curves in Figure 2.6 are associated with this method. While the nominal stress approach offers sufficient accuracy for many cases, it is less reliable for welded details, where the calculated stresses may not accurately reflect fatigue behaviour, as the stress concentrations at the welds are not captured [11].

Hot spot stress approach
An alternative approach is the hot spot stress (HSS) method, which estimates the fatigue strength by focusing on the structural stress at critical locations where fatigue cracks are likely to initiate, such as weld toes [11]. Unlike the nominal stress approach, which considers the average cross-sectional stress, the HSS method captures stress concentrations caused by structural geometry, but excluding local notch effects. Hot spot stresses are determined by extrapolating stresses from two points at a specified distance from the joint [9], as visualised in Figure 2.7. These stresses can be obtained using finite element modelling or strain gauge measurements [11]. Guidelines for extrapolation are provided in design standards, such as the "Richtlijnen Ontwerp Kunstwerken" (ROK) by Rijkswaterstaat [12]. Although there are fewer available S-N curves for this method compared to the nominal stress method, the HSS approach is known to provide a more accurate fatigue strength assessment [11].
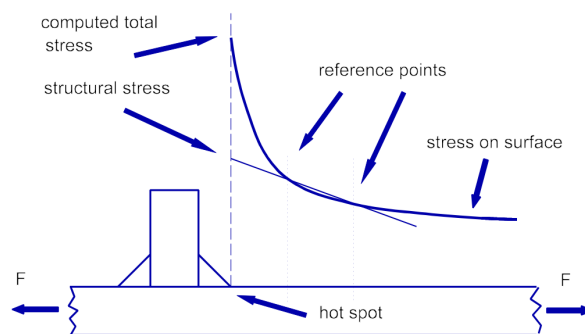
Figure 2.7: Hot Spot Stress method: extrapolation of stresses [9]

Effective notch stress approach
A limitation of the hot spot stress method is its inability to include non-linear notch effects caused by sudden geometric changes, such as cross-section reductions or holes. The effective

notch approach can effectively address this issue. This method utilises an effective notch contour, a simplified shape of the stress concentration effects, to replace the actual complex contour. It is particularly effective for capturing critical stress concentrations where fatigue failure is most likely to occur [11].

Comparison of methods
Each of these methods has advantages depending on the application. The hot spot stress and effective notch approaches are particularly suitable for components with high stress concentrations, such as welded joints [9]. Abdelbaset and Zhu [11] compared these methods for estimating the fatigue performance of an orthotropic steel deck. Their findings showed that both the nominal stress and hot spot stress approaches were effective for analysing the joint between the longitudinal stiffener and deck plate. However, when assessing the joint between the longitudinal stiffener and cross beam, the effective notch and hot spot stress methods provided more reliable fatigue predictions.

Analysis of stress history: cycle counting
Fatigue loading usually involves variable amplitude loading, consisting of different load spectra with consecutive high and low peaks (maxima and minima) that change their amplitudes and frequencies during the loading history. These variations cause fluctuations in stress, forming stress cycles. However, identifying representative stress cycles is more challenging for stochastic loads: unpredictable loading conditions such as vehicle traffic on a highway or wind forces acting on a bridge. To simplify the complexity of such loads, cycle counting methods are used to break down load spectra into discrete stress cycles, enabling fatigue damage calculations [8].

The *Rainflow Counting Method* is widely used to process complex load histories into discrete cycles. It effectively isolates relevant relevant stress cycles while discarding non-damaging ones [8], allowing the accurate fatigue damage prediction. A useful analogy to explain this method is visualising the stress-time history as a pagoda roof, where stress cycles are determined by the distances water droplets travel as they fall from different roof levels [9].

Another commonly applied technique is the *Reservoir Counting method*, which models the stress-time history as a reservoir being filled with water. Water is drained from the peaks, and the stress cycle is defined by the largest drop before completely emptying that peak of the reservoir [9]. Figure 2.8 illustrates this principle.
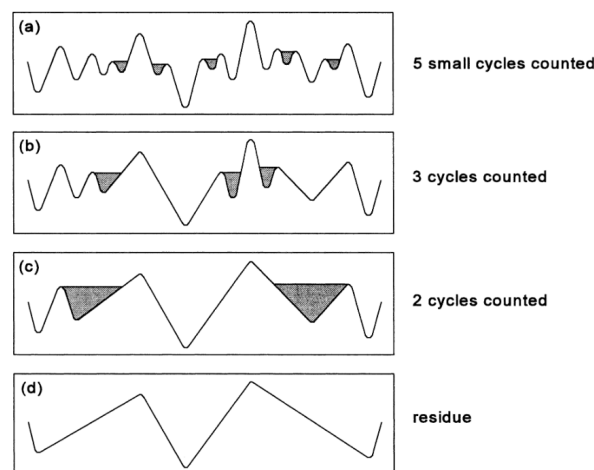
Figure 2.8: Principle of reservoir counting method [8]

Damage calculation

Once the significant stress cycles have been identified, the final step is to calculate the accumulated fatigue damage. A widely used approach for this is the Miner's rule, also known as the linear damage rule, given in Equation 2.5 [9]. This method assumes that fatigue damage accumulates linearly with each load cycle, but only considering cycles that exceed the fatigue limit [8]. As shown in the formula, total fatigue damage is obtained by summing up individual damage fractions. Fatigue failure is predicted to occur when the cumulative damage reaches or exceeds a threshold of 1 [9]. A key limitation of this method is that it disregards cycles below the fatigue limit, which can result in an overestimation of fatigue life. To mitigate this issue, alternative approaches have been developed, including S-N curve extrapolation [8] and non-linear damage accumulation models [9].

$$D = \sum_{i=1}^{I} \frac{n_i}{N_i} \qquad (2.5)$$

where:

- D = fatigue damage
- n_i = number of applied cycles at stress level i,
- N_i = number of cycles to failure at stress level i from the corresponding S-N curve [9].

2.2. Orthotropic Steel Decks

Orthotropic Steel Decks are a common bridge deck type for steel bridges. In the Netherlands, between the 1960s and 1980s, 70-80% of the steel bridges built featured an OSD [1]. Orthotropic steel decks offer many benefits, such as being lightweight while providing a high load-carrying capacity. Due to their modular construction, they can be installed relatively quickly as well [11].

This section provides an introduction the structural composition, benefits, and applications of orthotropic steel decks, as well as analysing their structural behaviour through the concept of "structural systems". Moreover, the vulnerability of orthotropic steel decks to fatigue failure is discussed, and guidelines for fatigue design are summarised. The section also explores strengthening solutions to extend the fatigue life of orthotropic steel decks.

2.2.1. Structural composition

As illustrated in Figure 2.9, an orthotropic steel deck consists of a deck plate, longitudinal stiffeners, crossbeams, and main girders. The deck plate distributes traffic loads in both longitudinal and transverse direction [13]. The crossbeams support the deck plate in transverse direction, while the longitudinal stiffeners reinforce the deck plate along the bridge's length. The orthotropic steel deck is fully integrated into the bridge's superstructure, functioning as the top flange of both the crossbeams and main girders, resulting in a rigid and cost-efficient design [14].

The longitudinal stiffeners may have an an open profile (e.g. bulb shaped) or closed profile (e.g. trough), with the latter depicted in Figure 2.9. Open stiffeners offer advantages in fabrication, inspection, and maintenance, whereas closed troughs provide superior flexural and torsional rigidity while requiring fewer welds. However, trapezoidal-shaped closed ribs, commonly referred to as troughs, experience high local stresses and deformations due to their complex geometry, which can lead to fatigue cracking [1].

Cross-section bridge deck with orthotropic deck structure

View on underside of bridge deck

longitudinal girder /
trough profile

crossbeam

deck plate

main girder
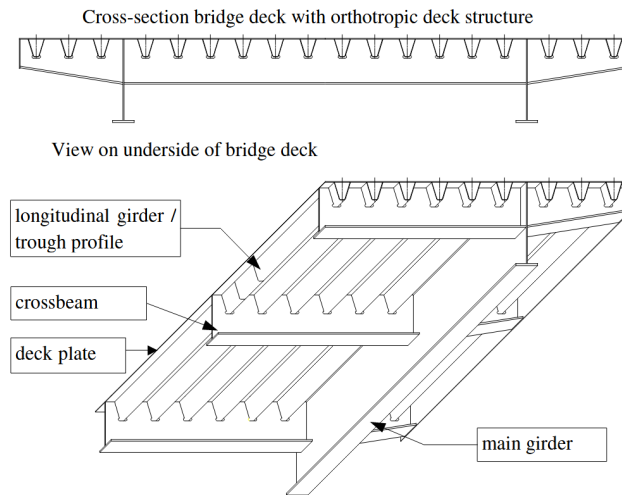
Figure 2.9: Structural composition of orthotropic steel deck [1]

2.2.2. History and application

The use of orthotropic steel decks began in the 1930s [14] as a means to reduce dead weight of bridges, benefiting from the low cost of steel and labour at the time [15]. However, their widespread adoption occurred in the 1960s, driven by advancements in cold-forming techniques that enabled the efficient production of trapezoidal and V-shaped stiffeners (troughs). These innovations allowed for longer spans of the longitudinal stiffeners, up to five metres, and significantly reduced fabrication costs. Another key development was the introduction of cut-outs in crossbeams, which allowed stiffeners to pass through. These cut-outs had standard geometry, but could be adjusted according to the size of the stiffeners. These developments standardised the assembly process and production of orthotropic steel decks [4]. Further supporting the increased use of OSDs was the introduction of high strength structural steel and advancements in welding techniques [15].

In the Netherlands, a significant portion of the national road network includes steel bridges with OSDs. De Jong [1] estimated that around 100 orthotropic steel decks exist on the highway network, with many more on secondary roads (*N-wegen*). Most of these decks feature trapezoidal stiffeners and deck plates typically 10 mm thick for fixed bridges and 12 mm thick for movable bridges. Historically, fatigue resistance was not a primary design consideration and deck plate thickness was determined mainly by static resistance.

Orthotropic steel decks are widely used in plate-girder, box-girder, cable-stayed, and truss bridges [1] due to their design flexibility and ease of integration with other structural elements. They are particularly advantageous in long-span bridges, where their weight advantage over concrete bridges is beneficial, and in movable bridges, where minimising dead weight is critical [15]. Beyond bridges, stiffened steel deck plates are also common in offshore structures and ship industry, where they similarly endure high fatigue loading under dynamic conditions [13].

2.2.3. Structural systems

The deck of a bridge experiences fluctuating vehicle loads of different amplitudes. The load path due to such loading is as follows. The wheel load is first distributed by the asphalt surface layer and then transferred to the deck plate. Next, the load continues its path to the longitudinal stiffeners, which are supported by the crossbeams. From there, the wheel loads are transferred to the main girders [11], after which the loads are carried to the substructure.

Local deck plate deformation

Panel deformation

Longitudinal deflection of stiffeners

Crossbeam in-plane flexural

Local behaviour of crossbeam

Distortion of stiffeners

Global displacement mechanism
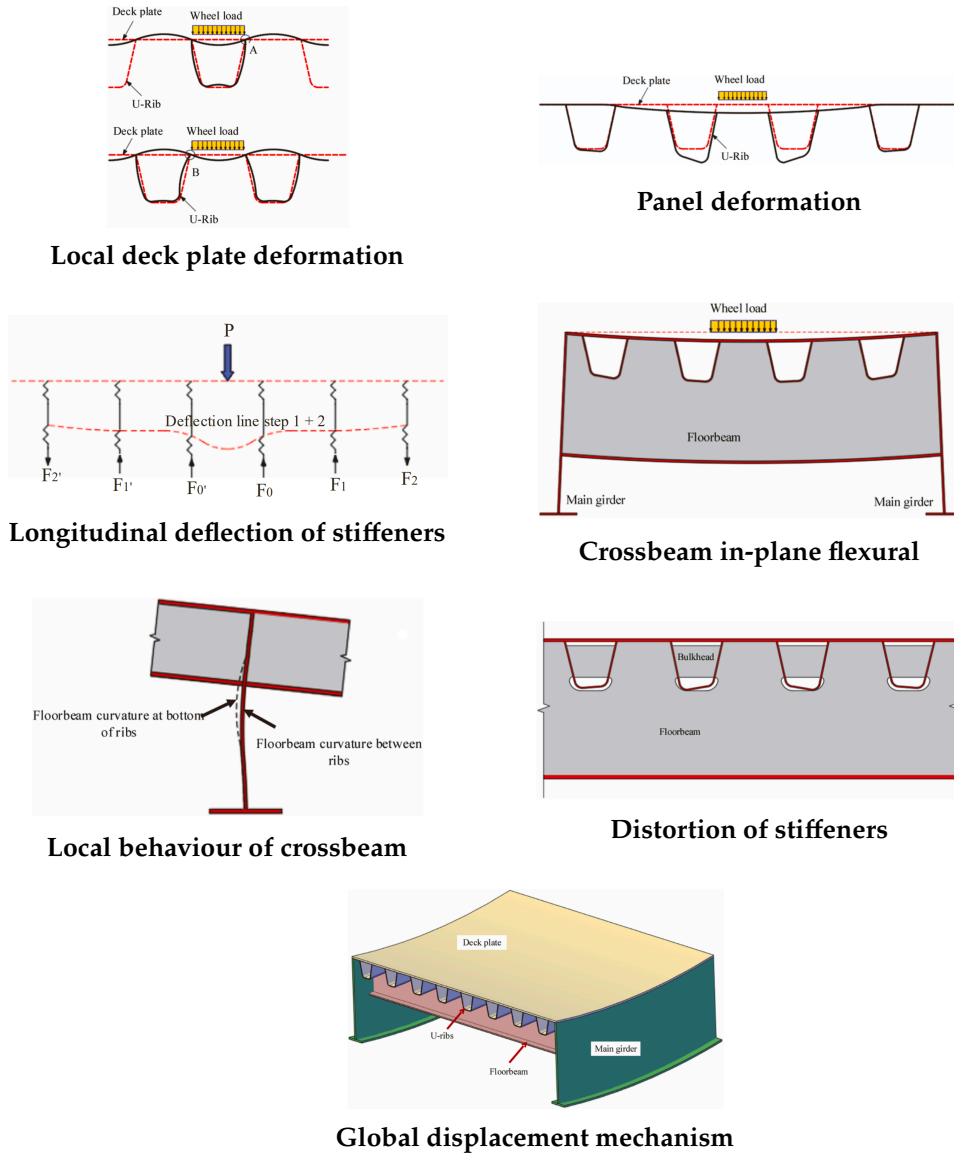
Figure 2.10: Deformation systems of an Orthotropic Steel Deck [11]

According to Connor et al. (2012) [14], during this load transfer different deformations occur on multiple levels of the structural system. These deformation levels, also called behavioural mechanisms, help explain which systems contribute to the stresses in the various parts of the orthotropic steel deck. Figure 4.2 illustrates these deformation mechanisms. Each mechanism is detailed below:

1. **Local deck plate deformation**
   During the transfer of the wheel loads from the deck plate to the trough walls, the deck plate deforms, primarily influenced by trough spacing and deck plate thickness. The resulting stresses are local and depend on the magnitude and distribution of wheel loads through the asphalt layer. Although this system does not cause strength-related concerns, it significantly affects the fatigue behaviour of trough-to-deck-plate joints.

2. **Panel deformation**
   This mechanism captures the transverse load distribution across the troughs. The deformation of the panel is quite complex due to its two-dimensional load distribution

behaviour when subjected to out-of-plane loading. It results from the differential displacement of the stiffeners.

3. **Longitudinal deflection of stiffeners**
   Individual stiffeners transfer loads in the longitudinal direction to the crossbeams and act as continuous beams supported by discrete, flexible supports (crossbeams).

4. **Crossbeam in-plane flexure**
   The crossbeams span between the main girders and are loaded with in-plane flexure. The stresses that occur in the crossbeams include in-plane (flexural and shear) and out-of-plane components (due to stiffener rotations).

5. **Local behaviour of crossbeam (distortion)**
   The in-plane distortion of the crossbeam web (due to horizontal shear and vertical displacement of the rib) and out-of-plane distortion stiffener web influence the local behaviour of the crossbeams. This affects the fatigue behaviour of the trough-to-crossbeam joints.

6. **Distortion of stiffeners**
   Out-of-plane distortion of the ribs occurs when the wheel load is positioned at mid-span of two crossbeams and offset from the stiffener axis. The cut-out at the crossbeam location also influences this deformation.

7. **Global displacement mechanism**
   This system describes the deformation of the main girders and the orthotropic panel system. It can be evaluated through structural analysis.

2.2.4. Vulnerability to fatigue

Fatigue cracking is a major concern in orthotropic steel decks due to the cyclic loading from traffic and the complex weld detailing of the deck. As a result, the design of OSDs is governed more by live load effects than by dead loads, making fatigue the primary limit state [14]. The fatigue resistance of these decks is strongly influenced by the quality of welds and the fabrication techniques used [14].

Earlier designs of orthotropic steel decks did not account for fatigue to the extent that is now standard in the design process. Fatigue-related issues have been documented since the early 1970s, with numerous bridges showing damage. One of the earliest research cases into fatigue was the Severn Bridge in the United Kingdom, for which experimental tests were performed in 1971, aimed to assess the effects of heavy traffic loads on fatigue performance. Many bridges constructed at the time used one-sided fillet welds for trough to deckplate joints, which resulted in high stress concentrations and significant fatigue cracking. The example mentioned in Section 1.1, the Van Brienenoord bascule bridge in Rotterdam, played a crucial role in advancing fatigue-related research in the Netherlands. Despite the use of advanced welding processes during construction, fatigue cracks appeared within just seven years of service. These cracks, located at the joint between the trough and deckplate above the crossbeam, were substantial, ranging from 100 mm to 700 mm in length, resulting in the need for replacement of the deck with a thicker plate [15].

Locations of fatigue cracking

Fatigue cracks can develop at various locations in the bridge deck, primarily originating at welds. Kolstein [4] identified the following fatigue-critical joints in an orthotropic steel deck:

- Trough to deckplate joint
- Trough to crossbeam joint

- Trough to deckplate to crossbeam joint
- Crossbeam to deckplate joint
- Longitudinal web (main girder web) to deckplate joint
- Butt joints in deckplate
- Trough splice joint

Abdelbaset and Zhu [11] argue that the trough to deckplate joint, trough to crossbeam joint and the deckplate- and stiffener splices are often the most critical locations for fatigue cracking. These three joint types are examined below, along with the trough to deckplate and crossbeam joint, which has been identified as highly vulnerable in the case study bridge deck analysed in this thesis (see Section 3.1).

(a) Trough to deckplate joint

(b) Trough to crossbeam joint
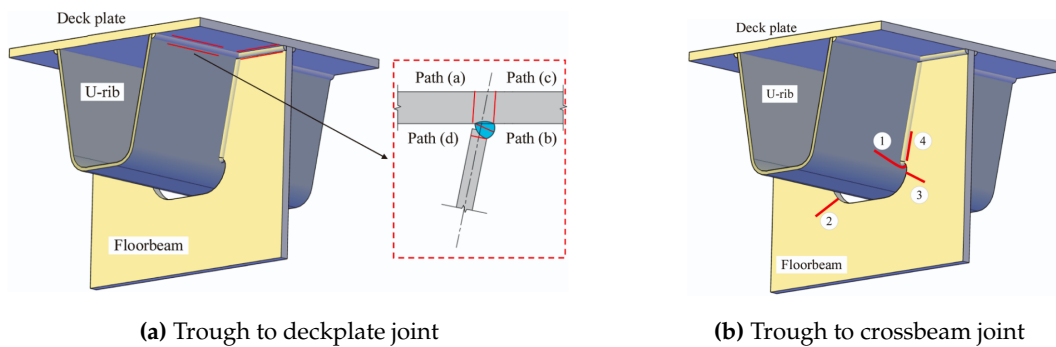
Figure 2.11: Fatigue-critical joints of an orthotropic steel deck [11]

Trough to deckplate joint

Fatigue cracks in this joint typically initiate at the weld root or toe and are found in the span between crossbeams. The crack propagates either through the deck plate (a & c), the weld throat (b) or web of the stiffener (d), as illustrated in Figure 2.11a. Cracks initiating at the weld root are considered the most critical, as they are often undetectable by visual inspection. For example, cracks that propagate through the weld (*path b in the Figure*) start at the weld root and extend through the weld towards the outer surface of the trough web, then continue longitudinally along the weld. This crack type generally does not pose immediate safety concerns, as load redistribution allows the deckplate to remain functional. However, if the crack deviates from the weld direction and extends into the deckplate or trough web, structural integrity can be compromised [11].

Trough to deckplate and crossbeam joint

In bridge decks with continuous longitudinal stiffeners, the intersection where the deckplate, stiffener and cross beam meet, directly above the crossbeam, is particularly susceptible to fatigue cracking. Localised wheel loads induce a hogging moment in the deckplate at this connection, resulting in high stress concentrations. Unlike the trough to deckplate joint, which is located between crossbeams, this joint experiences additional stresses from load transfer through the crossbeam itself. Cracks typically initiate inside the trough at the weld root, making early detection challenging. Over time, they propagate through the full thickness of the deckplate before extending longitudinally along the trough-to-deckplate weld [4]. This crack path is similar to *path a* depicted in Figure 2.11a, but with the initiation point at the intersection with the crossbeam.

Trough to crossbeam joint

The fatigue behaviour of the trough to crossbeam joint depends on whether the stiffener is continuous (extending through the crossbeams) or cut to fit between the crossbeams. Additional factors influencing fatigue performance include the stiffener cross-section and the presence and shape of cut-outs in the crossbeams. This joint is one of the most complex fatigue details in orthotropic steel decks due to the difficulty in controlling its fatigue sensitivity [11]. Figure 2.11b displays the possible crack paths for a bridge deck with continuous troughs and cope holes, showing cracks propagating in the crossbeam or stiffener web.

Deckplate- and stiffener splices

Splices can be executed by welding or bolting. While welded splices are more cost-effective, they offer lower fatigue resistance. A one-sided full penetration weld with a backing strip is usually applied. Fatigue cracks in stiffener splices generally originate at the weld root at the bottom of the stiffener or at the weld connecting the stiffener to the backing strip. In deckplate splices, cracks commonly initiate at the transverse groove weld or at the end of trough-to-deckplate longitudinal weld [11].

2.2.5. Fatigue design

This subsection outlines the approach to fatigue design for orthotropic steel decks. It covers the classification of fatigue-critical details as defined in the *Richtlijnen Ontwerp Kunstwerken* (ROK) for use with the hot spot stress method. Additionally, it presents fatigue load models according to the Eurocode and provides guidelines for applying finite element modelling in fatigue assessment.

Fatigue-critical details

The *ROK* provides an overview of the fatigue-critical details to be considered during fatigue assessment when using the hot spot stress method. Three types of decks are distinguished: decks with cut-out troughs, decks with pierced troughs without recess and decks with intermediate welded troughs [12]. In total, 27 critical details are defined across these three deck types, some of which are applicable to all three, while others specific to certain cases. This thesis focuses on a case study bridge deck with continuous troughs passing through cut-outs in the cross beams (the first deck type category). For this geometry, 20 fatigue-critical details must be considered. However, 2 details, 4a and 4b, are excluded from the assessment because these details are prescribing detailing for the design, with which they can be considered non-critical for fatigue assessment. As a result, 18 details are taken into account during assessment, which are provides in Tables 2.1 and 2.2. These tables provide the list of the fatigue-critical details, accompanied by visual illustrations.

For each critical detail, the *ROK* specifies one or more detail categories with corresponding reference fatigue strengths at 2 million cycles ($\Delta\sigma_c$). Additionally, it provides requirements regarding the execution of the joint, such as weld thicknesses. The *ROK* also explains how to extract stresses and extrapolate the hot spot stress for each detail. Furthermore, it offers guidance on finite element modelling choices, such as mesh sizes. explanations from the *ROK* for details 1c and 2b, which are considered in this thesis (as outlined in Section 3.1), can be found in Appendix C.
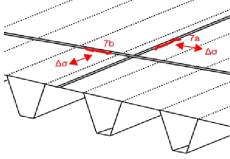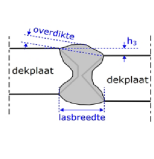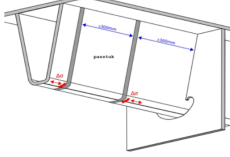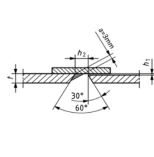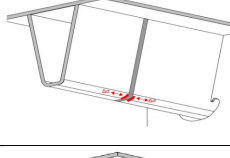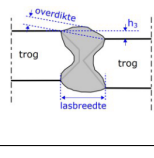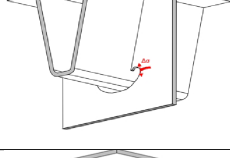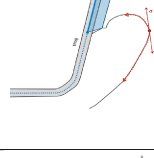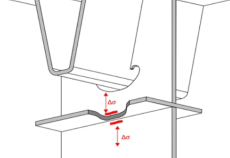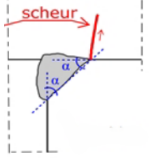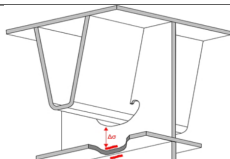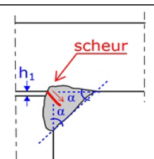
Fatigue Load Models

Fatigue in bridge structures is caused by the repeated stress fluctuations resulting from traffic loading. The characteristics of the stress spectrum, such as amplitude and frequency, are influenced by multiple factors, including vehicle dimensions, axle loads, vehicle spacing, and traffic composition.

Detail	Explanation	Location in OSD	Illustration
1a	Crack in deck plate starting from weld toe, growing outside of trough.		
1c	Crack in deck plate starting from weld root, growing inside of trough. Weld between trough and deckplate.		
2a	Crack in trough starting from weld toe.		
2b	Crack in trough-to-deckplate weld starting from weld root.		
3a	Crack in trough starting from weld toe, due to vertical stresses. Weld between trough and support plate.		
3b	Crack in trough starting from weld toe, due to horizontal stresses. Weld between trough and support plate.		
5	Crack in deck plate starting from weld toe. Weld between deck plate and support plate.		
6a	Crack in support plate starting from weld toe. Weld between deck plate and support plate.		
6b	Crack in weld starting from weld root. Weld between deck plate and support plate.		

Table 2.1: Critical details of OSD according to ROK (Part 1 of 2) [12]

Detail	Explanation	Location in OSD	Illustration
7a/7b	Crack in deckplate from weld toe of longitudinal/transverse weld between deckplate sections.		
8a	Crack in trough or trough fitting from weld toe between fitting and trough.		
8b	Crack in trough from weld toe at trough extension.		
9	Crack in support plate from edge of cope hole.		
10a/11a	Crack in support plate from weld toe with intermediate flange, crack above/below flange.		
10b/11b	Crack in support plate from weld root with intermediate flange, crack above/below flange.		

Table 2.2: Critical details of OSD according to ROK (Part 2 of 2) [12]

The Eurocode, NEN-EN 1993-1-9 [10], defines five fatigue load models. For a fatigue assessment, adopting a single appropriate model is sufficient. These load models serve different purposes. Load Models 1 and 2 are intended to verify whether an infinite fatigue life can be assumed, whereas Load Models 3 to 5 are designed for direct fatigue life estimation using fatigue strength curves (as explained in Section 2.1.2). Fatigue Load Model 3 uses a single vehicle, while Fatigue Load Model 4 is based on a set of equivalent heavy vehicles. *FLM4* is divided into two variants: *FLM4a* and *FLM4b*. *FLM4a* considers only stress ranges and is typically applied to steel structures, while *FLM4b* also takes into account maximum stress levels, making it more suitable for concrete structures. Fatigue Load Model 5, on the other hand, uses actual traffic measurements to estimate the fatigue life.

Among these options, *FLM4a* is the most commonly applied model for fatigue analysis of orthotropic steel decks. The *ROK* [12] also prescribes *FLM4a* as the default model for fatigue assessment of steel bridges, although *FLM5* may be used in specific cases, subject to approval by Rijkswaterstaat.
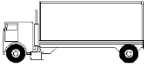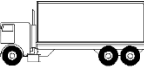
VEHICLE TYPE			TRAFFIC TYPE			
1	2	3	4	5	6	7
			Long distance	Medium distance	Local traffic	
LORRY	Axle spacing (m)	Equivalent axle loads (kN)	Lorry percentage	Lorry percentage	Lorry percentage	Wheel type
	4,5	70 130	20,0	40,0	80,0	A B
	4,20 1,30	70 120 120	5,0	10,0	5,0	A B B
	3,20 5,20 1,30 1,30	70 150 90 90 90	50,0	30,0	5,0	A B C C C
	3,40 6,00 1,80	70 140 90 90	15,0	15,0	5,0	A B B B
	4,80 3,60 4,40 1,30	70 130 90 80 80	10,0	5,0	5,0	A B C C C

Figure 2.12: Vehicle types from Fatigue Load Model 4 [16]
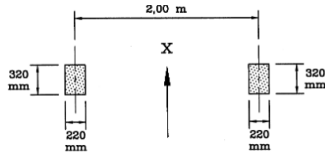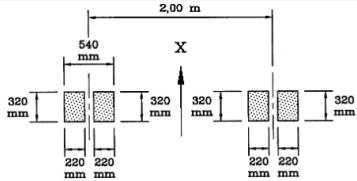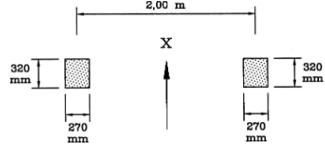
WHEEL/AXLE TYPE	GEOMETRICAL DEFINITION
A	
B	
C	

Figure 2.13: Wheel/axle types from Fatigue Load Model 4 [16]

FLM4 includes five standardised heavy vehicles representing typical motorway traffic in Europe, as given in Figure 2.12. The vehicles differ in wheel type, with the corresponding wheel geometries shown in Figure 2.13. It is important to note that the most recent version of the *ROK* specifies a wheel length of 220 mm instead of the 320 mm stated in the Eurocode. This adjustment is not applied in this thesis. Axle loads vary across the vehicle types, and three traffic categories are distinguished: long distance, medium distance, and local traffic. Each category has a specific distribution of vehicle types, with long distance traffic generally involving heavier vehicles and a higher total number of equivalent axle loads.

To account for transversal load placement, a range of load positions must be considered. This is crucial as there is variation in the driving path between vehicles. The centre of this load spread should be positioned at the most critical transverse position for each detail, which is identified individually. Figure 2.14 illustrates this load spread for detail 2a/2b. A maximum of three transverse load spreads should be evaluated per critical detail.
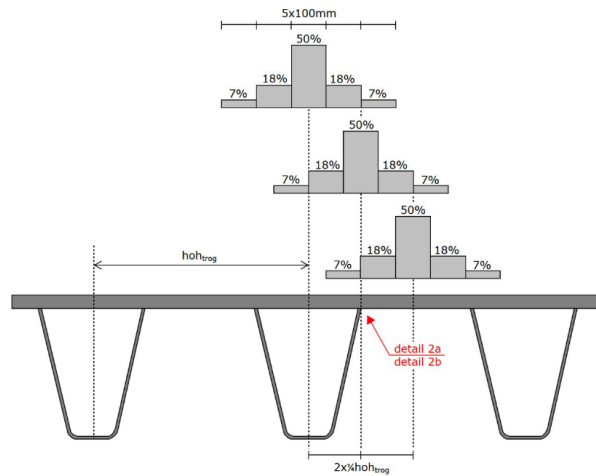
Figure 2.14: Transverse load distribution: example for position of weaves [12]

Use of Finite Element Modelling
Accurate estimation of the peak stresses at fatigue-critical details is crucial in fatigue assessment. In cases involving complex geometries, finite element modelling (FEM) is used for stress calculation. The hot spot stress (HSS) method, explained in Section 2.1.3, is often applied in combination with FEM, and its use has become increasingly widespread since the implementation of numerical modelling [13]. Design codes that outline the implementation of the HSS method, such as the *ROK*, also provide detailed recommendations on modelling choices. This is important, as FEM results are highly sensitive to mesh size, element type, and modelling assumptions, especially in zones near welds and geometric discontinuities, where high stress singularities occur [13].

Regarding element type, both solid and shell elements may be used. However, *ROK* specifies that, at minimum, the steel structure should be modelled using shell elements, while the asphalt and ZOAB layers, if present, should be modelled with solid elements. Alternatively, the steel structure can also be represented by solid elements, with the requirement of explicit weld modelling. Shell elements are often preferred due to lower computational costs. However, the use of shell elements involves simplifications which may reduce the accuracy of results if not handled carefully. When using shell elements, 8-node quadrilateral elements placed at the mid-plane of the steel plate are typically employed [13]. The *ROK* specifies a requirement of at least four integration points and prohibits three-node elements in zones used for stress

extraction. The element size is directly linked to the distance of the extrapolation points from the hot spot stress point [12].

The *ROK* also defines the extent of the finite element model and prescribes that modelling the full width of the bridge deck is required, while recommendations regarding the length differ per bridge type. For large span fixed bridges, a local sub-model can be employed with the length at least two times the longest heavy vehicle.

Aygul (2012) [13] discusses various approaches for modelling welds, such as locally increasing the plate thickness, or using oblique elements at weld zones. The *ROK* [12] specifies that elements should be thickened from the intersection point at the joint towards the weld toe. This has to be done symmetrically, even for single-sided welds. Guidelines on the increased thickness value are provided as well.

2.2.6. Strengthening methods

When significant fatigue damage is detected in an orthotropic steel deck, a mitigation strategy must be defined to ensure continued service of the structure. The available approaches include repair, strengthening, or a combination of both. In cases where the deck's fatigue resistance is regarded as insufficient for current or expected traffic demands, strengthening becomes necessary.

Prior to implementing strengthening measures, a thorough inspection must be performed, and fatigue cracks exceeding a critical size should be repaired. Cracks of limited size may be left unrepaired, provided that a fatigue assessment demonstrates that the desired remaining service life can still be achieved without repair of these cracks. Additionally, the ultimate load-bearing capacity of the deck in its cracked state must be sufficient [1].

In recent years, considerable research has been conducted regarding fatigue strengthening techniques for OSDs, resulting in the development of several promising methods. These methods can be applied across the entire bridge deck, targeted to specific traffic lanes, or for localised repairs, depending on the severity of fatigue damage, traffic intensity, and maintenance requirements. This subsection introduces several strengthening techniques.

Ultra-High Performance Concrete (UHPC) overlay

A widely adopted strengthening method for orthotropic steel decks is the application of an Ultra-High Performance Concrete (UHPC) overlay. This technique involves casting an UHPC layer over the entire bridge deck surface to improve stiffness, reduce stress concentrations, and extend fatigue life. Figure 2.15 illustrates the strengthening procedure.
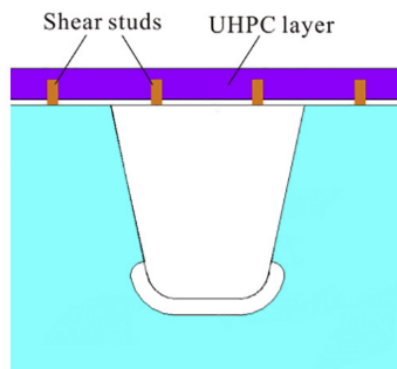
Figure 2.15: Ultra-High Performance Concrete overlay [17]

Studies have demonstrated significant stress reductions using UHPC overlays, reductions up to 70.9% observed at the trough to deckplate joint. However, effectiveness at other joins, such as the trough to crossbeam joint, is more limited. To address fatigue-critical details effectively, a significant overlay thickness of around 50 mm is typically required [18]. Despite its effectiveness, one of the main disadvantages is the considerable self-weight of the overlay, which imposes significant dead load to the structure. This additional weight may require further strengthening of other structural components as their load-bearing capacity may be exceeded.

This strengthening method has been applied for numerous bridges, with varying success. The performance is affected by different parameters: bond conditions between the steel deck and UHPC, surface preparation, long-term durability of the hybrid interaction [18]. The UHPC overlay can also be enhanced by adding prestressing tendons, resulting in a higher effectiveness of the strengthening due to induced compressive stresses in the steel deck. However, this addition does require more complex installation and achorage detailing [18].

Bonded steel plate
An alternative strengthening method involves bonding a steel plate directly onto the existing deck using a thin adhesive layer. This forms a composite system that improves fatigue performance by redistributing stresses. Experimental studies have shown a notable reduction in stresses. However, the bonded system's primary vulnerability lies in the vulnerability to shear failure of the adhesive layer [19]. Teixeira de Freitas et al. (2010) [19] also investigated a sandwich system that replaced the adhesive with a polyurethane core. This alternative is lighter but generally less effective in mitigating fatigue issues and is more sensitive to temperature variations. Results from the study demonstrated that the stresses of the trough to deckplate joint reduced by 55% with the bonded steel plate and by 45% with the sandwich system.

(a) Bonded steel plate system

(b) Sandwich system with polyurethane core
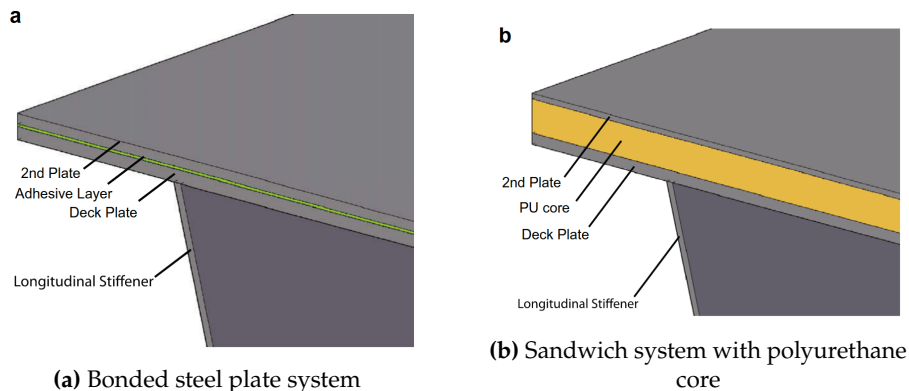
Figure 2.16: Bonded steel plate strengthening techniques [19]

Bonded steel plates of smaller size have also proven useful for repair of fatigue damage. Wang et al. (2023) [20] demonstrated that adhesively bonded steel patches could effectively prolong the fatigue life of orthotropic steel decks and reduce the growth of existing cracks.

Bolted steel plate
One method for strengthening orthotropic decks involves mechanically bolting a steel plate to the existing deck. This approach was explored for the fatigue renovation of the Second Van Brienenoord bridge deck, aiming to reduce installation time and minimise the additional weight on the structure compared to the UHPC overlay procedure. The design team, consisting of engineering firms Arup and Royal HaskoningDV, considered various configurations, using

either single or multiple steel plates, with or without an epoxy layer between the strengthening plate and the bridge deck. This solution could not be applied for the Second Van Brienenoord bridge due to the need for further investigation and testing to ensure its reliability and effectiveness [5]. After extensive testing with which the associated risks could be mitigated, the bolted steel plate solution was successfully implemented at the Suurhoff bridge. The solution involved a 30 mm steel plate attached to the deck plate by preloaded injection bolts, with an epoxy mid-layer between the plates. Figure 2.17 illustrates the components of the strengthening design. The long installation time needed for installing a UHPC overlay, approximately 33 weeks for a highway bridge [5], was reduced to just four weeks [6] with the bolted steel plate technique. The large thickness of the strengthening plate was chosen to be on the safe side [6].
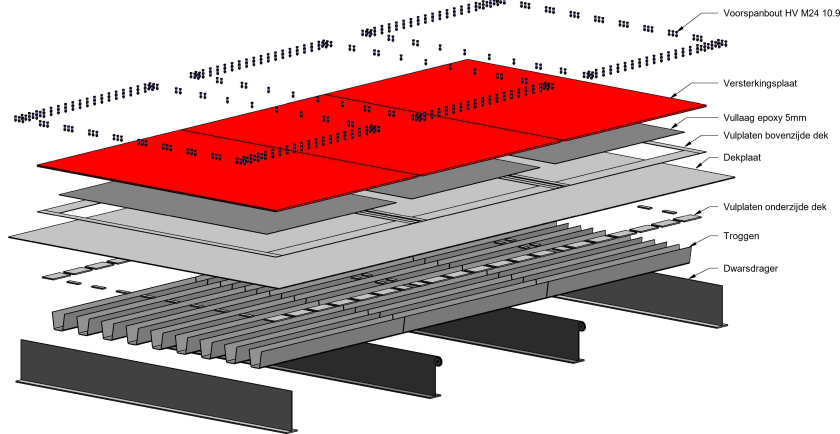
Figure 2.17: Strengthening solution with bolted steel plates for Suurhoff bridge [6]

Fibre-Reinforced Polymer

Fibre-Reinforced Polymer (FRP) plates offer a light-weight strengthening solution. These plates can be mechanically fastened or bonded to the bridge deck. However, concerns about long-term durability [18] remain a drawback. Studies have demonstrated that FRP angles can effectively reduce stresses at the trough to deckplate joint [11].

Emergency repair

In the event of sudden fatigue failure, emergency repair is necessary. In the past, the "gutsen-lassen" method (also known as the "oplasplaat" method in Dutch) was used. This repair procedure does not involve actual repair of the fatigue crack but instead involves placing a steel plate above the cracked location and welding it along its perimeter to the deck plate with fillet welds. A significant disadvantage of this method is that the welds have limited fatigue capacity. Over time, new cracks often develop in these welds, leading to detachment of the strengthening plate from the deck plate. This can result in damage to the asphalt layer, which poses safety concerns. Due to these issues, this emergency repair solution is no longer used in practice [5].

2.3. Blind bolts

This section presents a study of various blind bolt types to provide an overview of the options available on the market. The aim is to identify the most suitable type for the strengthening design proposed in this thesis. The comparison between blind bolt technologies and selection of a blind bolt for the design is performed in Section 3.3.

2.3.1. Introduction

Traditional bolts consist of a threaded shaft (body), head, nut and washer, as shown in Figure 2.18. The shaft prevents lateral movement of the connected structural elements, while the head and nut apply pressure to the top and bottom sides of these elements respectively, preventing vertical movement. Tightening the nut with a specified torque causes the bolt to elongate, generating a tensile force known as the preload force. This force is essential for clamping the surfaces of together [21]. There are different bolt variations available, depending on the application and needed properties. For structural applications, high-strength friction grip bolts are commonly used for their ability to achieve high pretension and provide slip-resistant connections. Injection bolts are particularly effective in structures subjected to fatigue loading, offering high stiffness and fatigue resistance [22].
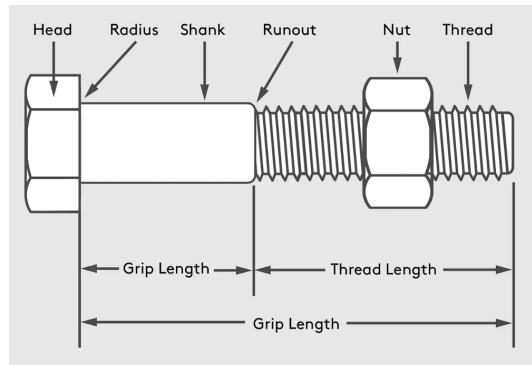
Figure 2.18: Components of traditional bolt [23]

For certain applications, it is not desirable, or even possible, to have access to both sides of the connection during installation. Blind bolts are designed for situations where one-side access to the connection is required. For bridge deck strengthening with bolted plates, installing the connection from the top of the deck can significantly reduce installation time.

The development of blind bolts has been largely driven by the need for a reliable connection solution for hollow structural sections (HSS). Prior to this, welding was the primary method used to connect HSS components. However, welding has several drawbacks, such as long installation times and sensitivity to fatigue, which led to the development of alternative methods [24]. Most literature of blind bolts focuses on HSS connections.

2.3.2. Blind bolt types

There is a wide range of blind bolts available on the market, with Ajax and Lindapter bolts especially highlighted as readily available on the market [25]. Table 2.3 provides an overview of the main types found in literature. Four specific types are selected for further analysis: Hollo-Bolt, Ajax, Slip-Critical Blind Bolt, and Elliptical One-sided Bolt.

Hollo-Bolt

One of the most well-known blind bolt types is the Hollo-Bolt, developed by Lindapter. This is an expansion bolt that replaces the nut with an expanded sleeve. The bolt does not need close tolerance holes [32], and can be installed with a short installation time using standard hand tools [26]. The Hollo-Bolt consists of several components: head, collar, High Clamping Force (HCF) mechanism, sleeve (with four legs), threaded cone, and shank, as illustrated in Figure 2.19a. Tightening the bolt causes the threaded cone to move up, causing the sleeve to expand and clamp against the connection [32]. The High Clamping Force mechanism is available in M16 and M20 bolts, increasing the clamping force threefold when included [33].

Blind bolt type	Description	Locking mechanism
Lindapter Hollo-Bolt	Developed for steel-to-steel connections, specifically hollow sections [26].	Expansive sleeve
Extended Hollo Bolt	Has an extended shank which can anchor and thus provide higher stiffness. Useful for connections with concrete sections [25].	Expansive sleeve
Ajax	Multiple versions developed by Ajax Fasteners, including the Ajax ONESIDE. Aims to develop a high-strength steel connection [25].	Collapsing mechanism
Slip-Critical Blind Bolt (SCBB)	Capable of achieving the same pretension as conventional high-strength bolts [27].	Frictional interlock
Elliptical One-sided Bolt (EOB)	An innovative type of blind bolt with an elliptical head that bears against an elliptical hole [28].	Elliptical head
SHBS-PRO	The Self-tightening High-Strength Single-Side Bolt is developed for connecting closed steel sections [29].	Deformation sleeve that forms an anchor end
Flowdrill	Developed in the 90s using a thermal drilling technique to form a connection for tubular columns [30].	Thick collar created around the drilled hole for larger bearing surface
DHABB	The Double-Headed Anchored Blind Bolt is developed for concrete-filled steel tubes [31].	Anchored head

Table 2.3: Overview table of the considered blind bolt types

There are three variations of Lindapter Hollo-Bolt heads on the market: hexagonal, countersunk and flush fit, as shown in Figure 2.19b, differing in the amount of protrusion above the connection from standard to minimal to zero respectively. The Hollo-Bolt brochure mentions that there is also the possibility of developing a Hollo-Bolt with a customised head [26].

Performance
Studies by Elghazouli et al. (2009) [34] have examined the monotonic and cyclic behaviour of Hollo-Bolt connections, demonstrating that these bolts provide significant ductility and hardening. The capacity of the Hollo-Bolt is controlled by the sleeve rather than the shank, as the failure of the sleeve is found to be the main failure mode during shear testing [35]. Furthermore, Gao et al. (2022) [27] observed that the shear performance of the Hollo-Bolt is superior to that of standard bolts, with the sleeve contributing most of the strength. Regarding fatigue loading in shear, J. Wang et al. (2020) [36] found that Hollo-Bolts made from stainless steel exhibit higher fatigue resistance compared to standard bolts. However, when subjected to tensile fatigue loading, Hollo-Bolts show lower S-N curves than standard bolts if the difference between minimum and maximum loading is significant [37].

Preload
Under typical installation conditions, Hollo-Bolts may exhibit early separation under tensile loading when preloaded solely with the standard installation torque [35]. This issue can lead to insufficient slip resistance, and the bolts may loosen rapidly [27]. However, Wang et al. (2018) [39] reported that applying over-torque during installation can enhance the pretension.

(a) Components [38]

(b) Variations of bolt head [26]
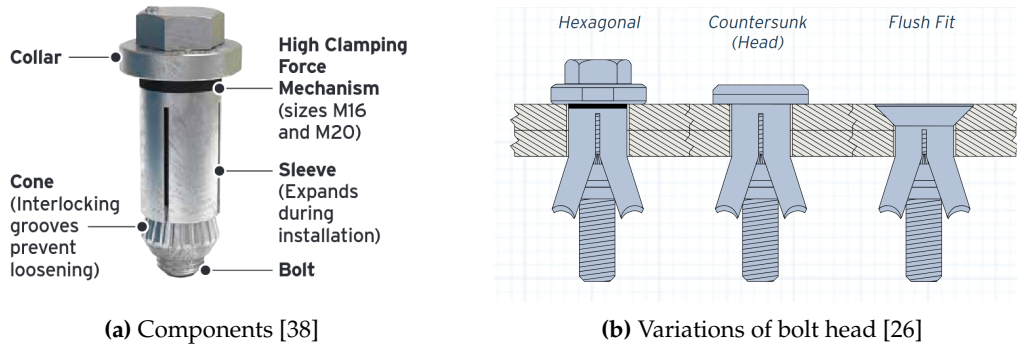
Figure 2.19: Visualisation of Hollo-Bolt

Their experimental study demonstrated that pretension values vary considerably with bolt diameter and the applied torque. The findings for Grade 8.8 bolts of diameters 12, 16 and 20 mm are summarised in Table 2.4. Standard installation torque values used were 80 Nm for M12, 190 Nm for M16, and 300 Nm for M20 bolts. M12 bolts reached pretension levels between 9-21 % of those for standard slip-resistant bolts, while M16 bolts achieved up to 60%. M20 bolts exhibited the highest performance, with pretension values up to 83% of a standard bolt when torqued to 400 Nm.

These results indicate that although Hollo-Bolts may not reach the same pretension levels as standard preloaded bolts, their performance under increased torque conditions can be significantly improved. However, the data also revealed that excessive torque may sometimes result in lower pretension. For instance, one M16 bolt subjected to double the recommended torque developed less pretension than under standard conditions. This is attributed to the malfunction of the High Clamping Force mechanism. It should be noted that these results were based on Hollo-Bolts with hexagonal heads and no available literature was found on pretension of Hollo-Bolts with other head types, such as countersunk.

Bolt size	Torque [Nm]	Pretension [kN]
M12	80	3.67
M12	80	10.05
M12	200	4.08
M12	To ultimate	12.96
M16	190	5.25
M16	190	7.55
M16	380	2.60
M16	To ultimate	64.81
M20	300	22.97
M20	300	71.58
M20	400	114.40
M20	To ultimate	84.59

Table 2.4: Hollo-Bolt torque and pretension experimental data [39]

Jiang et al. (2021) [40] studied the performance of altered versions of the Hollo-Bolt, referred to as NSHSBB and SSHSBB. The bolts offer significantly improved preload capabilities compared to standard Hollo-Bolts. For example, the NSHSBB and SSHSBB bolts achieve preload values as high as 100 kN for M16 bolts at 500 Nm torque. These improvements are attributed to changes in the bolt's geometry, including modifications to the sleeve and internal components, enhancing the clamping force.

Ajax bolt

Ajax connectors consist of a bolt, collapsible washer, flat washer, and a nut [41]. One variation of the system, the Nexgen2, is shown in Figure 2.20a. The installation mechanism of the Ajax bolt relies on a collapsible washer that is folded prior to insertion into the bolt hole and unfolds after placement using a specialised tool. This washer bears against the connection from the in-accessible side, while the nut is positioned and tightened on the accessible side of the connection [28]. A larger oversize hole is required compared to standard bolts to allow insertion of the collapsible washer [42], which may lead to local deformation and increased risk of pull-out failure.

Performance

The increased bolt hole clearance can result in a slip plateau under shear loading conditions [43]. When used as shear connectors between FRP panels and steel sections, Ajax bolts exhibit higher shear and tensile resistance under static loading compared to Hollo-Bolts. However, they tend to fail prematurely under cyclic loading due to early failure of the collapsible washer [44]. The Nexgen2 version was developed to improve shear resistance [45]. Hosseini et al (2020) [43] emphasise that preload plays a significant role in the fatigue behaviour of Ajax bolts.

Preload

The upgraded Nexgen2 bolt is capable of developing a high level of pretension. For instance, M20 Nexgen2 bolts can achieve a pretension force of approximately 142 kN [45].

(a) Ajax Bolt: Nexgen2 [45]   (b) Components of the SCBB [27]   (c) Components of EOB [28]
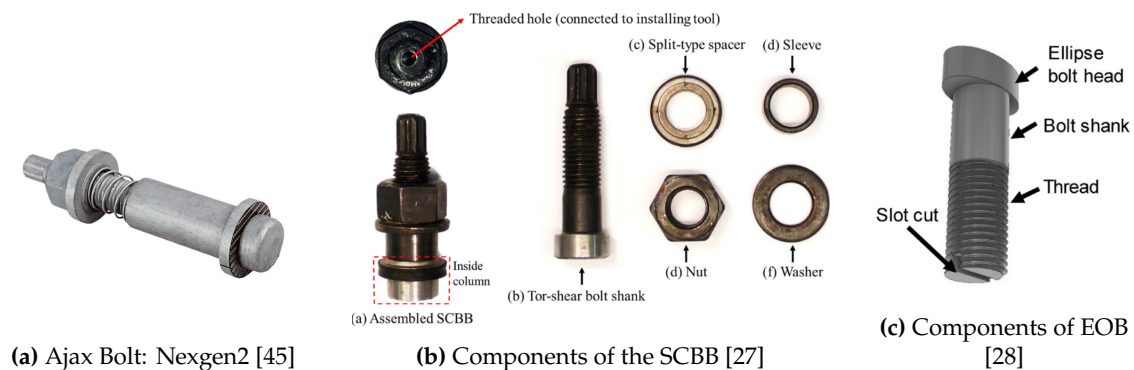
Figure 2.20: Overview of different blind bolt types and their components.

Slip-Critical Blind Bolt (SCBB)

The Slip-Critical Blind Bolt was developed because most blind bolt types cannot achieve a slip-critical connection. The SCBB achieves its slip-critical behaviour due to the high pretension force that can be developed in the bolt, thanks to its split-type washer. In addition to the washer, the bolt assembly consists of a tor-shear high strength bolt, washer, nut, and sleeve, as illustrated in Figure 2.20b. The sleeve is used to fill the oversized hole, improving shear capacity. Similarly to the Ajax bolt, the SCBB is installed with the nut on the accessible side of the connection. A specialised tool is required to facilitate installation [35].

Performance

Research by Wang et al. (2017) [35] concludes that the anti-slip capacity of the SCBB is sufficient for typical applications. Additionally, both the tensile and shear strength of the SCBB were found to be higher than nominal strength values [27]. Under cyclic loading, the SCBB also demonstrated satisfactory performance [35].

Preload

Tests were performed to verify the pre-tensioning force values, and the results were found to be satisfactory according to the Chinese code [35], finding values of the preload approximately 90% of a standard preloaded bolt. For instance, M24 SCBB bolts could achieve a pretension of approximately 240 kN.

Elliptical One-sided Bolt (EOB)

According to Wan et al. (2020) [28], the majority of the blind bolts on the market are inconvenient for installation and often require specialised equipment. To address these issues, a novel one-sided bolt design is proposed, resulting in a cost efficient and easy-to-install technique. The bolt consists of an elliptical bolt head, shank, and nut, as shown in Figure 2.20c. The elliptical bolt head is inserted through an elliptical bolt hole, after which the bolt is turned 90 degrees to allow for bearing against the interior plate side. From the accessible side to the connection, the nut is tightened. A slot cut at the tail of the bolt shank ensures that the bolt remains properly oriented during installation.

Static (shear) performance

The slippage of the EOB is excessive compared to a standard bolt, due to the significant bolt hole oversize on two sides of the bolt, and the slip distance is found to be three times large compared to a standard bolt [28]. Yang et al. (2024) [46] propose using a plug-in gasket to address this slippage issue and increase the initial joint stiffness. This additional component also helps to reduce stress concentrations and eliminate premature failure of the bolt hole. With the addition of a plug-in gasket, the shear performance of the EOB was significantly improved.

Preload

Yi et al. (2024) [47] investigated the pretension of EOBs and found that a pretension of 67.2 kN could be achieved for the M16 bolt and of 96 kN for the M20 bolt. The study suggests that higher preload values might be achievable. However, they were unable to explore this further due to limitations in the measurement equipment. Additionally, the study observed that after a prolonged time period of 128 days, the stable pretension remained 93% of the initial value.

3

Strengthening Design

This chapter introduces the case study and presents the concept of the strengthening design. The use of steel plates for the strengthening of orthotropic steel decks has shown several advantages over the commonly used UHPC overlay, such as reduced weight and shorter installation time. This thesis explores the potential of steel plate strengthening by developing a strengthening design for a case study bridge deck: the orthotropic steel deck of the Second Van Brienenoord bridge. Due to Arup's involvement in the bridge's assessment, extensive knowledge on the fatigue assessment of the deck is available, making it a suitable case for this study. While orthotropic steel decks vary in geometry and fatigue damage, the findings from this case study may offer valuable insights into the feasibility of strengthening similar bridge decks experiencing comparable fatigue issues.

The chapter begins with the introduction of the case study, followed by the explanation of the strengthening design concept developed for the bridge deck. Next, the selection process for the blind bolt technology used in the design is described. Furthermore, the design parameters studied in the thesis are introduced, outlining the strengthening schemes variations considered. Finally, the methodology for evaluating the performance of the different strengthening schemes is presented.

Figure 3.1: Van Brienenoord bridges: Second Van Brienenoord bridge on the left (western arch) [48]

3.1. Case study: Second van Brienenoord bridge deck

The section begins with general information about the bridge, followed by a summary of the geometrical and material properties of the bridge deck. Finally, the fatigue assessment of the deck is discussed, identifying two fatigue-critical details that will be the focus of this thesis.

3.1.1. General information

The Van Brienenoord bridge spans 1.3 km over the Nieuwe Maas river in Rotterdam. It consists of two separate arch bridges, each connected to a bascule bridge. The bridge is a critical link in the A16 highway, one of the busiest highways in the Netherlands. The First van Brienenoord bridge was constructed in 1965, but 20 years later it was no longer sufficient to handle the growing traffic. The construction of the Second Van Brienenoord bridge, located adjacent to the first bridge, was completed in 1990. The bridge consists of three lanes in both traffic directions [49], totalling six traffic lanes. Figure 3.1 shows the two bridges, with the Second Van Brienenoord bridge on the left.

Strengthening of bridge deck

After approximately 20 years of service, Rijkswaterstaat appointed engineering firms Arup and Royal HaskoningDHV to conduct a local fatigue assessment Second Van Brienenoord bridge deck. The goal was to evaluate the fatigue performance of the orthotropic steel deck and explore possible repair and strengthening options [50]. The assessment indicated the need for strengthening, and several strengthening strategies were developed. As an alternative to the heavy UHPC overlay, the concept of using bolted steel plates was proposed [5], as explained in Section 2.2.6. However, the risks associated with this novel method could not be sufficiently mitigated without further experimental studies [5], and it was ultimately decided to implement the UHPC overlay method.
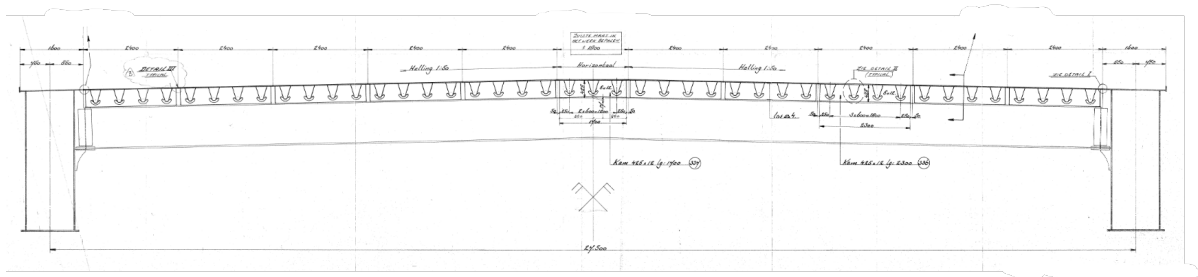
Figure 3.2: Cross-section Second Van Brienenoord bridge deck [51]

3.1.2. Properties of the bridge deck

Geometrical properties

The Second Van Brienenoord bridge is a plate girder bridge with an orthotropic steel deck. The longitudinal stiffeners are shaped as trapezoidal troughs, continuous over their length, passing through the cross beams. The cross section of the bridge deck is shown in Figure 3.2. Appendix A provides the complete overview of technical drawings of the bridge deck. A description follows of the various components of the bridge deck.

Cross beams

The cross beams are welded I-profiles, as shown in Figure 3.3a. They are connected to the longitudinal stiffeners and deck plate via support plates with a height of 425 mm, placed on top of the cross beams [51]. The cross beams are spaced 3.645 m apart, except at the bearings, where a spacing of 3.342 m is implemented [50].

(a) Cross-section of cross beam with support plate

(b) Cross section of trough at joint with cross beam [51]

Figure 3.3: Geometry of cross beam and longitudinal stiffener in mm

Orthotropic deck

The deck consists of a 12 mm thick deck plate, longitudinally stiffened by 6 mm thick troughs. The troughs are continuous and pass through cut-out openings in the support plates. The cut-outs follow the shape of the stiffeners, but also provide additional free space underneath for accessing crossing welds, referred to as a "cope hole" [50]. The geometry of the stiffener, support plate, and cope hole is illustrated in Figure 3.3b.

Material properties
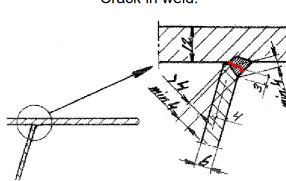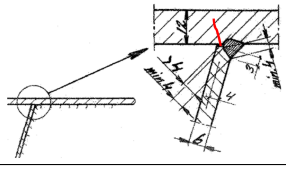
The components of the orthotropic deck and the cross beams are made of steel grade Fe 510, equivalent to S355 steel. The weld material is assumed to have the same strength as the parent material [52]. The Young's Modules is assumed to be 210.000 MPa, a common value for steel.

3.1.3. Fatigue details of the bridge deck

As discussed in Section 3.1.1, an extensive fatigue assessment was conducted for the Second Van Brienenoord bridge deck by Arup. The critical weld details for fatigue assessment were identified, and damage at these details estimated over different time periods. Two critical details were highlighted in the assessment due to their high predicted damage values [52]. These details, illustrated in Table 3.1, are referred to as detail 2b and detail 1c, as classified in the *ROK* (see Section 2.2.5).

The hot spot stress extraction procedure will be carried out according to the *ROK*, instead of following the extrapolation procedure used in the Second Van Brienenoord strengthening report. The latter employed different extrapolation points, deviating from those prescribed in the *ROK* [5]. A complete description of the critical details as specified by the ROK can be found in Appendix C.

Detail 2b

Detail 2b is located in the trough to deckplate joint, with a crack forming in the longitudinal weld connecting the two components, starting from the weld root. The predicted damage at this detail was found to be 33.8 over a period of 30 years.

Detail 1c

Detail 1c is located at the joint between the deckplate, support plate and trough, with a crack forming in the deck plate starting from the weld root. The predicted damage was found to be 23.3 over a period of 30 years.

Detail	Weld	HSS Extraction (ROK)	Predicted Damage 1990–2019
2b	Trough to deck plate weld: Crack in weld.	Stresses extracted at 20 mm and 40 mm from the weld root	33.8
1c	Intersection of deck, support plate and trough: Crack in deck plate.	Stresses extracted at 0.5 and 1.5 times the deck plate thickness from the weld root	23.3

Table 3.1: Selected critical details and predicted damages [5, 52, 12]

3.2. Design Concept

This section describes the concept developed for the strengthening of the case study bridge deck. The design focuses on strengthening of the slow lane using a blind-bolted steel plate, with the primary objective of improving the fatigue performance of the two fatigue-critical details identified earlier. The section begins by presenting the design objectives. Next, the scope of the strengthening is defined, followed by a description of the components that make up the design. Finally, the anticipated influence of the strengthening on the structural behaviour of the orthotropic steel deck is discussed.

3.2.1. Design objectives

The primary objective of the strengthening design is to reduce hot spot stresses in the bridge deck, thereby extending its fatigue life. This is the key focus, as minimising stress concentrations at critical details directly enhances the durability of the structure. In addition to this, the design also aims to:

- Minimise installation time, ensuring that strengthening can be implemented efficiently with minimal disruption

- Limit additional weight, preventing excessive load increase on the existing structure while still achieving effective strengthening

- Develop a partial strengthening solution, allowing for targeted strengthening of regions with critical fatigue damage

3.2.2. Scope of strengthening

A strengthening design is developed for the Second Van Brienenoord bridge deck, as introduced in Section 3.1. The fatigue-critical details targeted in this study are *detail 2b*, located in the trough to deckplate joint, and *detail 1c*, located in the joint between the deckplate, stiffener and

support plate. While these details occur throughout the bridge deck, the most severe fatigue damage has been identified in the slow lane, which carries the heaviest traffic, making it the primary target for strengthening.

Bridge decks can be strengthened either over their entire area or in selected regions. In line with the stated design objectives of minimising the weight of the strengthening solution and targeting regions with the most severe fatigue damage, the scope is limited to this single lane. The selected critical details (*1c* and *2*) are located at the cross beam and between adjacent cross beams, respectively. The design is therefore tailored to improve these two details only and does not consider other potential fatigue-prone locations.

Depending on the outcome of the research, specifically the effectiveness of the design in reducing hot spot stresses extending fatigue life, the proposed solution may be suitable for strengthening heavy traffic lanes or as an emergency repair measure. The application of this concept to full deck strengthening is beyond the scope of this study.
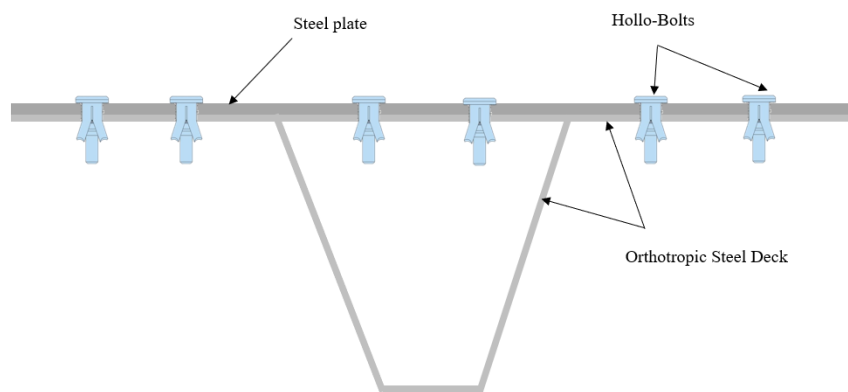
Figure 3.4: Visualisation of strengthening design components: blind bolts and thin steel plate

3.2.3. Design components
The concept of the strengthening design consists of a strengthening plate and blind bolts, as shown in Figure 3.4.

Strengthening plate
The design concept, developed to meet the aforementioned scope and objectives, utilises a thin steel plate to enhance fatigue capacity of the critical details of the case study bridge deck. Unlike the strengthening design used for the Suurhoff bridge, which incorporates bolted steel plates with an epoxy mid-layer, this design avoids epoxy by using a thin plate. It is assumed that the thin plate will be flexible enough to follow the deformation of the deckplate with greater ease. Furthermore, surface imperfections of both the deck plate and strengthening plate are disregarded, with the assumption that both plates are perfectly straight. In reality, gaps could form between the two plates, which may negatively affect the preloading of the bolts. However, this potential complication is not considered in this thesis.

Material properties
The strengthening plate is assumed to be made of the same steel grade as the orthotropic deck, S355, with an elastic modulus of 210.000 MPa, the same of the deck material.

Blind bolts

Blind bolts are used as connectors between the strengthening plate and bridge deck plate. While there have been limited applications of blind bolts for strengthening of bridges so far, the benefits of blind bolts, such as enabling one-sided access during installation, make them an attractive choice for this design. Additionally, blind bolts offer increased design flexibility, as they can be installed above closed stiffeners as well, potentially increasing the hybrid interaction between the strengthening plate and the orthotropic deck.

The blind bolts will act as shear connectors, fastening the strengthening plate on top of the existing deck plate. They need to have sufficient preload capacity to ensure proper hybrid interaction between the plates and to eliminate the possibility of slip, providing significant slip resistance.

3.2.4. Expected influence on structural behaviour

The addition of the strengthening is expected to influence several deformation mechanisms of the orthotropic steel deck (see Section 2.2.3). By increasing local stiffness in the strengthened lane, both local deck plate bending and panel deformations are reduced. Local deck plate deformation is most impacted by the strengthening, as the increased effective thickness reduces bending under wheel loads. This especially influences *detail 2b*, which is highly sensitive to local deck plate bending.

In contrast, *detail 1c*, located at the crossbeam, is also influenced by global deformation mechanisms. Although these mechanisms are less affected by the strengthening, the longitudinal deflection of the troughs is expected to decrease slightly due to the stiffer deck response. This change in deflection may result in altered load transfer to the crossbeams, which act as supports for the longitudinal stiffeners. The asymmetry introduced by strengthening only one lane could lead to local stiffness gradients at the interface between strengthened and unstrengthened regions. These gradients might introduce new stress concentrations or distortions. Such effects are not explicitly modelled in this study.

3.3. Choice of blind bolt type

This section explains the selection process of the blind bolt type used in this strengthening design. Various blind bolt technologies, with differing bearing mechanisms and mechanical properties, were reviewed in Section 2.3. Some of these bolts are already available on the market, while others are still in the development stage. The choice of the most appropriate bolt type for the strengthening design was made based on a set of selection criteria, summarised in Table 3.2. The four blind bolt types explained in detail in Section 2.3.2 are evaluated: the Hollo-Bolt, Ajax Bolt, Slip-Critical Blind Bolt (SCBB) and Elliptical One-sided Bolt (EOB). Each bolt was graded based on its ability to meet these criteria, with a tick (✓) indicating full compliance, a tilde (~) for partial compliance, and a blank for not meeting the criterion.

The literature review indicates that both the Ajax Bolt and SCBB can achieve at least 80% of the preload of a standard slip-resistant bolt. In contrast, the potential for effectively preloading the Hollo-Bolt and EOB remians uncertain, although they might be used with a lower preload compared to standard bolts. Most bolt types can be installed quickly, with the exception of the EOB, which requires elliptical bolt holes. Additionally, the high shear capacity of the EOB depends on the use of a plug-in gasket.

The SCBB is designed to provide significant slip resistance and high shear capacity, while the Ajax Bolt (*Nexgen2* prototype) also performs well in shear. The Hollo-Bolt generally has lower shear strength due to sleeve deformation but has been reported to offer higher shear

Criterion	Description	Hollo-Bolt	Ajax Bolt	SCBB	EOB
Preload	The preload of the bolt must be sufficient to achieve hybrid interaction between the strengthening and existing deck plate.	~	✓	✓	~
Availability on market	The blind bolt type must be accessible and developed by a manufacturer.	✓	✓		
Ease of assembly	The installation time of the bolt should be relatively short, and minimal specialised equipment should be needed.	✓	~	✓	
Shear performance	As the bolt acts as a shear connector, its shear capacity must be sufficient for both static and cyclic loading.	~	✓	✓	✓
Visible protrusion of bolt	A bolt with limited protrusion above the bridge deck is preferred. For fixed bridges, large protrusions create stress concentrations in the asphalt. For movable bridges, a thin wearing surface requires countersunk bolt heads.	✓			

Table 3.2: Merged table of selection criteria and evaluation of blind bolts

resistance in specific conditions. Moreover, the Hollo-Bolt can be installed with countersunk heads, reducing the bolt's protrusion above the strengthening plate. In contrast, the other three bolts require the nut to be placed on top of the connection, leading to a larger protrusion above the plate surface due to the nut's size.

Considering these factors, the Hollo-Bolt emerges as the most suitable option for the strengthening in this thesis. It is readily available on the market, can be assembled with ease and speed, and can be executed with limited protrusion of bolt. However, the choice of the preload property has to be taken with care, as is explained in the following subsection.

3.3.1. Bolt properties
The assumed properties of the Hollo-Bolt are provided here. More detailed information on installation procedures, for example the installation torque, and bolt geometry, for both hexagonal and countersunk heads, is provided in Appendix B. The safe working loads in tension and shear are also included in the Appendix. The bolts are assumed to have a strength grade of 10.9.

Preload and slip capacity
It is crucial that the connectors are slip-critical, as any slip would reduce the effectiveness of the hybrid interaction in the strengthening system. The bolts are designed following the guidelines for preloaded bolts from *NEN8703* [53], assuming a maximum slip deformation of 0.125 mm (see Figure B.4). The preload capacity and corresponding slip resistance are calculated according to *NEN-EN 1993-1-8*, assuming category C holds, which requires a slip-resistant connection in both serviceability and ultimate limit state [54].

Literature shows that the Hollo-Bolt can be preloaded with forces 3-83% lower than those of standard slip-resistant bolt. Therefore, it is not realistic to assume standard preload values. A reduction of the preload of 50 % is selected as acceptable. Table 3.3 gives an overview of the

standard preload values and the reduced preloads assumed for the Hollo-Bolt. The table also includes the resulting slip resistances for the Hollo-Bolt. A friction coefficient of 0.4 is used, based on surface treatment category B from *NEN-EN 1090-2* [55], assuming that the plates surfaces are hot-dip galvanised and painted with a zinc silicate.

Bolt size	Preload of standard bolt [kN]	Preload of blind bolt [kN]	Slip Resistance of blind bolt [kN]
M8	25.6	12.8	4.7
M10	40.6	20.3	7.4
M12	59.0	29.5	10.7
M16	109.7	54.8	19.9
M20	171.4	85.7	31.2

Table 3.3: Preload and slip resistance values, for Grade 10.9 [54]

Minimum spacings in bolt configuration

When multiple bolts are used in a configuration, their performance may be affected if placed too close to each other. To ensure proper load transfer and prevent interaction effects, the minimum spacings specified in Eurocode EN 1993-1-8 are applied (Table 3.5a). For fatigue-sensitive structures, additional spacing requirements are given in *EN 1993-1-9*, but these are less strict and therefore not governing (see Table B.1). The relevant spacing symbols are illustrated in Figure 3.5b. Installation guidelines provided by the manufacturer (see Appendix B.3) prescribe less strict spacing rules. To remain on the safe side, the Eurocode values are adopted as normative for the design.

Symbol	Min. spacing	M8	M10	M12	M16	M20
e_1	$\geq 1.2d_0$	16.8	21.6	24	31.2	39.6
e_2	$\geq 1.2d_0$	16.8	21.6	24	31.2	39.6
p_1	$\geq 2.2d_0$	30.8	39.6	44	57.2	72.6
p_2	$\geq 2.4d_0$	33.8	43.2	48	62.4	79.2

(a) Minimum spacings according to Eurocode, in mm [10]
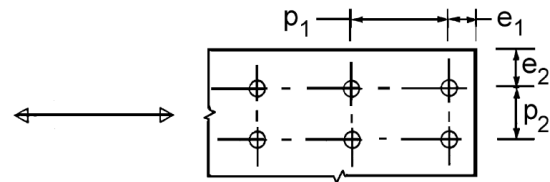
(b) Symbols for bolt spacings [56]

Figure 3.5: Minimum bolt spacings and their corresponding definitions

3.4. Design parameters

Since the two selected critical details differ in geometry and stress behaviour, separate strengthening designs are developed for each. Initially, each strengthening design is optimised individually per detail, after which they are combined into a single strengthening design. Despite the differences in detail behaviour, the general setup of the strengthening designs is similar, and the following explanation applies to both. Any minor differences between the two are pointed out along the way.

The key parameters varied in the strengthening design are:

- Bolt size,
- Strengthening plate thickness,
- Bolt configuration.

The bolt configuration is further defined with several sub-parameters that describe the arrangement of bolts in both the longitudinal and transverse directions relative to the troughs. In the longitudinal direction, two parameters are defined: *bolt row spacing* and *amount of bolt rows*. In the transverse direction, the amount of bolts inside and between troughs is varied, referred to as *amount of bolts per trough* and *amount of bolts between troughs*, respectively. Table 3.4 summarises the values considered for each design parameter, and Figure 3.6 provides a visual representation of these parameters.
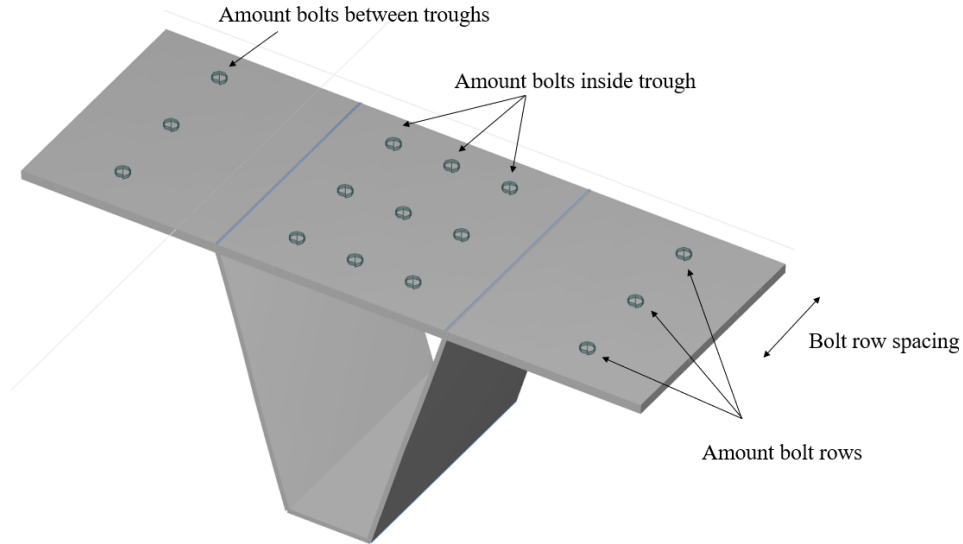
Figure 3.6: Visualisation of bolt configuration parameters

Plate thickness [mm]	Bolt size	Amount bolts inside trough	Amount bolts between troughs	Amount bolt rows	Bolt row spacing [mm]
8	M8	0	0	1	50
10	M10	1	1	2	100
12	M12	2	2	3	150
14	M16	3	3	4	200
16	M20	5	5	5	250
18				6	300
20				7	350
				8	400
				9	450
				10	500

Table 3.4: Possible values for strengthening design parameters

The *amount of bolts per trough* and *amount of bolts between troughs* are combined into a single parameter during the analysis, termed *amount of bolts transversal*, and defined as *amount of bolts per trough* x *amount of bolts between troughs* in the report. For example, a configuration with 2 bolts inside the trough and 3 in-between troughs would be denoted as 2 x 3. With this implementation, the total number of design parameters is limited to five. This number is further reduced in later stages, based on the outcomes of the parametric study.

3.4.1. Bolt configuration constraint based on bolt size

The feasible bolt configurations are constrained by the size of the bolts, as the required minimum spacing between bolts increases with diameter. Smaller bolts can be positioned more closely together, enabling denser configurations, while larger bolts require more space to ensure proper performance. As a result, the maximum amount of bolts that can be used inside or between troughs, as well as the minimum allowable bolt row spacing, depends on the selected bolt size. Table 3.5 summarises these practical limits for each bolt size.

Bolt Size	Amount of bolts per/between troughs	Minimum bolt row spacing (mm)
M8	1, 2, 3, 5	50
M10	1, 2, 3, 5	50
M12	1, 2, 3	75
M16	1, 2, 3	75
M20	1, 2	100

Table 3.5: Bolt configuration dependence on bolt size

3.5. Evaluation of strengthening schemes

To identify effective schemes that meet the strengthening design objectives, multiple design parameters are systematically varied. This leads to a large number of possible strengthening schemes: up to 75.000 variants when all combinations from Table 3.4 are considered. While a parametric model allows for the automated generation of these schemes, analysing the full set is computationally infeasible. Instead, a structured approach is adopted to reduce the number of variants and gain clearer insight into the influence of individual parameters.

3.5.1. Fatigue assessment: hot spot stress reduction

Fatigue performance is the primary design objective, assessed by evaluating the hot spot stress reduction in the two selected critical details. This reduction is quantified as:

$$\text{Hot Spot Stress Reduction} = 1 - \left(\frac{\sigma_{\text{after}}}{\sigma_{\text{before}}} \right) \tag{3.1}$$

where σ_{after} and σ_{before} are the hot spot stresses after and before strengthening, respectively.

The stresses are computed under fatigue loading based on Load Model 4, as defined in *NEN-EN 1991-2* [16]. An overview of the load model principles is provided in Section 2.2, while the specifics of the loading conditions implemented in this thesis are explained in the following chapter.

3.5.2. Parametric study

As explained in Section 1.6, a parametric study is performed to explore the influence of each design parameter on the hot spot stress reduction, as well as identify any interdependencies between parameters. The goal is to gain insight into which design choices have the largest impact on fatigue performance. The results of this study also guide the selection of strengthening schemes for further analysis.

3.5.3. Verifications

The selected strengthening schemes are checked for compliance with design requirements in both the Serviceability Limit State (SLS) and Ultimate Limit State (ULS). The bolts are designed as slip-resistant connections. For SLS, the applied shear forces must remain below the slip resistance of the bolts. In ULS, multiple verifications are necessary to ensure the robustness of the design. These typically include checks for stresses in the deck and strengthening plate, buckling, and the shear and axial capacity of the bolts [6]. However, due to the limitations of the scope of this study, only two loading scenarios are considered: thermal loading and Load Model 2 (LM2). These loading conditions were selected because they were identified as the most critical during the strengthening of the Suurhoff bridge [6]. In particular, the shear resistance of the bolts, especially near the edges of the strengthening plate, was found to be a key concern under thermal loading. Therefore, these two loading cases are prioritised for verification.

3.5.4. Evaluation criteria

The schemes that satisfy the verifications are evaluated using certain criteria, set up to quantify to what extent the schemes can realise the design objectives. The criteria are as follows:

- Fatigue life extension,
- Weight of the strengthening scheme,
- Installation time.

Numerical Modelling

This chapter describes the finite element (FE) model representing a section of the case study bridge deck. Given that evaluating the fatigue strength of welded details in orthotropic steel decks is often analytically infeasible, finite element analysis is the preferred approach. This chapter explains in detail the purpose of the model, components, mesh configurations, and applied loading and boundary conditions.

Following, the strengthening design introduced in Chapter 3, consisting of blind bolted steel plates, is incorporated into the FE model. A parametric model is developed to enable variation of the strengthening design parameters and generate multiple strengthening schemes.

The software used for the structural analysis is GSA Oasys (version 10.2). Grasshopper (Rhinoceros 3D, version 8) is employed as a parametric modelling tool, facilitating efficient modifications to the strengthening configuration.

4.1. Numerical model of bridge deck

The model simulates the fatigue behaviour of a single traffic lane of an orthotropic deck, focusing on two critical details susceptible to high stress concentrations. These are located in the middle of the modelled section. The model consists of beam and shell elements, arranged in such a way that the level of detailing increases from the outer edges towards the critical details. In this way, the critical responses of the bridge deck are captured and accurate hot spot stress prediction is possible, while maintaining computational efficiency. Since multiple strengthening schemes are analysed, reducing computational time is essential. This balance

(a) 3d view of the model

(b) Top view with dimensions
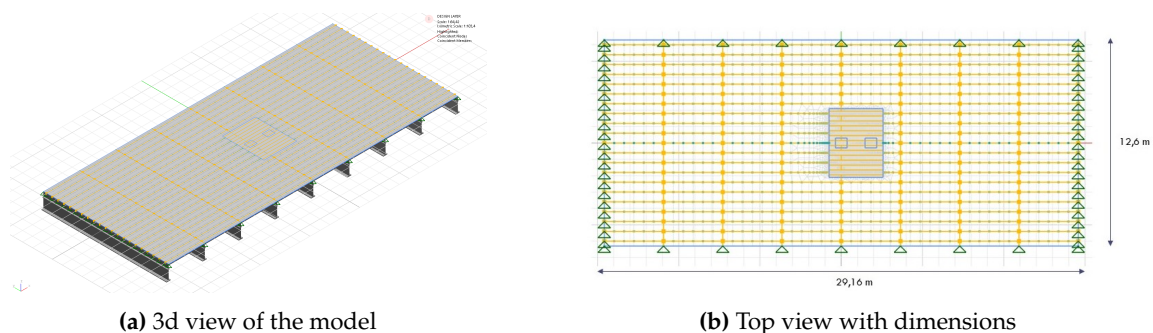
Figure 4.1: Finite element model of the bridge deck section

between accuracy and computational efficiency is a key aspect during the model set-up, and the various simplifications made to accommodate this trade-off are presented in this chapter.

4.1.1. Layout and geometry

The model represents a section of the 2nd Van Brienenoord bridge deck, as visualised in Figure 4.1. The slow lane, which is the lane of interest, is centrally located within this section. To ensure proper boundary conditions, the total modelled width is three times the width of the lane, amounting to 12.5 meters. In longitudinal direction, the deck spans between cross beams over eight spans, totalling 29.16 meters in length. It is important to note that the *ROK* prescribes that for fatigue assessment the bridge deck should be modelled over its complete width (see Section 2.2.5). This guideline is not implemented, as that would significantly increase the computation time.

Only the orthotropic steel deck components are modelled: the deck plate, longitudinal stiffeners, and cross beams. Main girders and actual supports are excluded, as they lie outside the section boundaries. Additionally, the asphalt layer is left out as a modelling simplification. The modelled components have the same geometrical properties as the case study deck.

4.1.2. Boundary conditions

In reality, cross beams span the entire bridge width and rest on main girders. However, in the model, they are cut off to fit the width of the modelled section and are supported using pinned supports. Similarly, the trough ends are represented by pinned supports as well. This way, only the translations are restrained at the ends. This results in a less stiff response than in reality, where these sections would offer some rotational resistance and bending moment capacity.

4.1.3. Levels of model detailing

To manage the trade-off between computational time and accuracy, the model is divided into three levels of detail, as visualised in Figure 4.2. The levels are explained below, starting with the most detailed *level 3*.

Level 3

The two critical details are located in *level 3*, which is modelled according to recommendations for FE modelling of fatigue details (see Section 2.2.5), with finely meshed shell elements to allow for extrapolation of stresses. The dimensions of *level 3* are the same for both details, with a length of 0.72 metres and a width equal to the trough-to-trough spacing, 0.6 metres. They are modelled at the expected locations of the fatigue details, *detail 2b* at the mid-span between two cross beams, and *detail 1c* at the cross beam. It is important to note that the two details are modelled separately; each is contained within its own finite element model, depending on which detail is being analysed.

Level 2

Inclusion of this level of detail throughout the entire model would result in excessive computational demands. Therefore, *Level 2* serves as an intermediate representation, maintaining sufficient accuracy while reducing computational complexity. This level still allows for the formation of all significant deformation mechanisms, such as the distortion of the cross beam and panel deformation, as it is modelled using shell elements, but with a coarser mesh. This is in line with the *ROK* which requires the steel structure to be modelled with shells (see Section 2.2.5). *Level 2* surrounds *level 3* and extends in the width to form the slow lane of 4.2 metres. The length of this region is defined by adding a 0.75 metres to the outer boundaries of the two critical details. This additional space allows for the application of strengthening over an appropriately extended length.

Level 1
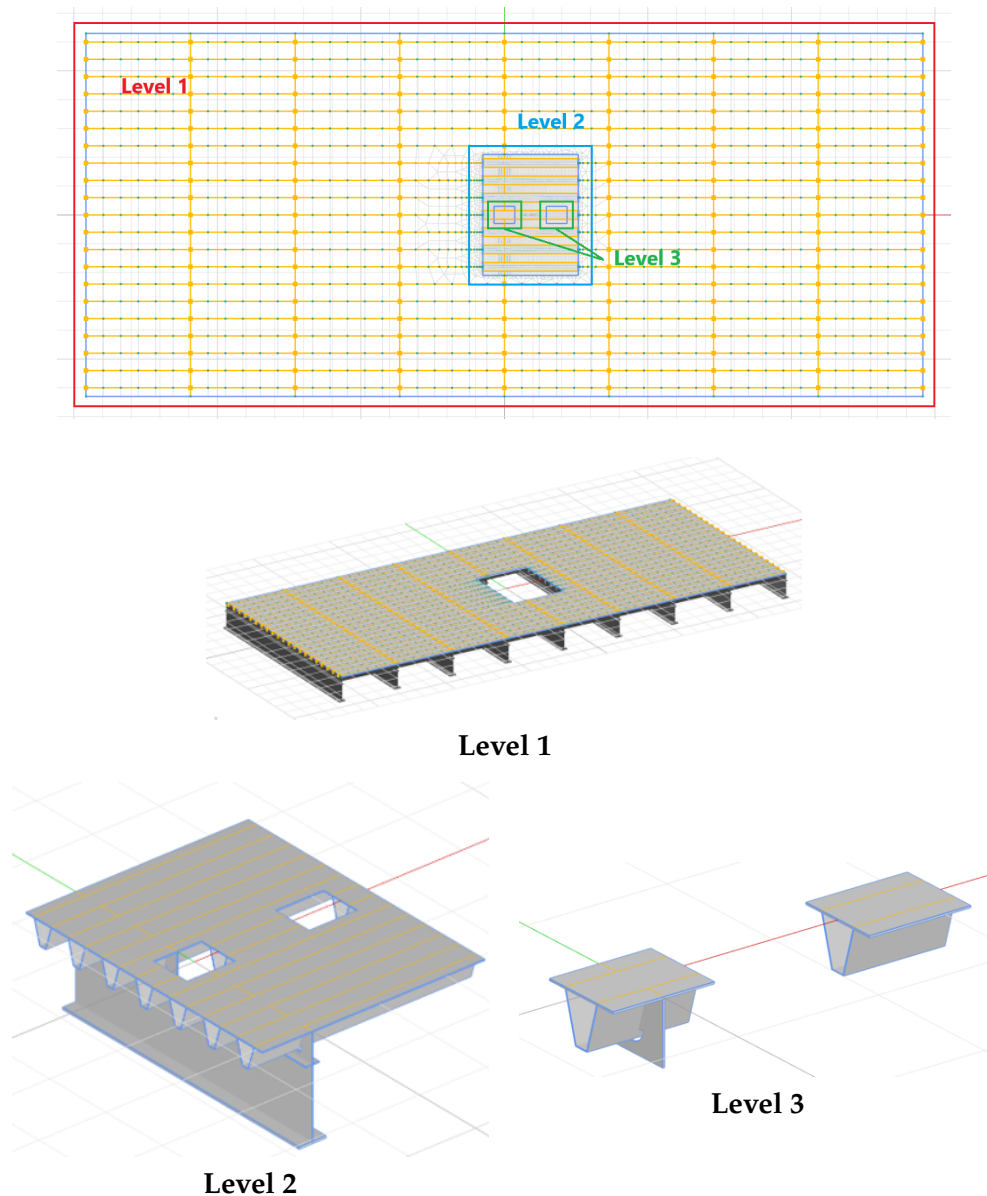
Level 3

Level 2

Figure 4.2: Three levels of detailing of the finite element model

Level 1

Level 1 is constructed around *Level 2* to establish the necessary boundary conditions for the model. In this level, the deck plate is represented with a very coarse mesh, and the troughs and cross beams are modelled as beam elements rather than shell elements.

4.1.4. Description of model components

The modelled components and corresponding mesh configurations are outlined below.

Level 1: beam elements region

In *Level 1*, the cross beams and troughs are modelled as beam elements. The cross-sectional properties of these beam elements are defined based on their geometry. They are attached to the deckplate at the top middle point of the cross-section. The deck plate is represented as a shell. The mesh size for the beam elements region is set to 600 mm, corresponding to the spacing between adjacent troughs.

Level 2: shell elements region

At this level, the mesh size is reduced to 50 mm to enhance the accuracy of the mechanical behaviour when approaching the region relevant for fatigue assessment. The troughs and cross beams are now modelled as shell elements. The rounding of the corners of the troughs is neglected in both *level 2* and *level 3*. The cope hole in the support plate is modelled using straight lines, ignoring the curvature of the hole, as shown in Figure 4.3a.

The connection of the cross beams and troughs which pass through both *level 2* and *level 1* is realised through the definition of pinned constraints. These constraints are imposed at the boundary nodes of the shell and beam representations of the troughs and cross beams.

(a) Cope hole detailing at *level 2*   **(b)** Cope hole detailing at *level 3*
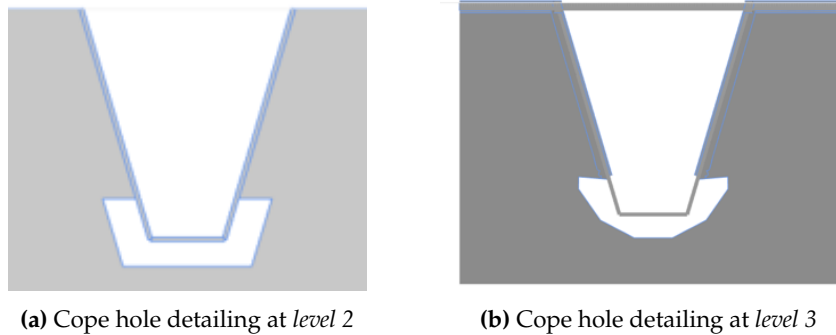
Figure 4.3: Modelling of support plate and cope hole at different levels

Level 3: detailed shell region for fatigue assessment

Level 3 is where the hot spot stress extraction for the two critical details occurs. This level consists of two regions: one at the cross beam, representing *Detail 1c*, and the other between two cross beams, focusing on *Detail 2b*. The mesh sizes are selected following the guidelines provided by ROK [12] for hot spot stress extraction: 6 mm for *Detail 2b* and 4 mm for *Detail 1c*. Further details on these mesh size selections are provided in Section 4.1.6. *Level 3* of *detail 1c* exclusively represents the support plate and not the attached cross beam, with the cross beam meshed according to the *Level 2* mesh size.

4.1.5. Loading conditions

A simplified fatigue load is applied, using a single wheel from a heavy vehicle, based on Eurocode Load Model 4, as shown in Section 4.1.5. Including the full set of load cases would lead to excessive computation time, which is not feasible for this parametric study. Instead, only the critical wheel position is considered, which is centrally placing the wheel inside the trough inside the *level 3* region, for both *details 2b* and *1c*. The second wheel of the axle is excluded from the analysis, as it falls outside of the width of the slow lane.

Wheel type C, applying a 45 kN load over an area of 270 x 320 mm^2, is used as it produces the highest hot spot stresses (Figure 2.13).

4.1.6. Extraction of hot spot stresses

Accurate hot spot stress extraction requires fine meshing and specific extrapolation point locations, as advised by the *ROK* [12]. Figure 4.4 shows the guidelines for the two critical details. For *detail 2b*, the *ROK* advises extrapolation points at 20 and 40 mm from the hot spot location. While this allows for larger mesh sizes, it is decided to implement a 6 mm mesh in order to be able to thicken the elements that represent the welds. For *detail 1c*, either a 4 mm or 12 mm mesh could be selected, with the preference for a finer mesh to increase accuracy of hot

spot stress prediction.

- **Detail 2b**: Weld between the trough web and deck plate. Extrapolation points at 21 mm and 39 mm. A mesh size of 6 mm is used.

- **Detail 1c**: Root of weld between the trough and deck plate. Extrapolation points at 0.5 and 1.5 times the plate thickness. A finer mesh of 4 mm is selected.
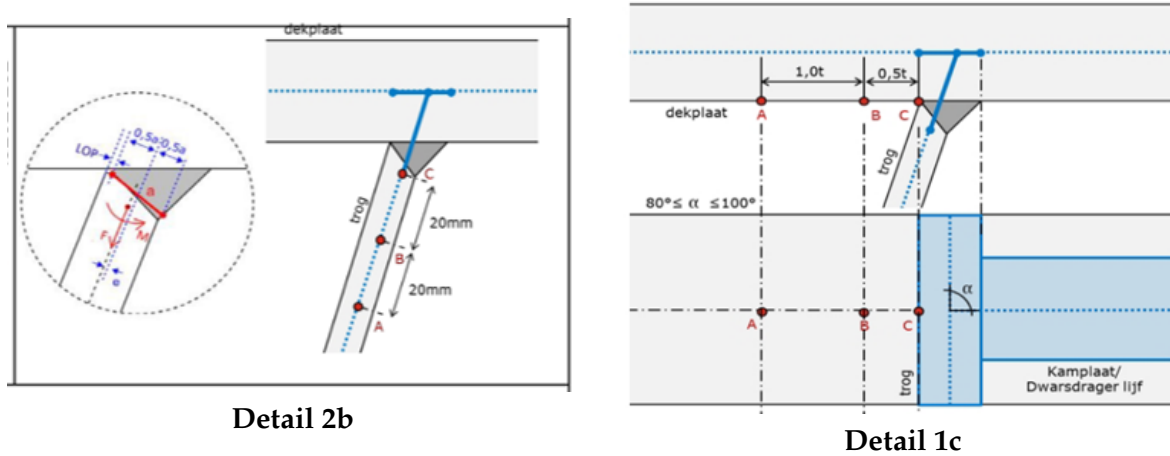
Detail 2b

Detail 1c

Figure 4.4: Guidelines for extrapolation of hot spot stresses according to ROK [12]

Modelling of welds

The modelling of welds is implemented by locally increasing the element thickness in accordance with *ROK* guidelines, 6 mm extra. For *detail 2b*, two rows of elements of the trough near the weld are increased to 12 mm, and similarly two rows of the deck plate to 18 mm thickness. Similarly, for *detail 1c*, the trough to deckplate joint is modelled in the same way. The joint between trough and support plate, and support plate and deck plate, follow the same principle, as can be recognised in Figure 4.5.
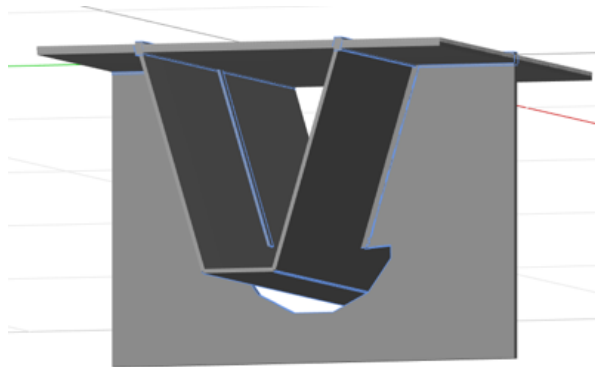
Figure 4.5: 3D view of level 3: detail 1c

4.2. Parametric model of strengthened bridge deck

This section begins with an explanation of how the finite element model is extended the components of the strengthening design: a shell plate representing the strengthening plate and elastic springs simulating the blind bolts. Following, the modelling assumptions and decisions made to represent the hybrid interaction between the two plates are discussed.

Finally, the workflow of the parametric model, developed in the visual programming software Grasshopper, is summarised.

4.2.1. Description of model components for strengthening

The two components of the strengthening design, the strengthening plate and blind bolts, must be properly modelled, to ensure accurate representation of the structural behaviour of the strengthened bridge deck, and consequently, accurate fatigue prediction. As two critical details are considered, two distinct strengthened bridge models are created: one for *detail 1c* and one for *detail 2b*. Figure 2.18 visualises the strengthened bridge deck for *detail 2b*.

(a) 3D view of strengthened bridge deck **(b)** Springs representing the blind bolts
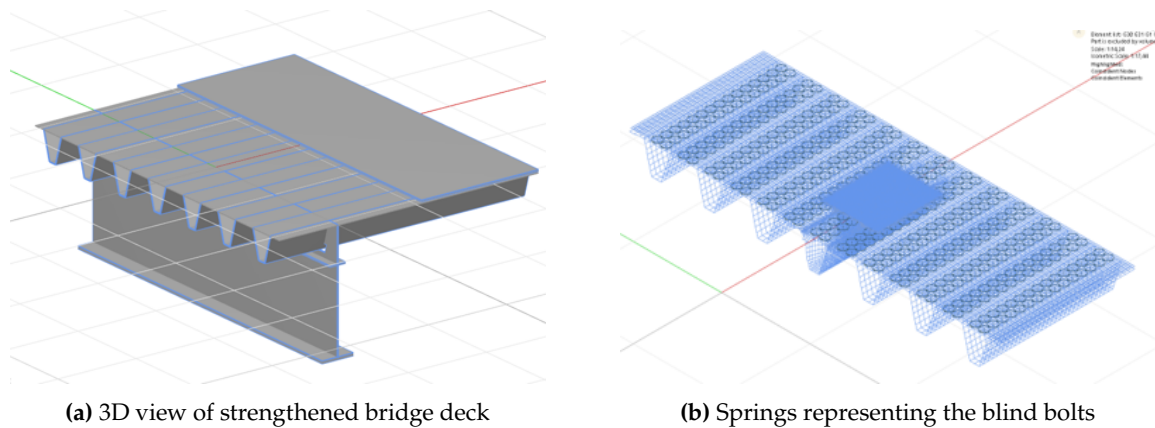
Figure 4.6: Visualisation of strengthened bridge deck for detail 2b

Strengthening plate

The strengthening plate is modelled as a shell, with varying thicknesses ranging from 8 to 20 mm. The plate extends across the entire width of *level 2*, with the length in longitudinal direction of 1.5 m. Depending on whether *detail 2b* or *1c* is considered, the strengthening plate is positioned centrally above the mid-span between cross beams or directly above the cross beam. The modelling levels of *level 2* and *level 3* are followed for the strengthening plate, resulting in a finer mesh over the critical detail, while the rest of the plate is meshed with a coarser mesh. The mesh size above the critical details is set to 6 mm, while the coarser mesh has a size of 25 mm. Initially, a 50 mm mesh was used to align with the bridge deck meshing, but this was later refined to allow greater flexibility in bolt placement.

An offset of half the plate thickness is applied to the elements representing the strengthening plate to ensure appropriate behaviour of the springs connecting the two plates. Similarly, an offset of half its thickness is also applied to the deck plate, but in the negative z-direction.

Crucial to a comparison of the hot spot stress results of various strengthening schemes is the mesh consistency across schemes. This is achieved by pre-meshing the bridge deck model and combining it afterwards with the meshed components from the strengthening. This ensures that the same extrapolation elements are used in the un-strengthened and strengthened model, providing reliable hot spot stress assessment. Furthermore, a selection of nodes for possible bolt placement is made prior to meshing, ensuring that these nodes are included in all strengthening scheme variants.

Hollo-Bolts

The blind bolts are modelled as discrete springs with a high axial stiffness, acting as rigid connection points in z direction, while their stiffness in x- and y- direction is related to their

shear capacity. The derivation of the shear stiffness is discussed in Appendix D, where the effects of different stiffness values on hot spot stresses and maximum shear forces in the springs are analysed. The study reveals that the shear stiffness of the springs significantly influences the hot spot stresses, with higher stiffness resulting in lower stress values. Since the design aims to be slip-resistant, a high stiffness, approaching infinity, is expected before slipping occurs. However, due to the inherent uncertainty in the behaviour of Hollo-Bolts, a conservative approach is taken, using a stiffness calculated based on the slip deformation graph shown in Figure B.4: $k_s pring = F_s lip/0.125mm$. A reduced preload is considered in the calculation of the slip capacity, as explained in Section 3.2.

Hybrid interaction between the plates
If the plates are only connected at the bolt locations, the hybrid interaction between the plates would not be representative of the actual behaviour, as the plates could pass through each other in certain regions. To address this, additional discrete springs with high axial stiffness and zero shear stiffness are placed at critical locations. The most critical location is the joint between the trough web and the deck plate, where *detail 2b* and *detail 1c* are located. At this location, a high density of axial springs is applied above the trough web to prevent the plates from passing through each other.

In the initial iteration, axial springs were applied across the entire strengthening plate region. However, it was later found that this overestimated the hybrid interaction, as gaps could not form. The placement of the axial springs was optimised through a sensitivity study, which examined different areas for spring application. The study also considered the use of non-linear, compression-only springs that allow for the formation of gaps. The results indicated that applying the springs exclusively within the *Level 3* region provided the most accurate hot spot stress results, comparable to the results with compression-only springs.

4.2.2. Workflow of parametric model
Figure 4.7 presents the workflow which was navigated to perform the fatigue assessment of various strengthening schemes. With this workflow, a strengthening scheme can be generated by adjusting a "slider" in Grasshopper, allowing for rapid results, such as hot spot stress predictions, within a few minutes.
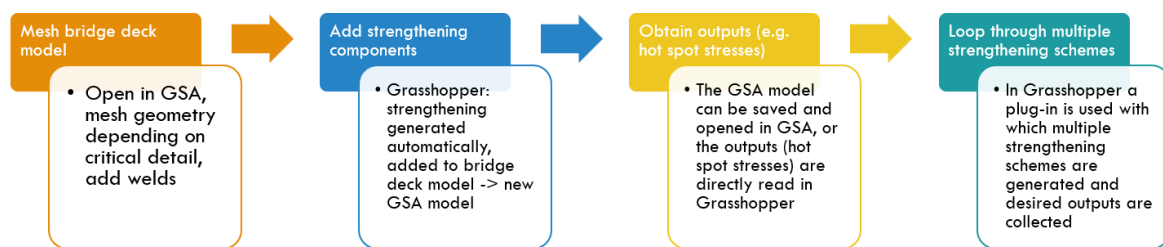
Figure 4.7: Workflow of GSA and Grasshopper for use of parametric model

5

Parametric Study Results

This chapter starts by presenting the results of the hot spot stresses of the Second Van Brienenoord bridge deck before strengthening. Understanding of the initial stress distributions is essential, as they provide a establish a reference point for evaluating the performance of various strengthening schemes. Following, the hot spot stresses of a baseline strengthening scheme are examined, showing the hot spot stress reduction due to the applied strengthening. A comparison is performed between various generated strengthening schemes in a parametric study, with the goal of quantifying the influence of different design parameters on fatigue stress reduction. Interdependencies between parameters are also explored. Based on the outcomes, a subset of strengthening schemes is selected for further analysis in Chapter 6.

5.1. Hot spot stresses prior to strengthening

The finite element model described in Chapter 4 is analysed under fatigue loading, with a single wheel positioned on the most critical location on the bridge deck. As outlined in Section 4.1.5, for both the detail in-between cross beams (*detail 2b*), as well as the critical detail above the cross beam (*detail 1c*), placing the wheel centrally above the trough, directly above the detail location, causes the highest hot spot stresses.
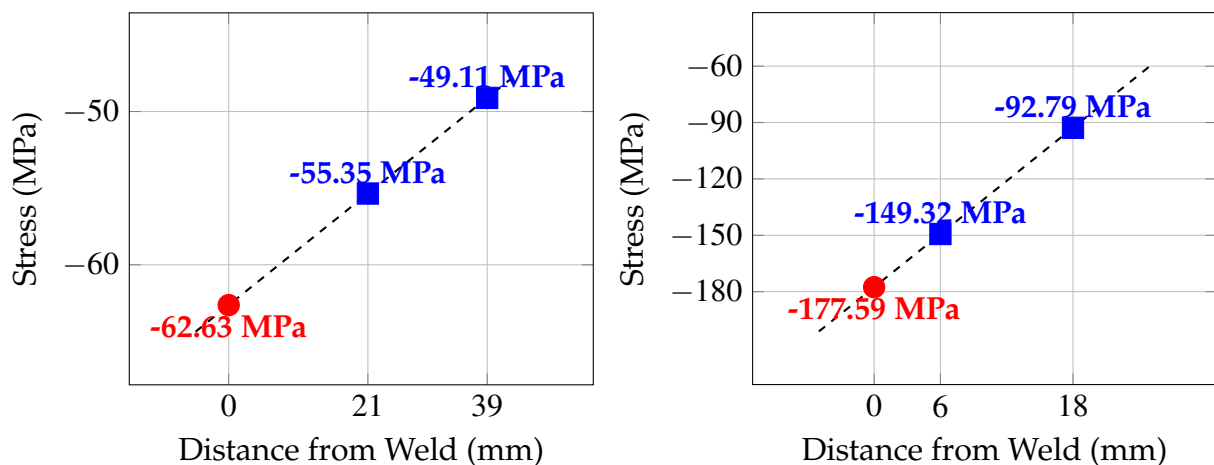
Figure 5.1: Comparison of hot spot stress extrapolation for two cases. The left plot represents detail 2b, while the right plot represents detail 1c.

49

The resulting bending stress distributions in the yy direction are shown in Figure 5.2, highlighting the elements used for hot spot stress extrapolation. These elements, marked in red (Figures 5.2a and 5.2c), provide a basis for estimating the peak stress values at the details through linear extrapolation, as as visualised in Figure 5.1. Linear extrapolation was applied as it requires less data points, compared to quadratic extrapolation, and provides a reasonable approximation of stresses. The coordinate system used in the Figures is as follows:

The hot spot stresses are as follows:

- **Detail 2b**: -62.63 MPa

- **Detail 1c**: -177.59 MPa

There is a significant difference in stress levels between the two details, likely because of the proximity of *detail 1c* to the cross beam. This creates additional constraints at the junction between deck plate and trough, leading to a region of stress concentration.

(a) Detail 2b - With extrapolation elements

(b) Detail 2b - Stress distribution

(c) Detail 1c - With extrapolation elements

(d) Detail 1c - Stress distribution
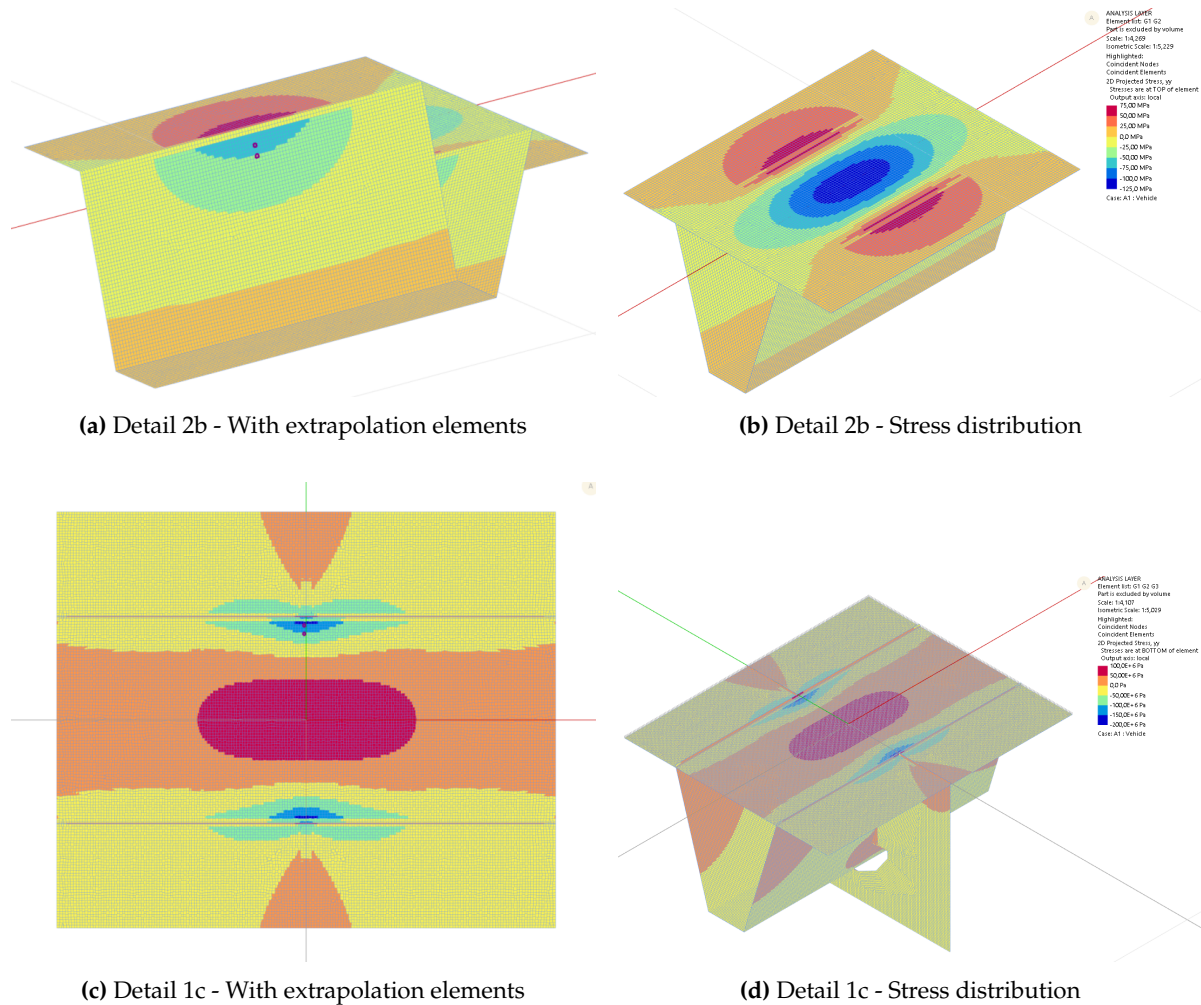
Figure 5.2: Comparison of stress distribution and extrapolation elements for details 2b and 1c

Detail 2b is located at the longitudinal weld between the trough web and deck plate, with the extrapolation elements located in the trough web. The hot spot stress point is positioned at the root of the weld, on the inner side of the trough web, according to the *ROK* [12]. The bending stresses observed in this region are compressive. Figure 5.2a shows the the bending stress distribution near the detail, forming a semicircular pattern that gradually diminishes with distance from the detail, indicating a region of stress concentration surrounding *detail 2b*. Figure 5.2b highlights the distribution of stresses in the deck plate, showing that positive bending moments occur in the deck plate underneath the vehicle load, and negative moments above the trough legs. This stress pattern is expected as the trough adds bending stiffness to the deck plate and resists deformation near the longitudinal weld. The region of high stresses is of limited size, confirming the localised nature of this critical detail.

Detail 1c , which is positioned at the root of the weld in the bottom of the deck plate, experiences compressive stresses due to positive bending moments occurring at the joint between trough, deck plate and cross beam. At this joint, stress concentrations occur, as can be seen in 5.2d, with the stresses increasing inwards from the longitudinal weld into the trough, with peak values just next to the weld. Figure 5.2c shows the location of the extrapolation elements inside of this stress concentration region. These high localised stress occur due to the presence of the cross beam, which also causes localised stress peaks in the deck plate region between two troughs as there the support plate is welded to the deck plate. Unlike *detail 2b*, *detail 1c* is strongly influenced by the behaviour of the cross beam, making the critical detail more affected by global deformation of the orthotropic deck.

To summarise, the stress distribution of *detail 2b* follows a more predictable pattern, whereas in *detail 1c*, stress localisation is more pronounced due to the presence of the cross beam. The found hot spot stresses are -62.63 MPa for *detail 2b*, and -177.59 MPa for *detail 1c*.

5.2. Effect of design parameters on hot spot stress reduction

The effectiveness of strengthening schemes is assessed by analysing their impact on reducing hot spot stresses. The section first introduces a baseline strengthening scheme to establish a reference case, followed by a parametric study where individual design parameters are varied systematically. The aim is to determine which parameters have the strongest influence on hot spot stress reduction.

Design Parameter	Value
Plate Thickness [mm]	16
Bolt Size	M16
Transversal Bolt Configuration	2 x 2
Bolt Row Spacing [mm]	100
Number of Bolt Rows	15*

Table 5.1: Baseline strengthening scheme for parametric study
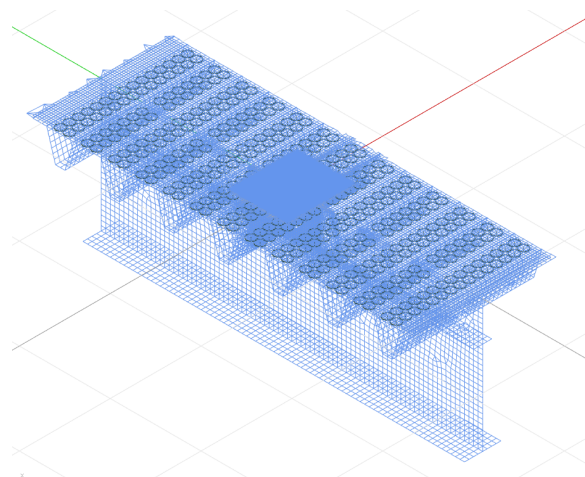
Figure 5.3: Baseline strengthening scheme detail 1c

Baseline strengthening scheme

A baseline strengthening scheme is defined, incorporating a 16 mm thick strengthening plate and M16 bolts. In longitudinal direction, the bolts are placed across the entire plate with a 100 mm spacing, and in transversal direction, a 2x2 configuration is applied. The baseline scheme of *detail 1c* differs only in the bolt row directly above the cross beam, where a 2x0 configuration is applied due to the presence of the cross beam. Here, the regions between troughs contain a support plate welded to the deck. The design parameters are provided in Table 5.1 and the baseline scheme for *detail 1c* visualised in Figure 5.3.

Detail	HSS Baseline Strengthening [MPa]	HSS Reduction Factor [-]
2b	-30.40	0.52
1c	-100.55	0.43

Table 5.2: Hot Spot Stresses of critical details after applying baseline strengthening scheme

(a) Detail 2b - With extrapolation elements

(b) Detail 2b - Stress distribution

(c) Detail 1c - With extrapolation elements

(d) Detail 1c - Stress distribution
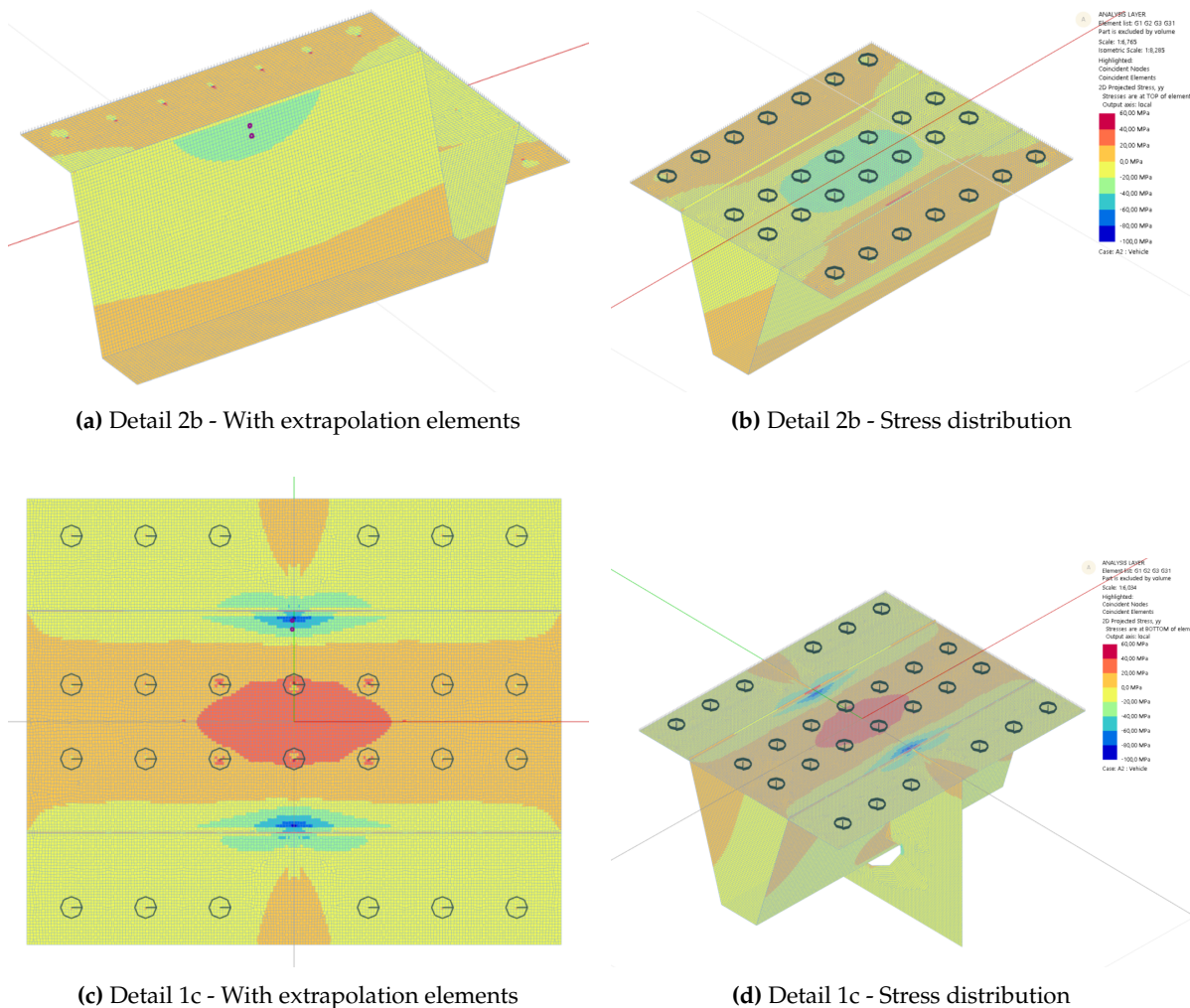
Figure 5.4: Comparison of stress distribution and extrapolation elements for details 2b and 1c - with baseline strengthening scheme

Applying this strengthening scheme results in a 52% hot spot stress reduction for *detail 2b* and a 43% reduction for *detail 1c*, as summarised in Table 5.2. The corresponding bending stress distributions of the details are shown in Figure 5.4, showing an overall reduction of stresses in the bridge deck. The hot spot stress reduction is slightly less effective for *detail 1c*, due to the influence of the cross beam. The strengthening plate cannot be fastened to the deck between troughs, limiting the ability of hybrid interaction between plates in those regions. Moreover, the cross beam undergoes its own deformation mechanisms, such as out-of-plane distortion and in-plane flexure (see Section 2.2.3), which are less affected by local strengthening. As a result, the stress distributions in *detail 1c* are influenced in a more complex manner compared to *detail 2b*.

Single parameter influence

A parametric study is conducted by varying one design parameter at a time, allowing for direct observation on its influence on hot spot stress reduction. The parameters are varied as follows:

- **Plate thickness**: 8 - 20 mm, step size of 2 mm
- **Bolt size**: M8 - M20
- **Bolt row spacing**: 100 - 500 mm, step size of 50 mm
- **Number of bolt rows**: 1 - 15, step size of 2
- **Transversal bolt configuration**: 0 - 3 bolts inside/between troughs

As the minimum spacing for a M20 bolt is 100 mm (Table 3.5), the bolt row spacing is varied from 100 mm and higher. Furthermore, it is decided to only look at uneven number of bolt rows, in order to ensure that every strengthening variation contains a bolt row centrally above the critical detail location. Three bolts are selected as the maximum number in the width of a trough or region between adjacent troughs. The impact of each parameter is discussed, with the results presented in Figure 5.5.

Parameter 1: plate thickness

Increasing the strengthening plate thickness consistently improves hot spot stress reduction. The reduction follows a near-linear trend in the lower thickness range, and starts to flatten around 16 mm, finally reaching 60% effectiveness at 20 mm thickness for both critical details. Noteworthy, *detail 2b* benefits more at a lower plate thickness, e.g. 10 mm, compared to *detail 1c*. This suggests that for *detail 2b* strengthening already achieves high efficiency even at moderate thicknesses, whereas *detail 1c* requires thicker plates to reach comparable effectiveness. For *detail 1c*, a strengthening plate of 8 mm thickness can result in a slightly negative hot spot stress reduction, meaning that the hot spot stress is actually higher than without strengthening. This suggests that the plate might be too thin to help with effective stress redistribution. Instead, it may act as a localised stiffened area, causing increased forces, and, consequently, higher stress concentrations.

Parameter 2: bolt size

Increasing the bolt size results in improvement of hot spot stresses, but in a limited manner. Across the varied sizes, M8 to M20, the difference in hot spot stress reduction is less than 3% for *detail 2b* and less than 2% for *detail 1c*. The influence of bolt size might be enhanced if a higher preload can be applied. This would improve the load transfer between the deck plate and the strengthening plate, benefiting their hybrid interaction, and distributing the load more effectively, which could further reduce hot spot stresses.

(a) HSS Reduction vs. Plate Thickness

(b) HSS Reduction vs. Bolt Size

(c) HSS Reduction vs. Bolt Row Spacing

(d) HSS Reduction vs. Number of Bolt Rows

(e) HSS Reduction vs. Amount of Bolts Transversally

HSS Reduction 2b   HSS Reduction 1c
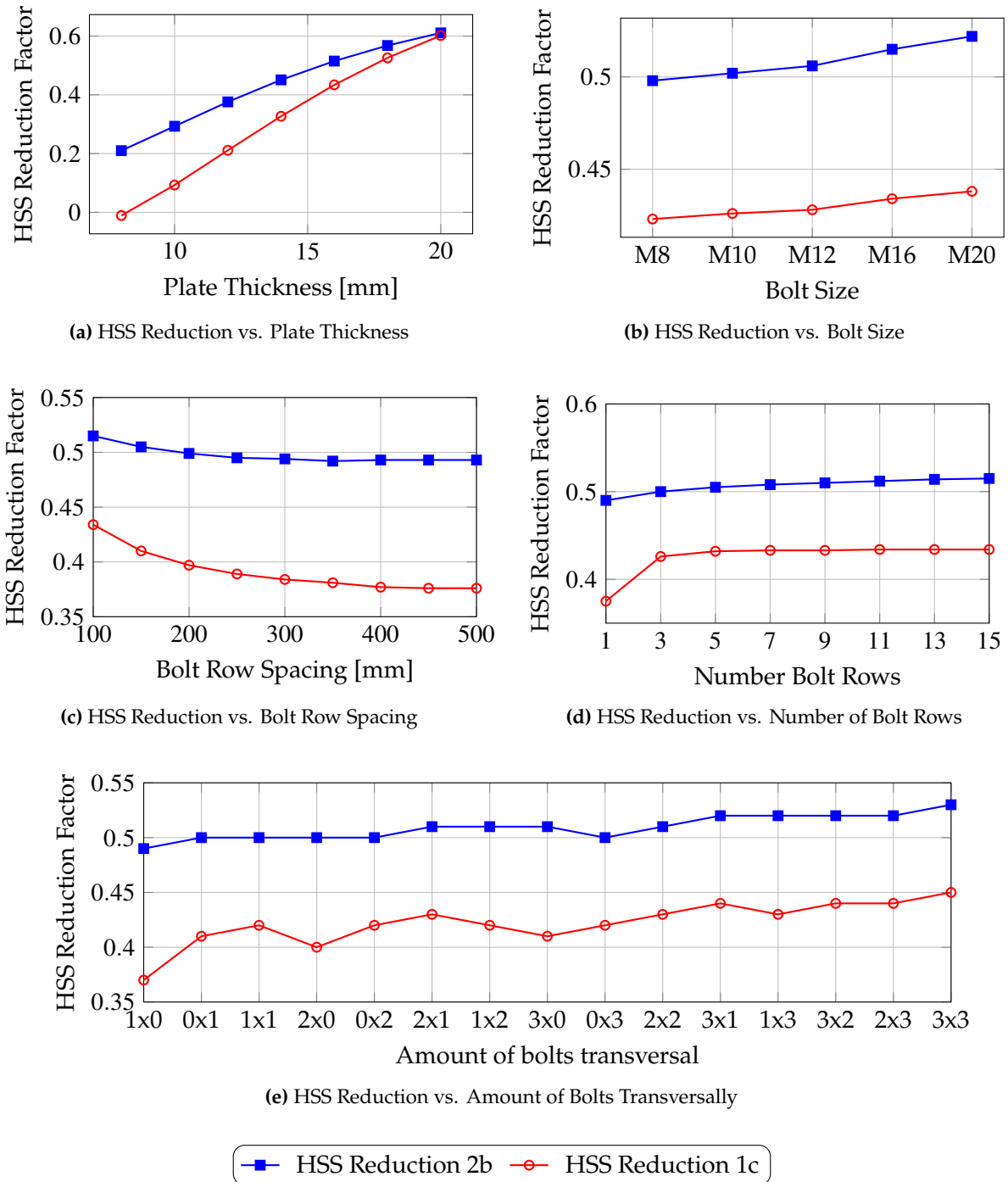
Figure 5.5: Overview of parametric study results

Parameter 3: bolt row spacing

With an increase of bolt row spacing, the number of bolt rows in longitudinal direction decreases. With a spacing of 100 mm, there is room for 15 bolt rows, while this reduces to only three bolt rows in case of a 500 mm spacing. The bolt row spacing has both impact on how close bolts are located to the critical detail longitudinally, as well as on the total number of bolts used to connect the plates. A higher stress reduction is observed with a smaller spacing, likely also because of a higher number of bolt rows. As the bolt row spacing increases, the reduction of stresses declines with a parabolic curve. The curve stabilises beyond 400 mm for *detail 1c*

and 250 mm for *detail 2b*, indicating that *detail 1c* is more sensitive to bolt row spacing. This could be because of the limited amount of bolts above the cross beam, requiring the bolt rows adjacent to the centred bolt row more crucial in case of *detail 1c* than for *detail 2b*. Furthermore, *detail 1c* may require more bolts to achieve similar hybrid interaction as *detail 2b*, as the cross beam limits the flexibility between the plates.

Parameter 4: number of bolt rows
Increasing the number of bolt rows improves the reduction of hot spot stresses. For *detail 2b*, adding bolt rows enhances the HSS reduction at a diminishing rate, with the overall benefit remaining small. *Detail 1c* shows a significant decrease of hot spot stresses when going from one to three bolt rows, followed by a more gradual reduction. Eventually, the curve stagnates, indicating that there might be a limit to how much longitudinal placement of bolts can decrease the hot spot stress of *detail 1c*. It might be that the cross beam provides this limit, and that stress redistribution cannot be improved by adding more bolt rows. However, in general, the influence of the number of bolt rows remains higher for *detail 1c* compared to *detail 2b*.

Parameter 5: transversal bolt configuration
The bolt configuration in transversal direction with respect to the stiffeners has notable effect on the hot spot stress reduction, especially for *detail 1c*. Symmetrical bolt configurations, e.g. 1x1, 2x2 and 3x3, progressively improve the reduction of stresses. For *detail 1c*, placing bolts only inside the troughs (e.g. 1x0, 2x0 and 3x0) is less effective than locating them between the stiffeners. Most probably, bolts are needed between the troughs to compensate for the "missing" bolts above the cross beam. For *detail 2b*, when having to choose between placing bolts only between or inside troughs, it is suggested to choose inside of troughs when multiple bolts are required, as e.g. 3x0 performs better than 0x3.

After the 3x3 configuration, the most effective for *detail 1c* are the configurations with three bolts placed inside the trough, and 1 or 2 bolts between adjacent stiffeners. The hot spot stresses of *detail 2b* are less sensitive to transversal bolt configuration compared to *detail 1c*, but still show improvement in HSS reduction with increase of bolts. Similarly as for *detail 1c*, the 3x2 configuration performs second-best. Placing three bolts inside and three between troughs leads to the highest stress reduction, 53% for *detail 2b* and 45% for *detail 1c*. The best performing configurations require bolts inside the closed stiffeners, indicating the benefit of the use of blind bolts. In case regular bolts would be used, assuming same properties for the bolt, the highest possible reduction, compared to a 3x3 configuration, would be 2.23% lower *detail 2b* and 2.29% lower for *detail 1c*.

Summary
After evaluating each parameter individually, plate thickness emerges as the most influential factor, showing the highest variability in stress reduction for both critical details. Particularly for *detail 1c*, the increase of thickness is crucial for significant reduction of hot spot stresses. For example, to reach a similar effectiveness as a 10 mm plate for *detail 2b*, a plate of 14 mm is needed for *detail 1c*.

Compared to *detail 2b*, the bolt configuration has a higher effect on hot spot stress reduction. From the three parameters related to configuration, number of bolt rows stands out, followed by the transversal bolt configuration and spacing between bolt rows. The bolt size remains the least significant factor, influencing *detail 1c* with less effect than for *detail 2b*.

For *detail 2b*, hot spot stress reduction is least sensitive to bolt row spacing, while transversal bolt placement has a stronger impact than bolt size or bolt row spacing. This indicates that the

positioning of bolts in transversal direction with respect to the troughs should be of higher focus for *detail 2b*, compared to the configuration in trough direction.

5.3. Interdependence between design parameters

Analysing the effect of a single design parameter at the time provides valuable insights, but does not capture potential interdependencies between parameters, e.g. if the bolt configuration has more impact on the hot spot stress reduction when a thinner plate is used. To address this, an alternative strengthening scheme is introduced, and its results are compared to the baseline scheme to identify parameter interdependencies.

Comparison with alternative strengthening scheme

The baseline strengthening scheme is quite robust, with a 16 mm deck plate and M16 bolts covering large part of the strengthening plate. In contrast, an alternative strengthening scheme is set up, with a thinner plate and fewer bolts. It includes a smaller bolt size (M10), more widely spaced bolt pattern in longitudinal direction (5 bolt rows spaced 200 mm apart) and an asymmetrical transversal bolt configuration. Figure 5.6 illustrates the scheme, while Table 5.3 summarises the design parameters. Applying this scheme gives a 16% reduction of hot spot stresses for *detail 1c*, and a 35% reduction for *detail 2b*.

Design Parameter	Value
Plate Thickness [mm]	12
Bolt Size	M10
Transversal Bolt Configuration	3 x 1
Bolt Row Spacing [mm]	200
Number of Bolt Rows	5

Table 5.3: Alternative strengthening scheme for comparison with baseline scheme
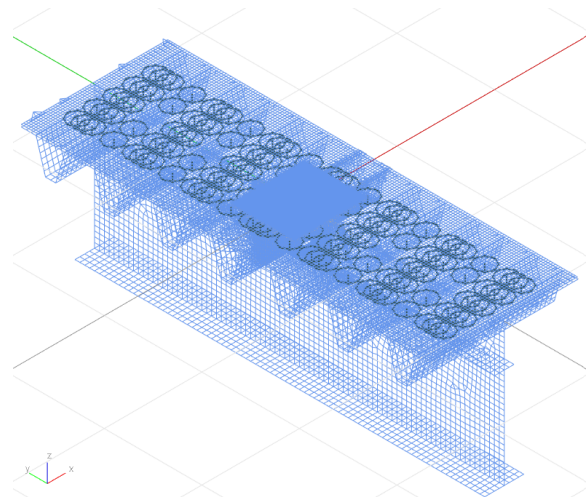
Figure 5.6: Alternative strengthening scheme detail 1c

Similarly as for the baseline strengthening scheme, the parameters of the alternative scheme are varied one by one and the effect on HSS reduction is observed. Table 5.4 shows the results of the study, together with the baseline strengthening scheme. The influence of a parameter on the HSS reduction is captured by the difference between maximum and minimum reduction of hot spot stresses that the parameter can achieve, noted down as a percentage.

The alternative scheme shows a higher influence of plate thickness on hot spot stress reduction compared to the baseline scheme, for both critical details. Meanwhile, the bolt size and bolt configuration show less influence on the HSS reduction. It is reasonable that the size and placement of the bolts simultaneously reduce, as with a smaller bolt size, the clamping force between the plates reduces, leading to diminished hybrid interaction at the connection points. In turn, as the alternative scheme contains a lower total number of bolts, the increase in bolt size, and consequently, clamping force, can only benefit few locations on the deck. The direct interdependency between number of bolt rows and row spacing is observed. In the alternative scheme, which uses a 200 mm spacing, the influence of additional bolt rows is

Design Parameter	Detail 2b		Detail 1c	
	Baseline Scheme	Alternative Scheme	Baseline Scheme	Alternative Scheme
Plate Thickness	40.09%	41.41%	61.30%	62.56%
Bolt Size	2.41%	0.99%	1.55%	1.50%
Bolt Row Spacing	2.29%	1.35%	5.83%	5.25%
Number Bolt Rows	2.49%	1.35%	8.88%	1.75%
Transversal Bolt Configuration	3.25%	0.83%	7.03%	2.96%

Table 5.4: Difference in HSS reduction between maximum and minimum parameter value: baseline vs alternative strengthening scheme

significantly lower, which is especially noticeable for *detail 1c*. The influence of the transversal bolt configuration decreases significantly for both details.

To summarise, an interdependence between plate thickness, bolt size and configuration is observed, with the influence of the plate thickness increasing when less bolts are used with a smaller bolt size.

Interaction analysis: transversal bolt configuration
The previous section highlights interdependence between the design parameters. In order to further investigate, a analysis is conducted focusing on the transversal bolt configuration, assessing the extent of its interaction with the strengthening plate thickness and size of bolts. The bolt row spacing and number of bolt rows are now kept intact, in order to eliminate their effect on the results out of the analysis. Their values are chosen according to the baseline strengthening scheme.

Interaction with plate thickness
Figures 5.7a and 5.7c show that the effect of transversal bolt configuration on hot spot stress reduction increases with a lower thickness of strengthening plate. For *detail 2b*, the difference between best and worst transversal configuration is 5.48%, while it drops to 2.79% for a 20 mm strengthening plate. Similarly, for *detail 1c* it changes from 8% with 10 mm thickness to 4.93% with 20 mm plate thickness. This suggests that when using a thinner strengthening plate, optimising the bolt configuration becomes more crucial, while in a strengthening scheme with a thicker plate, the plate is the primary contributor to stiffness improvement.

Interaction with bolt size
In Figures 5.7b and 5.7d, it is observed that applying larger bolts increases the influence of transversal bolt configuration on HSS reduction. Particularly, for configurations containing more bolts, e.g. 3x3, the choice of bolt size is significant, leading to 3% more hot spot stress reduction when using M20 bolts, compared to using M10 bolts (*detail 2b*). For *detail 1c*, this difference is slightly lower, amounting to around 2%. This implies that when using larger bolts, the transversal placement should be more optimised, to be able to make use of its higher hot spot stress reduction potential.

In summary, the choices regarding transversal bolt configuration are more critical for hot spot stress reduction in case of a thinner strengthening plate or when larger bolt sizes are employed.
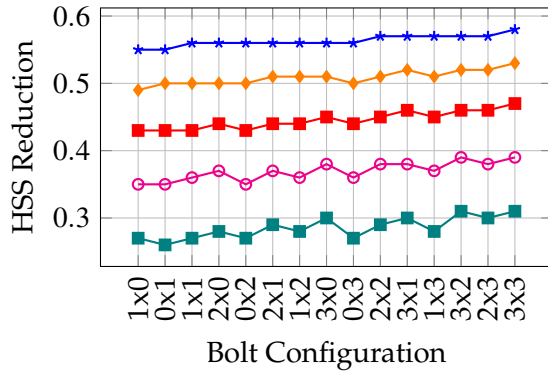
(a) Interaction bolt configuration and plate thickness: *detail 2b*
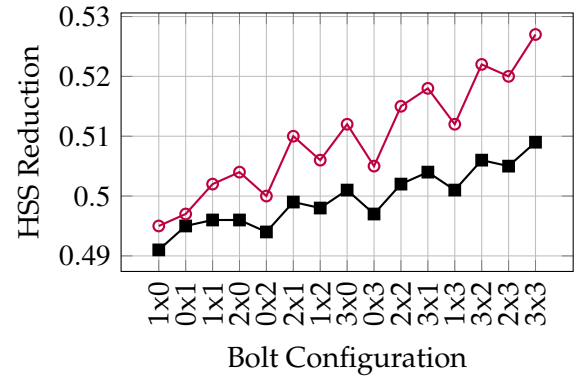
(b) Interaction bolt configuration and bolt size: *detail 2b*
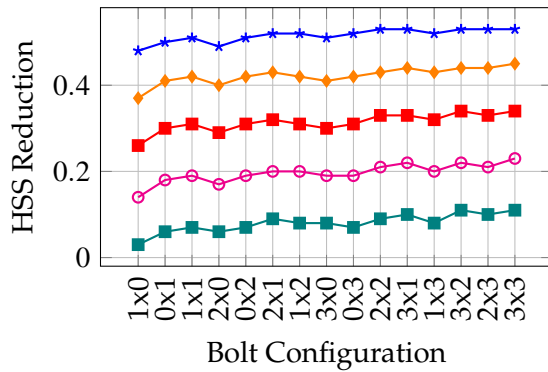
(c) Interaction bolt configuration and plate thickness: *detail 1c*

(d) Interaction bolt configuration and bolt size: *detail 1c*

Plate Thickness: 10 mm
Plate Thickness: 12 mm
Plate Thickness: 14 mm
Plate Thickness: 16 mm
Plate Thickness: 18 mm
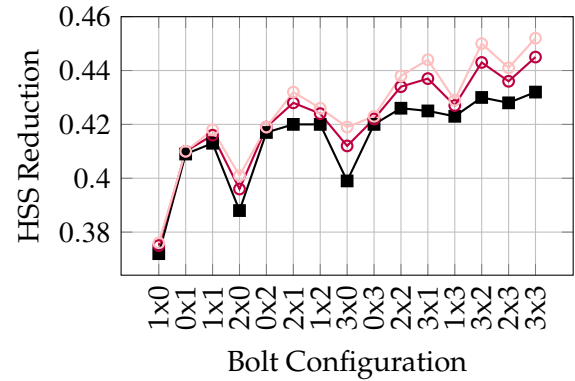
Bolt Size: M10
Bolt Size: M16
Bolt Size: M20
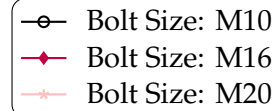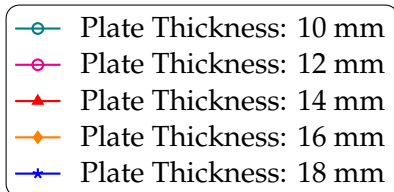
Figure 5.7: Analysis results: showing interaction between bolt configuration and plate thickness/bolt size based on HSS reduction.

5.4. Selection of strengthening schemes for further analysis

This section presents the selection of strengthening schemes which are further analysed in the following Chapter. Based on the findings from section 5.2 and 5.3, the most influential strengthening design parameters will be considered. Other parameters are fixed in order to reduce the number of strengthening schemes for the analysis.

Selection of design parameters

The following design parameters are further considered:

- **Plate Thickness**, 10 to 20 mm

- **Transversal Bolt Configuration**, maximum of three bolts inside/per trough

- **Bolt Size**, M16

The thickness of the strengthening plate is identified as the most influential parameter for reducing hot spot stresses. While a thicker plate results in higher reduction factors, it results in higher weight of the strengthening scheme. This trade-off will be considered in Chapter 6. The transversal bolt configuration also has significant effect on the reduction of hot spot stresses. Moreover, it is critical to analyse this parameter further, as the influence of blind bolts in the design can be studied with this parameter. While the bolt size shows limited influence on the hot spot stresses of the critical details, it is expected that it might be of significance in the static verifications of the strengthening scheme. Keeping this in mind, bolt sizes M16 and M20 are selected for further study.

The parameters that remain are fixed:

- **Bolt Row Spacing**, 100 mm
- **Number of Bolt Rows**, 15 bolt rows

It was found that the design parameters in longitudinal direction had limited impact on *detail 2b*, while their influence was more significant for *detail 1c*. For the latter, it was found that strengthening schemes with a minimum of five bolt rows are more effective for hot spot stress reduction, and that preferably that the bolts are installed as closely possible to the critical detail. It is decided to implement a spacing of 100 mm, and to consider bolt rows over the entire area of the strengthening plate, resulting in 15 bolt rows. The same is implemented for *detail 2b*, keeping in mind practical considerations regarding installation. Fixing these parameters allows for a focused investigation on the other design parameters.

Strengthening schemes for further analysis

The further considered strengthening schemes are presented. The hot spot stress reductions that result from the applied strengthening schemes are noted down. Here, the strengthening schemes containing M16 bolts are given, while Appendix E contains results for M20 bolts.

Detail 2b

Table 5.5 shows the hot spot stress reductions that can be achieved for *detail 2b* with a strengthening design containing M16 bolts. The effectiveness of the strengthening ranges from 26% hot spot stress reduction for a 10 mm plate to 62% reduction with a 20 mm strengthening plate. For a certain strengthening plate thickness, the difference between lowest and highest hot spot stress reduction is around 3 - 5%, decreasing for larger thicknesses. The highest reduction of hot spot stresses is achieved with a 3x3 transversal bolt configuration.

Table 5.5: Hot spot stress reduction for different thicknesses and bolt configurations: *detail 2b*, M16 100 mm fully bolted

Thickness	1x0	0x1	1x1	2x0	0x2	2x1	1x2	3x0	0x3	2x2	3x1	1x3	3x2	2x3	3x3
10	0.27	0.26	0.27	0.28	0.27	0.29	0.28	0.30	0.27	0.29	0.30	0.28	0.31	0.30	0.31
12	0.35	0.35	0.36	0.37	0.35	0.37	0.36	0.38	0.36	0.38	0.38	0.37	0.39	0.38	0.39
14	0.43	0.43	0.43	0.44	0.43	0.44	0.44	0.45	0.44	0.45	0.46	0.45	0.46	0.46	0.47
16	0.49	0.50	0.50	0.50	0.50	0.51	0.51	0.51	0.50	0.51	0.52	0.51	0.52	0.52	0.53
18	0.55	0.55	0.56	0.56	0.56	0.56	0.56	0.56	0.56	0.57	0.57	0.57	0.57	0.57	0.58
20	0.59	0.60	0.60	0.60	0.60	0.61	0.61	0.61	0.61	0.61	0.61	0.61	0.62	0.62	0.62

Detail 1c

In Table 5.5 the hot spot stress reduction factors are summarised for *detail 1c*. M16 bolts are employed in the schemes. The effectiveness of the strengthening starts at 3% - 11% reduction of hot spot stresses for a 10 mm plate, while it reached up to 61% for strengthening schemes with 20 mm thick plates. For a certain strengthening plate thickness, the difference between lowest and highest hot spot stress reduction is around 5 - 8%, decreasing for larger thicknesses. The highest reduction of hot spot stresses is achieved with a 3x3 transversal bolt configuration.

Table 5.6: Hot spot stress reduction for different thicknesses and bolt configurations: *detail 1c*, M16 100 mm fully bolted

Thickness	1x0	0x1	1x1	2x0	0x2	2x1	1x2	3x0	0x3	2x2	3x1	1x3	3x2	2x3	3x3
10	0.03	0.06	0.07	0.06	0.07	0.09	0.08	0.08	0.07	0.09	0.10	0.08	0.11	0.10	0.11
12	0.14	0.18	0.19	0.17	0.19	0.20	0.20	0.19	0.19	0.21	0.22	0.20	0.22	0.21	0.23
14	0.26	0.30	0.31	0.29	0.31	0.32	0.31	0.30	0.31	0.33	0.33	0.32	0.34	0.33	0.34
16	0.37	0.41	0.42	0.40	0.42	0.43	0.42	0.41	0.42	0.43	0.44	0.43	0.44	0.44	0.45
18	0.48	0.50	0.51	0.49	0.51	0.52	0.52	0.51	0.52	0.53	0.53	0.52	0.53	0.53	0.53
20	0.56	0.58	0.59	0.57	0.59	0.60	0.60	0.59	0.60	0.60	0.60	0.60	0.61	0.60	0.61

5.5. Conclusions

The fatigue analysis of the Second Van Brienenoord case study bridge deck showed hot spot stress value of -62.63 MPa at *detail 2b* and -177.9 MPa at *detail 1c*. With M16 bolts, the most effective strengthening schemes reduced the hot spot stresses up to 62% for *detail 2b* and 61% for *detail 1c*. These schemes contained a 20 mm thick strengthening plate and a bolt configuration consisting of three bolts inside the trough and three bolts between troughs.

The plate thickness is the most influential design parameter for both critical details, with *detail 1c* requiring larger thickness to achieve the same hot spot stress reduction as *detail 2b*. *Detail 1c* is significantly influenced by the bolt configuration, in both transversal and longitudinal directions. It benefits from close placement of bolt rows to the detail, thus calling for a smaller spacing. For both details, the possibility of placing blind bolts inside troughs increases the hot spot stress reduction.

6

Strengthening Scheme Selection

This chapter presents a final evaluation of the selected strengthening schemes from the parametric study (Chapter 5). The analysis includes estimated fatigue life extension, static verifications under ultimate limit state conditions, and a comparative assessment of the schemes in terms of added weight, installation time, and fatigue life gain.

6.1. Fatigue Life estimates

The fatigue assessment of the Second Van Brienenoord bridge deck [52] resulted in damage estimates of the fatigue-critical details of the deck: 33.8 for *detail 2b* and 22.3 for *detail 1c*. These values correspond to 30 years of usage.

To estimate the gained fatigue life after applying strengthening, a a simplified approach is adopted instead of the detailed damage prediction method presented in Chapter 2.1, which involves cycle counting and accumulated fatigue damage calculations. This choice is driven by the need to evaluate multiple strengthening schemes efficiently within a limited time period. The post-strengthening damage is estimated using Equation 6.1, which expresses the damage of the strengthened bridge deck as the ratio of hot spot stresses after and prior to strengthening, raised to the power 5, and multiplied by the damages from the fatigue assessment.

$$D_{\text{new}} = \left(\frac{\sigma_{\text{new}}}{\sigma_{\text{old}}} \right)^5 D_{\text{old}} \tag{6.1}$$

A damage value below 1 ($D_{\text{new}} =< 1$) indicates that the strengthened bridge is expected to not experience fatigue failure within the selected service life, which in this case is 30 years. For simplicity, it is assumed that at the start of the service life, the strengthened bridge deck does not contain any existing fatigue damage. In reality, this is different and fatigue damage can be expected, especially if the bridge deck has been used for a significant time.

As this study investigates the trade-off between fatigue life extension, strengthening weight and installation time, looking into strengthening schemes which provide a shorter fatigue life, e.g. 10 or 20 years, is also of interest. For the fatigue life calculation, it is assumed that the damages obtained for 30 years can be scaled linearly. As explained in Chapter 2.1, fatigue cracks grow with a non-linear propagation speed, starting off slower and growing more rapidly after a certain crack length is reached. Moreover, over the years, the weight and number of heavy vehicles has been rapidly growing, adding to the non-linearity of damage

accumulation. As follows, it is assumed that a linear approximation of damage accumulation is on the conservative side.

The analysed fatigue life values are 5, 10, 15, 20, 25 and 30 years. The damages for the critical details are scaled, and the reduction of hot spot stresses required to reach $D_{new} =< 1$ is obtained for each fatigue life target. Figure 6.1 visualises these hot spot stress reduction requirements. By comparing these requirements with the hot spot stress reductions obtained from various strengthening schemes (see Section 5.4), it can be identified which schemes meet the fatigue life extension target.
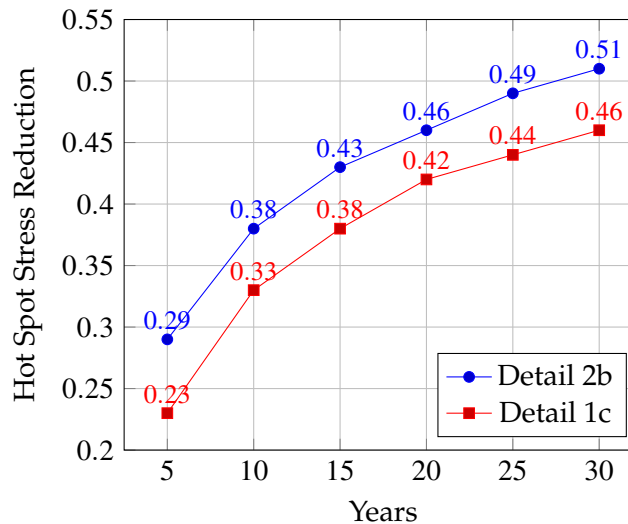
Figure 6.1: Hot Spot Stress Reduction vs. Additional Fatigue Life

Detail 2b

Table 5.5 from Chapter 5 presents the achievable hot spot stress reductions for *detail 2b*, using strengthening schemes with M16 blind bolts spaced 100 mm longitudinally. These results are evaluated against the required stress reductions derived in Figure 6.1 to determine which strengthening schemes meet specific fatigue life targets. The corresponding findings are summarised in Table 6.1.

Fatigue Life (years)	Min. Plate Thickness (mm)	Possible Configurations
5	10	2x1, 3x0, 2x2, 3x1, 3x2, 2x3, 3x3
10	12	3x0, 2x2, 3x1, 3x2, 2x3, 3x3
15	14	all
20	14	3x1, 3x2, 2x3, 3x3
25	16	all
30	16	2x1, 1x2, 3x0, 2x2, 3x1, 1x3, 3x2, 2x3, 3x3

Table 6.1: Minimum plate thickness and possible configurations for different fatigue life requirements: *detail 2b*.

The analysis shows that a 10 mm strengthening plate provides sufficient hot spot stress reduction to gain fatigue life of 5 years, whereas a minimum thickness of 16 mm is required to

achieve a fatigue life extension of 25 to 30 years. For the maximum considered time period of 30 years, increasing the plate thickness beyond 16 mm does not yield further benefits. However, if achieving a longer fatigue life gain than 30 years is desired, larger plate thicknesses may become beneficial. Furthermore, the table highlights the most efficient bolt configurations for each fatigue life category. In most cases, the optimal solutions, i.e. those that achieve the required fatigue life with the lowest hot spot stress reduction, involve placing bolts inside the troughs, highlighting the advantage of the use of blind bolts in the strengthening.

Detail 1c

For *detail 1c*, the hot spot stress reduction that can be achieved with strengthening schemes containing M16 bolts with 100 mm spacing are given in Table 5.6. Similarly, the reduction factors are evaluated against the requirements found for different fatigue life extension categories, resulting in proposed strengthening configurations per fatigue life target. Table 6.2 summarises the results.

In contrast to *detail 2b*, *detail 1c* requires a larger plate thickness of 14 mm to achieve a fatigue life gain of 5 years. For an increased service life of 30 years, *detail 1c* needs to be strengthened with an 18 mm thick plate. It is noticeable that the required plate thickness is higher for *detail 1c* compared to *detail 2b*, indicating that strengthening *detail 1c* requires a higher material investment to achieve similar fatigue life targets.

Fatigue Life (years)	Min. Plate Thickness (mm)	Possible Configurations
5	14	all
10	14	2x2, 3x1, 3x2, 2x3, 3x3
15	16	all, except for 1x0
20	16	1x1, 0x2, 2x1, 1x2, 0x3, 2x2, 3x1, 1x3, 3x2, 2x3, 3x3
25	16	3x1, 3x2, 2x3, 3x3
30	18	all

Table 6.2: Minimum plate thickness and possible configurations for different fatigue life requirements: *detail 1c*.

To summarise, the fatigue assessment of the Second Van Brienenoord Bridge deck resulted in damage estimates of 33.8 for *detail 2b* and 22.3 for *detail 1c*, corresponding to 30 years of usage. Strengthening schemes were evaluated on how much fatigue life they can achieve, resulting in a list of proposed strengthening configurations for different fatigue life categories (5 to 30 years). For *detail 2b*, a 10 mm strengthening plate is sufficient for 5 additional years of fatigue life, while a minimum of 16 mm is needed for 25–30 years. However, *detail 1c* requires 14 mm for 5 years and 18 mm for 30 years, indicating a higher material investment than *detail 2b*. The most efficient configurations often involve placing bolts inside troughs, utilising the advantage of blind bolts.

6.2. Static verifications of strengthening schemes

In addition to fatigue assessments, static verifications were conducted to ensure that the strengthening schemes can withstand ultimate limit state conditions. This is crucial, as premature failure of the strengthening should be prevented. This section presents the results from the static verifications performed for the strengthening schemes selected in Section 5.4.

The verification process included assessing the slip capacity of the bolts under two loading

conditions:

- **Temperature loading**: Perimeter bolts at the edges of the strengthening plate experience high shear forces due to thermal loading. A uniform temperature of 10 degrees Celsius is applied to the strengthening plate.

- **LM2 loading**: Verifying that the bolts can sustain high shear forces due to heavy vehicle tire. A single wheel load of 200 kN is applied on most critical position.

The bolts are verified in Ultimate Limit State, according to the following Unity Check (Equation 6.2). For the material factor, $\gamma_{M3} = 1.25$ is assumed, to be on the conservative side, as there is uncertainty regarding the preload, and thus slip capacity, of Hollo-Bolts. For the loading factor, $\gamma_F = 1.5$ is used, as both thermal and vehicle loading are variable loading conditions. The shear force V_{Ed} is the maximum shear force occurring in the bolts, and is found as $\sqrt{V_{Ed_x}^2 + V_{Ed_y}^2}$.

$$\frac{V_{Ed} \cdot \gamma_F}{F_{slip}/\gamma_{M3}} \leq 1.0 \qquad (6.2)$$

Temperature loading
The temperature loading was found to be more critical for both *detail 2b* and *detail 1c* compared to the loading according to Load Model 2, resulting in unity checks in the range of 0.63 to 1.41. Tables 6.3 and 6.4 present the findings, with the unity checks higher than 1.00 marked red. The results are similar for *detail 2b* and *detail 1c*, which is expected, as the strengthening plates are of the same size.

Table 6.3: Unity Checks for shear in bolts due to temperature loading: *detail 2b*

Thickness	1x0	0x1	1x1	2x0	0x2	2x1	1x2	3x0	0x3	2x2	3x1	1x3	3x2	2x3	3x3
10	1.10	1.05	0.97	0.88	0.86	0.80	0.88	0.73	0.74	0.75	0.84	0.82	0.66	0.72	0.64
12	1.18	1.13	1.05	0.95	0.92	0.86	0.95	0.79	0.80	0.81	0.79	0.89	0.71	0.77	0.69
14	1.26	1.19	1.11	1.00	0.97	0.91	1.01	0.84	0.84	0.86	0.73	0.95	0.76	0.82	0.73
16	1.32	1.24	1.16	1.05	1.01	0.96	1.06	0.89	0.89	0.90	0.70	1.00	0.80	0.86	0.77
18	1.37	1.28	1.21	1.09	1.05	1.00	1.11	0.92	0.92	0.94	0.69	1.04	0.83	0.90	0.80
20	1.41	1.32	1.25	1.12	1.08	1.03	1.15	0.95	0.95	0.97	0.68	1.08	0.86	0.93	0.83

Table 6.4: Unity Checks for shear in bolts due to temperature loading: *detail 1c*

Thickness	1x0	0x1	1x1	2x0	0x2	2x1	1x2	3x0	0x3	2x2	3x1	1x3	3x2	2x3	3x3
10	1.09	1.06	0.96	0.87	0.87	0.79	0.87	0.73	0.73	0.74	0.68	0.81	0.65	0.71	0.63
12	1.18	1.13	1.04	0.93	0.93	0.85	0.94	0.79	0.79	0.80	0.74	0.88	0.71	0.76	0.68
14	1.25	1.20	1.10	0.99	0.98	0.90	1.00	0.84	0.84	0.85	0.79	0.93	0.75	0.81	0.73
16	1.31	1.25	1.16	1.04	1.03	0.95	1.05	0.88	0.88	0.89	0.82	0.98	0.79	0.85	0.76
18	1.36	1.29	1.20	1.08	1.06	0.98	1.09	0.91	0.92	0.92	0.86	1.02	0.82	0.88	0.79
20	1.41	1.33	1.24	1.11	1.10	1.02	1.13	0.94	0.95	0.96	0.89	1.06	0.85	0.91	0.82

The most susceptible bolts are the ones located on the edges of the strengthening plate, as can be noticed in Figure 6.2, where the shear forces in y direction are displayed (transverse direction with respect to the troughs). Moreover, strengthening schemes with larger thicknesses of the strengthening plate are more sensitive to thermal loading, as the thermal expansion difference grows with increasing thickness. This leads to higher stresses at the interface between the plates, which in turn produces greater forces in the connecting bolts. As a result, half of the strengthening schemes with a 20 mm thickness do not satisfy the verification.
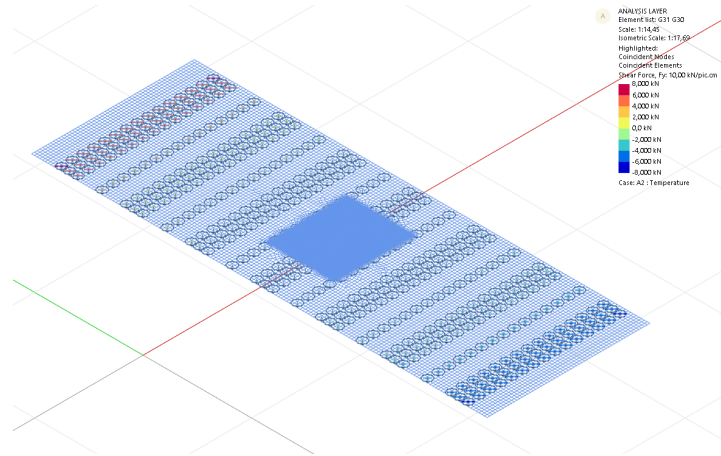
Figure 6.2: Shear forces due to temperature loading in strengthening scheme with 3x1 configuration: *detail 2b*.

However, the unity checks which are above 1 can be mitigated: by adding more bolts close to the edges of the strengthening plate. Since the high shear forces are concentrated in those regions, it is advised to apply a larger amount of bolts in close proximity to the edge, e.g. three bolts. This is assumed to satisfy the verifications, as all bolt configurations with three bolts had unity checks under 1.

Loading according to LM2
The shear bolts can sustain the vehicle loading according to Load Model 2. For *detail 2b*, the most critical positioning of the wheel was found in the centre of the trough in longitudinal direction, and moved 50 mm in the transverse direction. For *detail 1c*, the critical position of the wheel is centrally above the trough in transverse direction and moved 30 mm in longitudinal direction away from the cross beam. For both critical details, the unity checks were found to be under 1 for all considered strengthening schemes. The outcomes of the Load Model 2 verifications are given in Appendix E. Note that the model is optimised for the fatigue loading, especially in terms of hybrid interaction between the plates, realised by applying axial springs on locations where cooperation is expected. This should be taken into account when interpreting the results of the LM2 verification.

6.3. Final strengthening scheme selection

In this section, the critical details are combined in a unified design, in order to quantify the trade-off between fatigue life, weight of strengthening, and the installation time of different strengthening schemes. A single plate thickness is selected per solution, while keeping the bolt configuration separate per critical detail. It is assumed that the transition between the two details occurs at 0.75 m from the cross beam, as this was found to be a sufficiently large strengthening region for *detail 1c*. On the other hand, *detail 2b* can occur anywhere between two cross beams, and will cover a larger region of the vehicle lane, with a length of 2.145 m per section. It is assumed 15 bolt rows are needed for *detail 1c* in longitudinal direction and 22 bolt

rows for *detail 2b*, taking into account a spacing of 100 mm.

A selection is made of strengthening schemes with different fatigue life estimates, strengthening plate thicknesses and bolt configurations. For each strengthening scheme, the weight is estimated and installation time predicted. The calculations are based on a 30 m2 area of the heavy vehicle lane, assuming that the width of lane is 3 metres.

Weight of strengthening
The strengthening solution consists of steel plates and Hollo-Bolts. The weight is calculated with Equation 6.3, assuming that the contribution of the steel plate is much more significant than of the bolts, thus not including the latter in the calculation. The density of steel is assumed to be $7850 kg/m^3$.

$$W = \rho_s A_p t_p \tag{6.3}$$

where:

- W = total weight of strengthening solution [kg]
- ρ_s = density of steel [kg/m^3]
- A_p = area of strengthening plate [$m3$]
- t_p = thickness of strengthening plate [m]

Installation time
The prediction of the installation time is performed based on the Second Van Brienenoord bridge strengthening [5], using the time estimates made there. Due to the strengthening consisting of only two components, the installation is quite straightforward. Firstly, the top layer is removed from the bridge deck and the deck cleaned, after which waterjetting and gritblasting is performed. For the Suurhoff bridge, it was found that 53 hours were needed for these activities for an area of 3000 m2. These procedures are the same for each strengthening scheme, and are not included in the comparison. The following assumptions are made [5]:

- **Marking bolt holes**: 250 bolt holes per hour
- **Drilling holes**: 150 bolt holes per hour
- **Clean drilling oil**: entire area in 1 hour
- **Sandblasting**: entire area in 1 hour
- **Painting**: 12m2 per hour
- **Drying of paint**: 2h
- **Install plates**: 10 min per plate
- **Install bolts**: 5 bolts per minute

Important to note is that these estimates assume that some activities can be performed in parallel, assuming multiple working teams, which may differ in reality depending on the availability and resources of the contractor. Moreover, as these estimations do not include the initial cleaning and preparation of the deck, the final installation time estimates are optimistic and serve primarily for comparison between strengthening alternatives.

As can be noticed, the number of bolts is crucial for the installation time, while the strengthening plate mainly contributes to the additional weight added on the bridge deck. With all the

above-mentioned assumptions considered, the approximations of installation time and weight are performed. Table 6.5 summarises the findings. The bolt configurations annotated with a * do not satisfy the ultimate limit state verifications, as shown in previous section. However, it is assumed that this can be mitigated with adjustments to the bolt configuration, by increasing the bolt density in the most critical areas: on the edges of the strengthening plate.

The calculated installation time ranges from 10 to 18.5h, indicating a difference of 8 hours between the alternatives with lowest and highest installation time. The additional weight added to the bridge deck differs from 3297 kg to 4710 kg, increasing linearly with a larger plate thickness. If a longer fatigue life is desired, the strengthening concept with a 18 mm plate, 1x0 bolt configuration for *detail 2b* and 1x1 configuration for *detail 2b* stands out, providing a lower installation time compared to its alternatives: 11.5 hours. Interestingly, some of the strengthening schemes that achieve lower fatigue life, e.g. 5 years, score worse in terms of installation time compared to the longer fatigue life options, due to the higher number of bolts required. While these values are approximations, they provide a baseline for comparison between strengthening schemes.

Strengthening Configuration				Design Objectives		
Conf 2b	Conf 1c.	Bolt	Plate (mm)	Life (yrs)	Weight (kg)	Install Time [h]
1x1*	2x2	M16	14	5	3297	15
2x2	3x3	M16	16	25	3768	18.5
1x1*	3x0	M16	18	30	4239	14
2x2	3x1	M16	14	10	3297	18
1x0*	1x1*	M16	18	30	4239	11.5
2x1	1x1*	M16	16	20	3768	14.5
2x0*	2x0*	M16	16	20	3768	13
0x1*	1x0*	M16	14	5	3297	10
2x0*	1x1*	M16	16	15	3768	13
1x1*	1x1*	M16	20	30	4239	13

Table 6.5: Proposed Strengthening Configurations. Weight and Installation Time approximated for 30 m2 area.

7

Conclusions

In this thesis, the effectiveness of strengthening orthotropic steel decks using blind bolted steel plates was evaluated through numerical modelling. The primary research question was to determine the extent to which such a strengthening solution can contribute to extending the fatigue life of orthotropic steel decks. The research was conducted for a single case study, the Second Van Brienenoord bridge deck, for which two critical details were considered: *detail 2b*, located in the trough to deck plate joint with a crack forming in the weld, and *detail 1c*, located in the joint between trough, deck plate and cross beam, with a crack growing in the deck plate. The design incorporated Hollo-Bolts, assumed to achieve 50% of the preload of standard bolts.

A finite element model was developed to assess various strengthening schemes and observe their effect on hot spot stress reduction. The five design parameters considered were the plate thickness, bolt size, bolt row spacing, number of bolt rows, and transverse bolt configuration. A selection of strengthening schemes was evaluated based on fatigue life extension, ULS verifications, weight, and installation time.

The main conclusions of the research are presented here:

1. Hot spot stress reduction up to 61% is achievable with the application of blind-bolted steel plate strengthening.

2. The strengthening concept is more effective for *detail 2b* compared to *detail 1c*, particularly when strengthening plates of smaller thicknesses are used.

3. The thickness of the strengthening plate is the most influential design parameter for reducing hot spot stresses. For *detail 2b*, the transverse bolt configuration is second most important, whereas for *detail 1c*, it is the number of bolt rows.

4. The bolt configuration has higher impact on the hot spot stress reduction of *detail 1c* compared to *detail 2b*.

5. The strengthening design is viable for both short-term and long-term strengthening of orthotropic steel decks, with plate thicknesses ranging from 10 mm to 18 mm depending on the targeted fatigue life extension and detail location.

6. The strengthening design allows for multiple bolt configurations, offering flexibility in application, and can be adjusted to conform to temperature verifications in ultimate limit state.

7. A balance can be achieved between plate thickness, bolt quantity, weight of the strengthening, and installation time. Increasing plate thickness reduces the number of bolts required, thereby shortening installation time, at the expense of additional structural weight.

8. The Hollo-Bolt is identified as the most suitable blind bolt type for strengthening of orthotropic steel decks, owing to its availability on the market, ease of assembly, and suitability for countersunk installations.

8
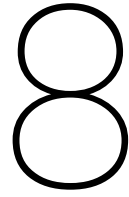
Recommendations

This chapter provides recommendations based on the findings of this thesis. The potential of blind bolted steel plates for extending the fatigue life of orthotropic steel decks has been demonstrated, but several aspects require further investigation to reduce uncertainties and validate the assumptions made in this study. The following recommendations are structured into three categories: experimental testing, additional analysis, and practical implications.

8.1. Experimental testing

Experimental testing is essential to validate the assumptions made in this study and reduce uncertainties related to the mechanical behaviour of the proposed strengthening solution.

8.1.1. Bolt properties: preload and slip resistance

One of the main sources of uncertainty is the preload and slip resistance of the Hollo-Bolt, which directly influence the hybrid interaction between the strengthening plate and the deck. As discussed in Section 2.3, experimental data show wide variation in preload values for Hollo-Bolts, ranging from 3% to 83% of the preload of a standard slip-resistant bolt. Although the High Clamping Force (HCF) mechanism can improve performance, particularly for M16 and M20 bolts, over-torquing can lead to premature failure. In this thesis, a 50% preload reduction was applied.

Laboratory testing should be conducted to quantify the actual preload and slip capacity of the Hollo-Bolt. Preload can be assessed by applying torque and measuring the resulting axial force in the bolt. Slip resistance should be evaluated using bending tests, such as three-point bending, on sections of the deck plate with the strengthening plate attached. These tests can determine the maximum shear force that can be sustained before a critical slip displacement is reached.

Both hexagonal and countersunk head Hollo-Bolts should be tested, as current data are based exclusively on the hexagonal type. If preload or slip resistance proves insufficient, bolt geometry may need to be modified, as indicated in Section 2.3, where improved preload was achieved through bolt design modifications.

8.1.2. Validation of results from numerical modelling

To confirm the reliability of the finite element model and the predicted hot spot stresses of the critical details, experimental validation is recommended. A physical segment of the deck

plate and a single trough, with the strengthening plate bolted on, should be fabricated. Either full-scale or scaled segments can be used. A patch load simulating a single wheel is applied, and strain gauges placed at the extrapolation points to measure strain responses. These can then be converted to hot spot stresses and compared to the numerical results.

8.2. Additional analysis

Further analysis is necessary to improve the accuracy of the fatigue life predictions and to broaden the applicability of the proposed strengthening method.

8.2.1. Fatigue assessment and damage calculation

In this thesis, fatigue performance was evaluated by comparing hot spot stresses under a single critical wheel load, and fatigue life was estimated based on simplified assumptions. Additionally, the damages that were considered in this simplified calculation were based on past data (1990 - 2019) and future increases in heavy traffic not taken into account.

Instead, a complete fatigue assessment according to Eurocode, as described in Section 2.1.3, should be performed, including multiple vehicle types and loading scenarios, stress history analysis, and damage accumulation calculations. A comprehensive assessment would yield more reliable fatigue life predictions.

8.2.2. Application to different geometry and critical details

The current analysis was limited to a single case study bridge deck and two critical details (*detail 2b* and *detail 1c*). Although the strengthening proved effective for these locations, further research is needed to assess its performance on bridge decks with different geometries (such as discontinuous longitudinal stiffeners) or other fatigue-critical details. The *ROK* identifies over 20 critical details that may require strengthening. Investigating these would involve developing additional finite element models and tailoring the strengthening design to each case.

8.3. Implementation and practical considerations

Assuming that a complete fatigue assessment has been carried out and the strengthening solution has been deemed effective for a specific bridge deck, this section outlines the practical considerations necessary for implementation. These recommendations are particularly relevant for infrastructure owners such as Rijkswaterstaat, who may consider applying the strengthening concept in practice.

Further work is required to address aspects related to execution, durability, and integration with existing structures. The following subsections highlight key aspects that must be investigated or developed to enable safe and effective implementation.

8.3.1. Interaction between the strengthening and deck

The effectiveness of the strengthening solution depends heavily on the interaction between the steel plate and the orthotropic steel deck. This study assumes ideal conditions, where the plates and deck surfaces are flat and in full contact. In reality, variations in deck flatness, local unevenness, or manufacturing tolerances may cause gaps between the plate and the deck. This may prevent the bolts from achieving full preload or lead to uneven contact pressures.

It is recommended to investigate whether the bolts can draw the plate into contact during installation, or if additional measures such as epoxy mid-layers are required. Potentially, compressible interlayers could be applied, but they require validation for long-term fatigue performance.

8.3.2. Applicability for emergency repair

This study focused on one heavy traffic lane and considered strengthening applied over the whole lane area. To be able to apply the feasibility of this strengthening concept as an emergency repair solution, further investigation into smaller strengthening plate sizes is required, focusing on localised fatigue damage mitigation rather than full lane coverage.

8.3.3. Durability

Environmental durability is another important aspect. Entry of moisture through bolt holes or between plates may lead to corrosion, especially since the steel plates are covered with asphalt, which can be porous or trap water.

References

[1]   F.B.P. de Jong. "Renovation techniques for fatigue cracked orthotropic steel bridge decks". PhD thesis. Delft: TU Delft, 2006. URL: https://repository.tudelft.nl/record/uuid: 239bdb2c-b59f-40d2-91b7-367139dbad13 (visited on 10/01/2024).

[2]   Dan Snyder. *Steel Orthotropic Decks*. en. May 2020. URL: https://www.shortspansteelbr idges.org/steel-orthotropic-decks/ (visited on 03/26/2025).

[3]   H.H. Snijder and B.H. Hesselink. "Repair, strengthening and upgrading of steel bridges in The Netherlands". In: (Jan. 2017). DOI: 10.2749/vancouver.2017.1177. URL: https: //doi.org/10.2749/vancouver.2017.1177.

[4]   M.H. Kolstein. "Fatigue Classification of Welded Joints in Orthotropic Steel Bridge Decks". PhD thesis. TU Delft, 2007.

[5]   MC Renovatie Bruggen, R. Gibson, and M. Rikken. *2e van Brienenoordbrug: Alternative Fatigue Strengthening*. June 2018.

[6]   MC Renovatie Bruggen et al. *Existing Suurhoff Bridge: Lifting bridge deck strengthening*. Mar. 2021.

[7]   *Material Fatigue Definition*. URL: https://www.comsol.com/multiphysics/material-fatigue (visited on 02/16/2025).

[8]   Jaap Schijve. *Fatigue of Structures and Materials*. Second Edition. Delft: Springer, 2009.

[9]   A. Hobbacher. *Recommendations for Fatigue Design of Welded Joints and Components*. Dec. 2008.

[10] *NEN-EN 1993-1-9+C2 - Eurocode 3: Design of steel structures - Part 1-9: Fatigue*. Sept. 2012.

[11] Hesham Abdelbaset and Zhiwen Zhu. "Behavior and fatigue life assessment of orthotropic steel decks: A state-of-the-art-review". In: *Structures* 60 (Feb. 2024), p. 105957. ISSN: 2352-0124. DOI: 10.1016/j.istruc.2024.105957. URL: https://www.sciencedirect.com/ science/article/pii/S2352012424001097 (visited on 10/01/2024).

[12] Rijkswaterstaat. *RTD 1001 Engineering Design Guidelines*. Jan. 2021.

[13] Mustafa Aygül, Mohammad Al-Emrani, and Shota Urushadze. "Modelling and fatigue life assessment of orthotropic bridge deck details using FEM". In: *International Journal of Fatigue* 40 (July 2012), pp. 129–142. ISSN: 0142-1123. DOI: 10.1016/j.ijfatigue.2011.12. 015. URL: https://www.sciencedirect.com/science/article/pii/S01421123110034 34 (visited on 10/26/2024).

[14] Robert J. Connor. *Manual for Design, Construction, and Maintenance of Orthotropic Steel Deck Bridges*. English. Tech. rep. FHWA-IF-12-027. Jan. 2012. URL: https://rosap.ntl. bts.gov/view/dot/41395 (visited on 10/01/2024).

[15] A. Romeijn. *Steel Bridges Dictaat deel I*. Faculty of Civil Engineering and Geosciences, Oct. 2006.

[16] *NEN-EN 1991-2+C1 - Eurocode 1: Actions on structures - Part 2: Traffic loads on bridges*. Oct. 2015.

[17] Zhiwen Zhu, Ze Xiang, and Y. Edward Zhou. "Fatigue behavior of orthotropic steel bridge stiffened with ultra-high performance concrete layer". en. In: *Journal of Constructional Steel Research* 157 (June 2019), pp. 132–142. ISSN: 0143974X. DOI: 10.1016/j.jcsr.2019.02.025. URL: https://linkinghub.elsevier.com/retrieve/pii/S0143974X1830779X (visited on 10/02/2024).

[18] Haohui Xin et al. "Strengthening effects evaluation on fatigue damage of rib to deck joint in orthotropic steel deck". In: *Engineering Failure Analysis* 145 (Mar. 2023), p. 107041. ISSN: 1350-6307. DOI: 10.1016/j.engfailanal.2022.107041. URL: https://www.sciencedirect.com/science/article/pii/S1350630722010081 (visited on 10/02/2024).

[19] Sofia Teixeira De Freitas, Henk Kolstein, and Frans Bijlaard. "Composite bonded systems for renovations of orthotropic steel bridge decks". en. In: *Composite Structures* 92.4 (Mar. 2010), pp. 853–862. ISSN: 02638223. DOI: 10.1016/j.compstruct.2009.09.016. URL: https://linkinghub.elsevier.com/retrieve/pii/S0263822309003547 (visited on 10/02/2024).

[20] Xudong Wang et al. "Experimental study on fatigue behavior of cracked steel plates repaired with adhesively bonded steel patches". en. In: *Structures* 56 (Oct. 2023), p. 104915. ISSN: 23520124. DOI: 10.1016/j.istruc.2023.104915. URL: https://linkinghub.elsevier.com/retrieve/pii/S2352012423010056 (visited on 10/02/2024).

[21] *The Huyett Guide to Nuts and Bolts*. URL: https://www.huyett.com/blog/nuts-and-bolts (visited on 10/01/2024).

[22] Bruno Pedrosa, Linda Bücking, and Milan Veljkovic. "Steel-reinforced resin for bolted shear connectors: Confined behaviour under quasi-static cyclic loading". In: *Engineering Structures* 256 (Apr. 2022), p. 114023. ISSN: 0141-0296. DOI: 10.1016/j.engstruct.2022.114023. URL: https://www.sciencedirect.com/science/article/pii/S0141029622001699 (visited on 10/01/2024).

[23] *What are the different types of nuts and bolts?* en-us. URL: https://www.essentracomponents.com/en-us/news/solutions/fastening-components/what-are-the-different-types-of-nuts-and-bolts (visited on 04/06/2025).

[24] Mike Manor. "HSS Blind Structural Fasteners". en-US. In: *Steel Tube Institute* (May 2021). Running Time: 116. URL: https://steeltubeinstitute.org/resources/hss-blind-structural-fasteners/ (visited on 10/01/2024).

[25] Y.L. Li, T.M. Chan, and X.L. Zhao. "Review on blind bolted connections to concrete-filled steel tubes". en. In: *Thin-Walled Structures* 183 (Feb. 2023), p. 110444. ISSN: 02638231. DOI: 10.1016/j.tws.2022.110444. URL: https://linkinghub.elsevier.com/retrieve/pii/S026382312200996X (visited on 10/01/2024).

[26] *Hollo-Bolt*. en. URL: https://www.lindapter.com/product-category/hollo-bolt-solutions-safe-secure-steel-connections (visited on 10/01/2024).

[27] Xing Gao et al. "A novel slip-critical blind bolt: Experimental studies on shear, tensile and combined tensile–shear resistances". en. In: *Thin-Walled Structures* 170 (Jan. 2022), p. 108630. ISSN: 02638231. DOI: 10.1016/j.tws.2021.108630. URL: https://linkinghub.elsevier.com/retrieve/pii/S0263823121006868 (visited on 10/02/2024).

[28] Chuqi Wan et al. "Mechanical performance of novel steel one-sided bolted joints in shear". en. In: *Journal of Constructional Steel Research* 165 (Feb. 2020), p. 105815. ISSN: 0143974X. DOI: 10.1016/j.jcsr.2019.105815. URL: https://linkinghub.elsevier.com/retrieve/pii/S0143974X19310934 (visited on 10/03/2024).

[29] Shenggang Fan et al. "Experimental study of self-tightening high-strength single-side bolted joints under low cyclic loading". In: *Engineering Structures* 311 (July 2024), p. 118180. ISSN: 0141-0296. DOI: 10.1016/j.engstruct.2024.118180. URL: https://www.scienced irect.com/science/article/pii/S0141029624007429 (visited on 11/03/2024).

[30] John E France, J Buick Davison, and Patrick A Kirby. "Strength and rotational stiffness of simple connections to tubular columns using flowdrill connectors". In: *Journal of Constructional Steel Research* 50.1 (Apr. 1999), pp. 15–34. ISSN: 0143-974X. DOI: 10.1016/ S0143-974X(98)00236-3. URL: https://www.sciencedirect.com/science/article/ pii/S0143974X98002363 (visited on 11/03/2024).

[31] Yusak Oktavianus, Helen M. Goldsworthy, and Emad F. Gad. "Cyclic behaviour of individual double headed anchored blind bolts within CFST". In: *Journal of Constructional Steel Research* 133 (June 2017), pp. 522–534. ISSN: 0143-974X. DOI: 10.1016/j.jcsr.2017. 03.004. URL: https://www.sciencedirect.com/science/article/pii/S0143974X163 03704 (visited on 11/03/2024).

[32] Y. Liu, C. Málaga-Chuquitaype, and A. Y. Elghazouli. "Response and component characterisation of semi-rigid connections to tubular columns under axial loads". In: *Engineering Structures* 41 (Aug. 2012), pp. 510–532. ISSN: 0141-0296. DOI: 10.1016/j. engstruct.2012.03.061. URL: https://www.sciencedirect.com/science/article/ pii/S0141029612001861 (visited on 10/01/2024).

[33] constructionAdmin. *High Clamping Force Hollo-Bolt for Structural Connections*. en-GB. June 2013. URL: https://constructionmanagement.co.uk/high-clamping-force-hollo-bolt-structural-connecti/ (visited on 10/02/2024).

[34] A.Y. Elghazouli et al. "Experimental monotonic and cyclic behaviour of blind-bolted angle connections". en. In: *Engineering Structures* 31.11 (Nov. 2009), pp. 2540–2553. ISSN: 01410296. DOI: 10.1016/j.engstruct.2009.05.021. URL: https://linkinghub.elsevier.com/ retrieve/pii/S0141029609001990 (visited on 10/02/2024).

[35] Wei Wang et al. "Cyclic behavior of endplate connections to tubular columns with novel slip-critical blind bolts". en. In: *Engineering Structures* 148 (Oct. 2017), pp. 949–962. ISSN: 01410296. DOI: 10.1016/j.engstruct.2017.07.015. URL: https://linkinghub. elsevier.com/retrieve/pii/S0141029617308131 (visited on 10/02/2024).

[36] Jia Wang et al. "Fatigue behaviour of stainless steel bolts in tension and shear under constant-amplitude loading". en. In: *International Journal of Fatigue* 133 (Apr. 2020), p. 105401. ISSN: 01421123. DOI: 10.1016/j.ijfatigue.2019.105401. URL: https://link inghub.elsevier.com/retrieve/pii/S0142112319305055 (visited on 10/03/2024).

[37] Yanzhi Liu et al. "Fatigue behaviour of blind bolts under tensile cyclic loads". en. In: *Journal of Constructional Steel Research* 148 (Sept. 2018), pp. 16–27. ISSN: 0143974X. DOI: 10.1016/j.jcsr.2018.05.019. URL: https://linkinghub.elsevier.com/retrieve/ pii/S0143974X17307794 (visited on 10/03/2024).

[38] *Hollo-Bolt Countersunk Head Safe Working Loads*. 2024.

[39] Wei Wang et al. "Progressive collapse behaviour of extended endplate connection to square hollow column via blind Hollo-Bolts". en. In: *Thin-Walled Structures* 131 (Oct. 2018), pp. 681–694. ISSN: 02638231. DOI: 10.1016/j.tws.2018.07.043. URL: https://linkinghub.elsevier.com/retrieve/pii/S0263823118304452 (visited on 10/03/2024).

[40] *Experimental study on tensile behavior of blind bolt - Jiang - 2021 - ce/papers - Wiley Online Library*. URL: https://onlinelibrary.wiley.com/doi/abs/10.1002/cepa.1268 (visited on 04/08/2025).

[41] Olivia Mirza, Milner L, and Mashiri F. "Experimental Investigation of Retrofitting Techniques for Steel Bridge Girders Subject to Fatigue Failure". en. In: *Journal of Steel Structures & Construction* 04.01 (2018). ISSN: 24720437. DOI: 10.4172/2472-0437.1000138. URL: https://www.omicsonline.org/open-access/experimental-investigation-of-retrofitting-techniques-for-steel-bridge-girders-subject-to-fatigue-failure-2472-0437-1000138-98103.html (visited on 10/02/2024).

[42] J. Lee, H.M. Goldsworthy, and E.F. Gad. "Blind bolted T-stub connections to unfilled hollow section columns in low rise structures". en. In: *Journal of Constructional Steel Research* 66.8-9 (Aug. 2010), pp. 981–992. ISSN: 0143974X. DOI: 10.1016/j.jcsr.2010.03.016. URL: https://linkinghub.elsevier.com/retrieve/pii/S0143974X10000982 (visited on 10/03/2024).

[43] Seyedeh Maryam Hosseini et al. "Behaviour of blind bolt shear connectors subjected to static and fatigue loading". In: *Engineering Structures* 214 (July 2020), p. 110584. ISSN: 0141-0296. DOI: 10.1016/j.engstruct.2020.110584. URL: https://www.sciencedirect.com/science/article/pii/S0141029619334480 (visited on 10/03/2024).

[44] Gerhard Olivier et al. "Feasibility of bolted connectors in hybrid FRP-steel structures". en. In: *Construction and Building Materials* 383 (June 2023), p. 131100. ISSN: 09500618. DOI: 10.1016/j.conbuildmat.2023.131100. URL: https://linkinghub.elsevier.com/retrieve/pii/S0950061823008127 (visited on 10/03/2024).

[45] *NexGen2® Structural Blind Bolt Assembly*. en. URL: https://www.allfasteners.com.au/nexgen2-structural-blind-bolt-assembly (visited on 10/03/2024).

[46] Lichen Yang et al. "Shear performance of elliptical head one-sided bolt double-lapped joint with plug-in gasket". In: *Structures* 60 (Feb. 2024), p. 105809. ISSN: 2352-0124. DOI: 10.1016/j.istruc.2023.105809. URL: https://www.sciencedirect.com/science/article/pii/S2352012423018970 (visited on 10/03/2024).

[47] Weitong Yi et al. "Experimental and numerical study on mechanical performance of single shear bolted connections with novel elliptical one-sided bolts". In: *Structures* 62 (Apr. 2024), p. 106223. ISSN: 2352-0124. DOI: 10.1016/j.istruc.2024.106223. URL: https://www.sciencedirect.com/science/article/pii/S2352012424003758 (visited on 10/03/2024).

[48] *Verdwijnt brugwachtershuisje van de Van Brienenoordbrug?* nl. URL: https://dagblad010.nl/Politiek/verdwijnt-brugwachtershuisje-van-de-van-brienenoordbrug (visited on 03/02/2025).

[49] Jan van Helleman. *Van Brienenoordbrug Rotterdam - grootste brug Nederland*. nl-NL. Oct. 2014. URL: https://nieuws.top010.nl/van-brienenoordbrug-rotterdam.htm (visited on 10/11/2024).

[50] MC Renovatie Bruggen and R. Gibson. *Van Brienenoordbrug: Design Basis for Local Fatigue Assessment*. Aug. 2013.

[51] van de Graaf. *Technical drawing - bridge deck Second Van Brienenoord bridge*. Jan. 1986.

[52] MC Renovatie Bruggen and D. Tjepkema. *Van Brienenoordbrug: Phase 2 Assessment*. Jan. 2017.

[53] A.H.J.M. Vervuurt. *NEN 8703 RBK Staal Startdocument*. Delft, 2017.

[54] *NEN-EN 1993-1-8+C2/NB - National Annex to NEN-EN 1993-1-8 Eurocode 3: Design of steel structures - Part 1-8: Design of joints (includes C2:2009)*. Dec. 2011.

[55] *NEN-EN 1090-2 - Execution of steel structures and aluminium structures - Part 2: Technical requirements for steel structures*. Aug. 2018.

[56] *NEN-EN 1993-2+C1 - Eurocode 3: Design of steel structures - Part 2: Steel bridges*. Dec. 2011.

[57] *Hollo-Bolt Hexagonal Head Safe Working Loads*. 2024.

A
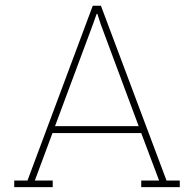
Second van Brienenoord Bridge Deck: Additional Information

A.1. Technical drawing

The technical drawing of the Second Van Brienenoord bridge deck is provided below.

Figure A.1: Second Van Brienenoord bridge deck [51]

B

Bolt Properties

B.1. Minimum spacings

Symbol	Minimum spacing	M8	M10	M12	M16	M20
e_1	$\geq 1,5d$	12	15	18	24	30
e_2	$\geq 1,5d$	12	15	18	24	30
p_1	$\geq 2,5d$	20	25	30	40	50
p_2	$\geq 2,5d$	20	25	30	40	50

Table B.1: Minimum spacings for structures exposed to fatigue loading [10]

B.2. Hollo-Bolt properties from manufacturer

Hexagonal Head Data ···
(Available in sizes M8, M10, M12, M16 & M20)

Collar

High Clamping Force Mechanism (sizes M16 and M20)

Cone (Interlocking grooves prevent loosening)

Sleeve (Expands during installation)

Bolt

High Clamping Force Mechanism (sizes M16 and M20)

Material: Carbon steel or stainless steel (see page 41 for corrosion protection options).

							Collar			Safe Working Loads (Factor of Safety 5:1)	
Product Code	Bolt Ø Z	Height H mm	Length B (max) mm	Clamping Thickness W mm	Outer Ply min t mm	Sleeve Outer Ø S mm	Ø D mm	A/F mm	Tightening Torque Nm	Tensile kN	Single Shear kN
HB08-1	M8	10.5	45	3 - 22	-	13.75	22	19	23	4.0	5.0
HB08-2	M8	10.5	65	22 - 41	-	13.75	22	19	23	4.0	5.0
HB08-3	M8	10.5	85	41 - 60	-	13.75	22	19	23	4.0	5.0
HB10-1	M10	12.5	49	3 - 22	-	17.75	29	24	45	8.5	10.0
HB10-2	M10	12.5	64	22 - 41	-	17.75	29	24	45	8.5	10.0
HB10-3	M10	12.5	84	41 - 60	-	17.75	29	24	45	8.5	10.0
HB12-1	M12	14.5	53	3 - 25	-	19.75	32	30	80	10.5	15.0
HB12-2	M12	14.5	73	25 - 47	-	19.75	32	30	80	10.5	15.0
HB12-3	M12	14.5	93	47 - 69	-	19.75	32	30	80	10.5	15.0
HB16-1	M16	18	67	12 - 29	8	25.75	38	36	190	21.0	30.0
HB16-2	M16	18	92	29 - 50	8	25.75	38	36	190	21.0	30.0
HB16-3	M16	18	112	50 - 71	8	25.75	38	36	190	21.0	30.0
HB20-1	M20	22.5	80	12 - 34	8	32.75	51	46	300	35.0	40.0
HB20-2	M20	22.5	110	34 - 60	8	32.75	51	46	300	35.0	40.0
HB20-3	M20	22.5	140	60 - 86	8	32.75	51	46	300	35.0	40.0

Figure B.1: Data of Hollo-Bolt with Hexagonal Head [57]

Countersunk Head Data ···
(Available in sizes M8, M10, M12 & M16)

Collar —

Cone
(Interlocking
grooves
prevent
loosening)

Sleeve
(Expands
during
installation)
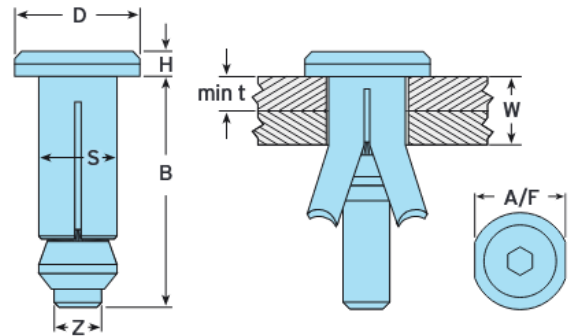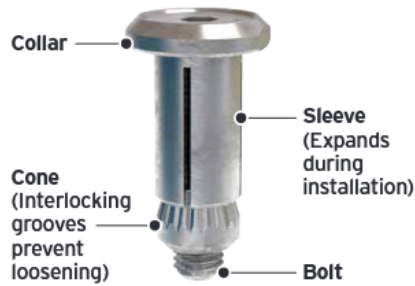
Bolt

Material: Carbon steel or stainless steel (see page 41 for corrosion protection options).

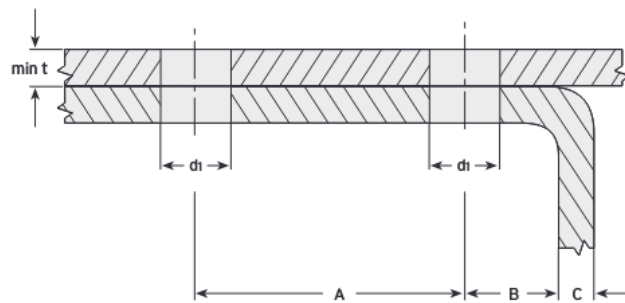| COUNTERSUNK HEAD DATA											
							Collar			Safe Working Loads (Factor of Safety 5:1)	
Product Code	Bolt Ø	Height	Length	Clamping Thickness	Outer Ply	Sleeve Outer Ø	Ø		Tightening Torque	Tensile	Single Shear
	Z	H	B (max)	W	min t	S	D	A/F			
		mm	mm	mm	mm	mm	mm	mm	Nm	kN	kN
HBCSK08-1	M8	5	45	3 - 22	-	13.75	22	19	23	4.0	5.0
HBCSK08-2	M8	5	65	22 - 41	-	13.75	22	19	23	4.0	5.0
HBCSK08-3	M8	5	85	41 - 60	-	13.75	22	19	23	4.0	5.0
HBCSK10-1	M10	6	44	3 - 22	-	17.75	29	24	45	8.5	10.0
HBCSK10-2	M10	6	64	22 - 41	-	17.75	29	24	45	8.5	10.0
HBCSK10-3	M10	6	84	41 - 60	-	17.75	29	24	45	8.5	10.0
HBCSK12-1	M12	7	48	3 - 25	-	19.75	32	30	80	10.5	15.0
HBCSK12-2	M12	7	73	25 - 47	-	19.75	32	30	80	10.5	15.0
HBCSK12-3	M12	7	93	47 - 69	-	19.75	32	30	80	10.5	15.0
HBCSK16-1	M16	8	62	12 - 29	8	25.75	38	36	190	21.0	30.0
HBCSK16-2	M16	8	92	29 - 50	8	25.75	38	36	190	21.0	30.0
HBCSK16-3	M16	8	112	50 - 71	8	25.75	38	36	190	21.0	30.0

HCF

Figure B.2: Data of Hollo-Bolt with Countersunk Head [38]

B.3. Installation guidelines Hollo-Bolt
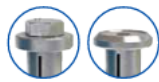
Preparation for installing Hollo-Bolt Hexagonal and Countersunk

Tool sizes for installing Hollo-Bolt Hexagonal

Hollo-Bolt Hexagonal			
Product Code	Spanner mm	Socket mm	Tightening Torque Nm
HB08	19	13	23
HB10	24	17	45
HB12	30	19	80
HB16	36	24	190
HB20	46	30	300

Type		Outer Ply	Clearance Hole Ø*	Hole Distances**		Edge Distances**
Hexagonal	Countersunk	min t mm	d1 mm	min A mm	min B mm	B + C mm
HB08	HBCSK08	-	14 (+1.0/-0.2)	35	13	≥ 17.5
HB10	HBCSK10	-	18 (+1.0/-0.2)	40	15	≥ 22.5
HB12	HBCSK12	-	20 (+1.0/-0.2)	50	18	≥ 25.0
HB16	HBCSK16	8	26 (+2.0/-0.2)	55	20	≥ 32.5
HB20	-	8	33 (+2.0/-0.2)	70	25	≥ 33.0

* For Hollo-Bolts with Hot Dip Galvanised Finish, drilling the clearance hole to the top tolerance is recommended.
** Ensure holes do not cut through the outer radius.

❯ Sizes M16 and M20 require outer ply thickness (min t) to be at least 8mm.

Tool sizes for installing Hollo-Bolt Countersunk

| Hollo-Bolt Countersunk			
Product Code	Spanner mm	Hexagon Key mm	Tightening Torque Nm
HBCSK08	19	5	23
HBCSK10	24	6	45
HBCSK12	30	8	80
HBCSK16	36	10	190

Figure B.3: Installation Guidelines for Hollo-Bolt Countersunk- and Hexagonal Bolt Head [57]

B.4. Deformation model for preloaded bolts
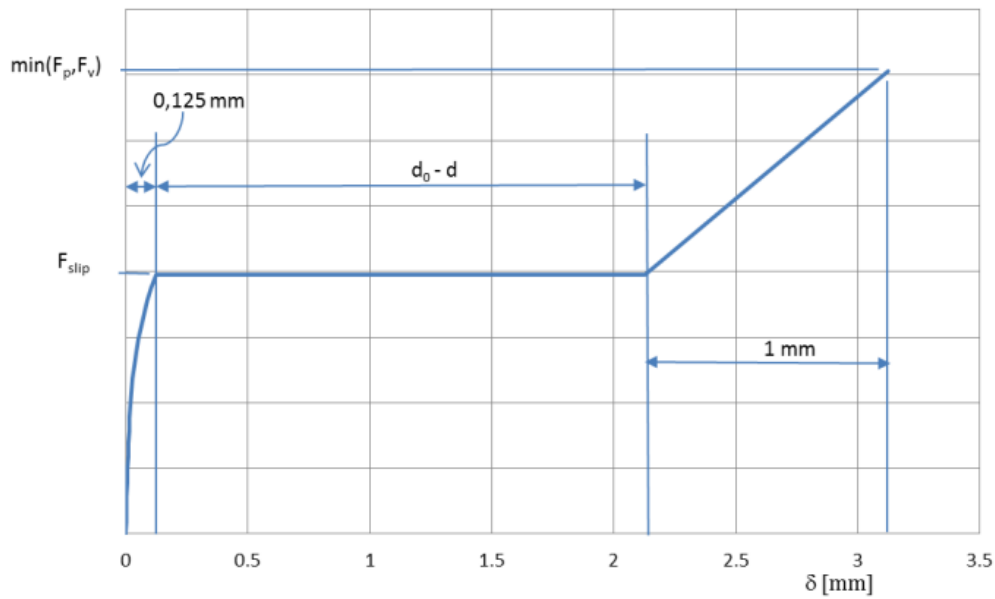
Figuur S1.1: Vervormingsmodel voor één voorgespannen bout in het vlak tussen twee platen

Figure B.4: Deformation model of 1 preloaded bolt connecting two plates [53]

C
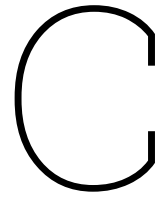
Critical Details

The ROK provides the following descriptions of the selected critical details for this thesis.
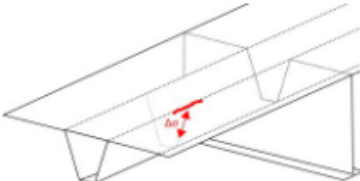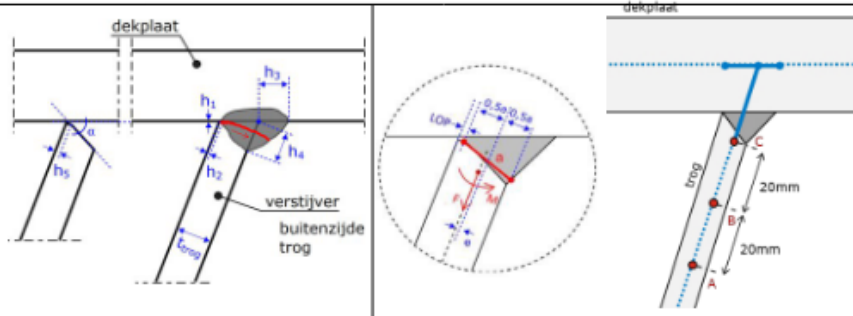
ROK-00919	Detail 2b-Fatigue of orthotropic driving floors-NEN-EN 1993-2							Bridge
Claim text	Detail 2b: TR-DP: crack in weld between trough and cover plate from the root of the weld							
Upper claim	ROK-00914							

Detail number	Description	Detail category	N_D	N_L	m_1	m_2	Detail category specific requirements
2b	Weld between the stiffener leg and the cover plate at a location between the cross girders.	125	10	100	3	5	auto glass
		112	10	100	3	5	hand weld (at fitting)
	Crack in the weld initiated from the weld root	**General implementation requirements**					

Slit

$h_1 = 0mm$

$h_1 < 0.5mm$ (<10% of length)

MDF[1] $\quad h_{1,mean} \leq 1.0$ mm

$h2_{,maximum} \leq 1.5$ mm

Weld extension[1] $\quad h3 = _{trough} +/-$

1mm $h_4 = t_{trog}$

$+/-$ 1mm

Welding geometry[1]
The weld must be flush to the deck and the trough leg. Breakthrough of the weld on the inside of the trough is not allowed.

Pre-processing
Trough leg bevel to a weld opening angle of 50° to 60°. $h_5 = 1mm$ (h_5) is the unbeveled part of the trough section).

NDO
Visual: 100 %; MT: all weld deposits + 10 % of weld length to be

Tension analysis:

The stress change should be determined from the normal force and the moment in the scale elements perpendicular to the weld. Both should be read directly at point C. If the results are doubtful, they can be extrapolated from points A and B. The stress variation at the weld root area should then be determined on the basis of the throat cross-section (a) of the weld measured perpendicular to the weld surface (this need not b e the smallest throat cross-section). The eccentricity due to the throat cross-section in relation to the trough centreline should be taken into account when determining the stresses at the weld root. When testing, MDF=1.5mm must be used in c o m b i n a t i o n with a weld extension (h_3 and h_4) equal to t_{trog}. Determine the stress in the weld according to the formula below:

$$\sigma w_{root} = \mp \frac{N_{trog}}{a} \quad \frac{6}{a^2} \left(M_{trog} + N_{trog} \cdot e_{trog} \right) + N_{trog}$$

Comments
The distance of the extrapolation points has been increased to a l l o w calculation with a large mesh. Due to the more or less completely linear stress build-up towards the weld, this does not affect the results.

[1] The MDF (maximum through-weld error), weld expansion and weld geometry s h o u l d b e verified by production tests in accordance with ROK par. 7.20.

Figure F00919: Detail 2b: TR-DP: crack in weld between trough and cover plate from the root of the weld

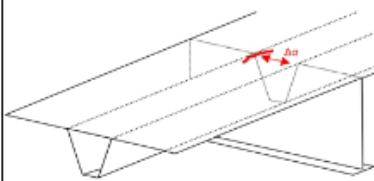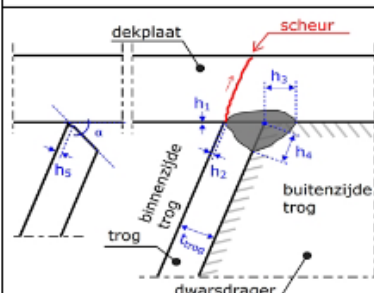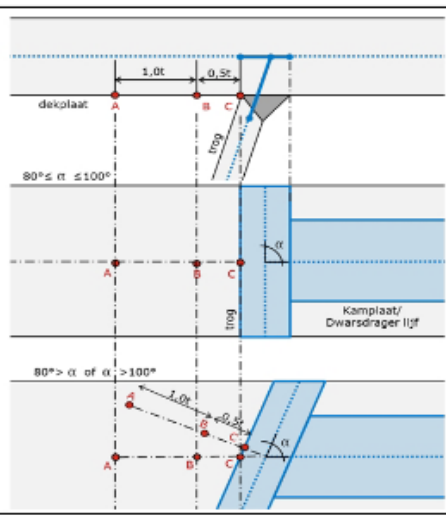**Figure C.1:** Detail 2b as according to ROK [12]

ROK-00917	Detail 1c-Fatigue of orthotropic driving floors-NEN-EN 1993-2	Bridge
Claim text	**Detail 1c: DP-TR**: crack in cover plate from root inside trough at location of a transverse support (troughs pierced)	
Upper claim	ROK-00914	

Detail-nummer	Beschrijving	Detail-categorie	N_D	N_L	m_1	m_2	Detailcategorie specifieke eisen
1c	Dekplaatscheur vanuit de laswortel van de trog-dekplaatlas ter plaatse van een dwarsdrager bij doorgestoken troggen.	200	20	300	3	5	$t_{dekplaat} \geq 18mm$
		188	25	200	3	5	$15mm \leq t_{dekplaat} \leq 17mm$
		167	30	100	3	5	$10mm \leq t_{dekplaat} \leq 14mm$

Algemene eisen m.b.t. uitvoering

Spleet	$h_1 = 0mm$
	$h_1 < 0,5mm$ (<10% van de lengte)
MDF[1]	$h_{2,gemiddeld} \leq 1,0$ mm
	$h_{2,maximaal} \leq 1,5$ mm
Lasuitbouw[1]	$h_3 = t_{trog} +/- 1mm$
	$h_4 = t_{trog} +/- 1mm$

Lasgeometrie[1]
De las moet vloeiend aanliggen aan het dek en het trogbeen.
Doorslag van de las aan de binnenzijde van de trog is niet toegestaan.
Voorbewerking
Trogbeen afschuinen tot een lasopeningshoek van 50° tot 60°. h_5=1mm (h_5 is het niet afgeschuinde deel van het trogdeel).
NDO
Visueel: 100 %; MT: alle lasaanzetten + 10 % van de laslengte als steekproef te kiezen op basis van de visuele inspectie.

Spanningsanalyse:

Lineaire extrapolatie vanuit A & B naar C. Mesh-afmeting $\leq 0,5t_{dekplaat}$, maar tussen knoop B en C dienen minimaal 2 elementen ($0,25t_{dekplaat}$) toegepast te worden. Extrapolatie is van de elementknopen in lijn met het lijf van de dwarsdrager/kamplaat (haaks op de trogwand). Indien hoek α kleiner is dan 80° of groter dan 100° dient de spanning bepaald te worden zowel loodrecht op de trog als parallel aan het lijf van de dwarsdrager/kamplaat (zie onderstaand Figuur). Spanningsrichting dient altijd gelijk te zijn aan de extrapolatierichting.

Opmerkingen

Bij dit detail horen aangepaste vermoeiingscurves. De cut-off limit ligt voor alle drie de categorieën ongeveer even hoog, echter ontwikkelen de dikkere platen minder snel schade dan de dunnere platen. Dit komt omdat het punt van schade (D=1) is afgestemd op het doorscheuren van de plaat. Voorbeeld, voor DC=200: N_C=2miljoen; N_D=20miljoen (m=3); N_L=300miljoen (m=5). Ter controle: met γ_{Mf}=1,15 ligt het afkaplimiet bij circa $0,235\sigma_c = 47$ MPa..

[1] De MDF (maximale doorlasfout), lasuitbouw en lasgeometrie dienen geverifieerd te worden middels productieproeven conform ROK par. 7.20.

Figure F00917: DP-TR: crack in cover plate from root inside trough at location of a transverse support (troughs pierced)

Figure C.2: Detail 1c as according to ROK [12]

D

Sensitivity Study: Shear Stiffness of Springs

These results were obtained with the initially made decisions regarding the hybrid interaction between the deck plate and strengthening plate: connecting them with additional discrete axial springs over the whole region of the strengthening plate. The sensitivity study regarding shear stiffness of the springs representing the bolts was performed for detail 2b. The results are shown below. An infinite stiffness is approximated with 1e9 kN/m. The other shear stiffness values are calculated using the formula $k_spring = F_slip/0.125mm$. When a percentage is included, it means that the shear stiffness is reduced with that percentage.

D.1. Effect of varying stiffness on hot spot stresses
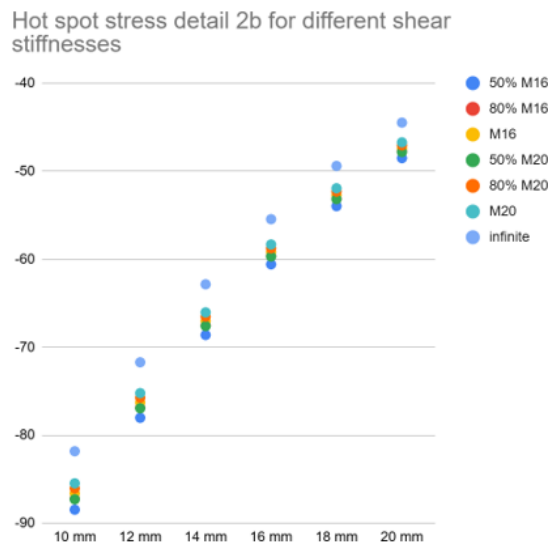
Figure D.1: Decreasing Hot Spot Stresses with Increase of Shear Stiffness of the Springs.

D.2. Effect of varying stiffness on shear forces in springs

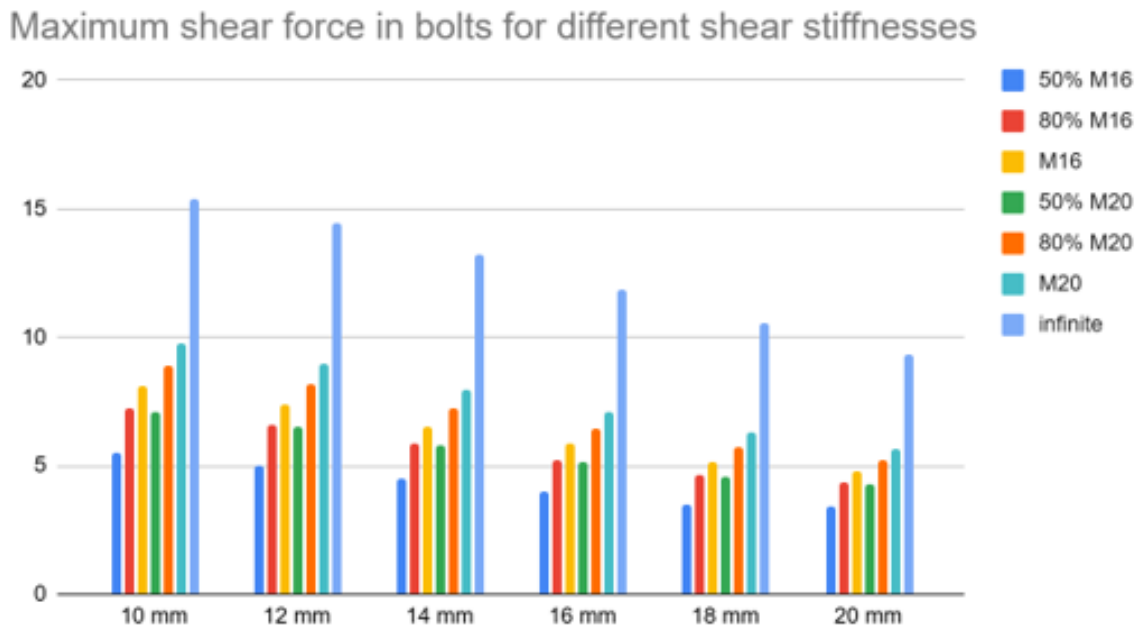**Figure D.2:** Increasing Shear Forces with Increase of Shear Stiffness of the Springs.

E

Strengthening Schemes: Additional Results

E.1. Hot Spot Stress Reductions for other strengthening schemes

Table E.1: Hot spot stress reduction for different thicknesses and bolt configurations: detail 2b, M20 100 mm fully bolted

Thickness	1x0	0x1	1x1	2x0	0x2	2x1	1x2	2x2
10	0.27	0.26	0.27	0.29	0.27	0.29	0.28	0.30
12	0.35	0.35	0.36	0.37	0.36	0.38	0.37	0.38
14	0.43	0.43	0.44	0.45	0.44	0.45	0.45	0.46
16	0.50	0.50	0.51	0.51	0.50	0.52	0.51	0.52
18	0.55	0.56	0.56	0.56	0.56	0.57	0.57	0.57
20	0.59	0.60	0.61	0.60	0.60	0.61	0.61	0.62

Table E.2: Hot spot stress reduction for different thicknesses and bolt configurations: detail 2b, M20 100 mm fully bolted

Thickness	1x0	0x1	1x1	2x0	0x2	2x1	1x2	2x2
10.00	0.03	0.06	0.07	0.06	0.07	0.09	0.08	0.10
12.00	0.14	0.18	0.19	0.18	0.19	0.21	0.20	0.22
14.00	0.26	0.30	0.31	0.29	0.31	0.33	0.32	0.33
16.00	0.38	0.41	0.42	0.40	0.42	0.43	0.43	0.44
18.00	0.48	0.50	0.51	0.50	0.51	0.52	0.52	0.53
20.00	0.56	0.58	0.59	0.58	0.59	0.60	0.60	0.61

E.2. Static verifications: Load Model 2

Table E.3: Unity Checks for shear in bolts due to LM2: detail 2b

Thickness	1x0	0x1	1x1	2x0	0x2	2x1	1x2	3x0	0x3	2x2	3x1	1x3	3x2	2x3	3x3
10	0.83	0.65	0.77	0.66	0.66	0.67	0.75	0.85	0.61	0.66	0.69	0.72	0.83	0.65	0.81
12	0.87	0.69	0.80	0.64	0.69	0.68	0.78	0.80	0.63	0.62	0.74	0.75	0.78	0.61	0.76
14	0.90	0.72	0.81	0.66	0.70	0.71	0.80	0.74	0.64	0.63	0.79	0.77	0.71	0.59	0.70
16	0.92	0.74	0.82	0.67	0.71	0.71	0.81	0.68	0.64	0.64	0.83	0.77	0.65	0.59	0.63
18	0.93	0.76	0.83	0.68	0.70	0.71	0.81	0.69	0.64	0.63	0.87	0.77	0.64	0.60	0.62
20	0.94	0.78	0.83	0.69	0.70	0.71	0.81	0.69	0.63	0.62	0.90	0.77	0.64	0.59	0.62

Table E.4: Unity Checks for shear in bolts due to LM2: detail 1c

Thickness	1x0	0x1	1x1	2x0	0x2	2x1	1x2	3x0	0x3	2x2	3x1	1x3	3x2	2x3	3x3
10	0.34	0.09	0.34	0.42	0.12	0.41	0.33	0.51	0.15	0.41	0.51	0.33	0.50	0.41	0.50
12	0.32	0.10	0.32	0.39	0.12	0.38	0.31	0.46	0.14	0.38	0.46	0.31	0.46	0.38	0.45
14	0.30	0.10	0.29	0.35	0.12	0.35	0.29	0.41	0.14	0.34	0.40	0.29	0.40	0.34	0.40
16	0.27	0.11	0.27	0.32	0.12	0.31	0.27	0.37	0.13	0.31	0.36	0.26	0.36	0.31	0.36
18	0.25	0.11	0.25	0.29	0.12	0.28	0.25	0.33	0.13	0.28	0.32	0.24	0.32	0.28	0.32
20	0.24	0.12	0.23	0.26	0.12	0.26	0.23	0.30	0.13	0.25	0.29	0.23	0.29	0.25	0.29